EurJIC
European Journal of Inorganic Chemistry

19/2013
1st July Issue

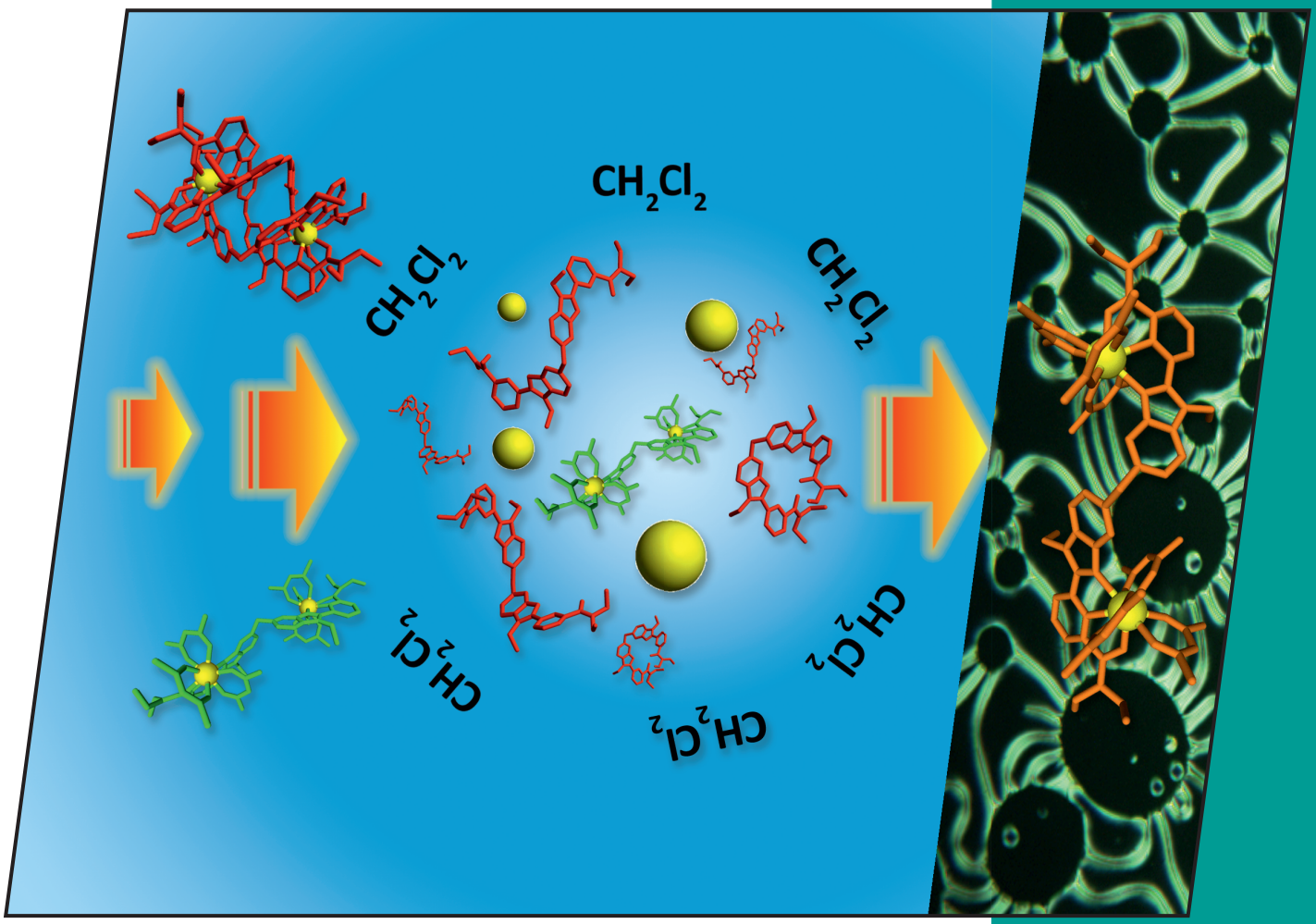

Cover Picture
Emmanuel Terazzi, Claude Piguet et al.
Single-Stranded Dinuclear Lanthanide Helicates

A Journal of
ChemPubSoc Europe

WILEY-VCH

www.eurjic.org

EJICFK (19) 3271–3440 (2013) · ISSN 1099-0682 · No. 19/2013

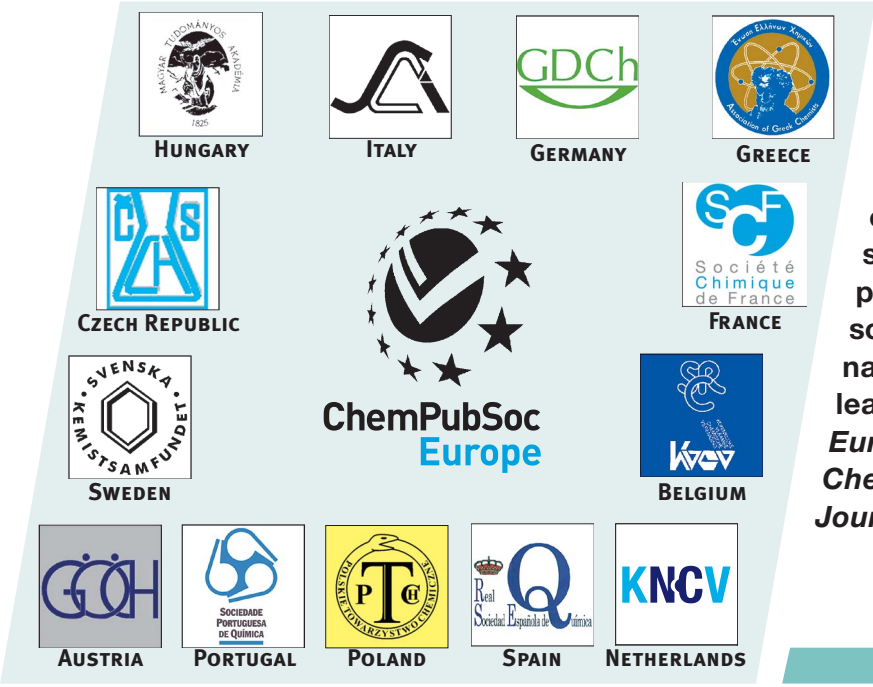

EurJIC is a journal of ChemPubSoc Europe, a union of 16 European chemical societies formed for the purpose of publishing high-quality science. All owners merged their national journals to form two leading chemistry journals, the *European Journal of Inorganic Chemistry* and the *European Journal of Organic Chemistry*.

Other ChemPubSoc Europe journals are *Chemistry – A European Journal*, *ChemBioChem*, *ChemPhysChem*, *ChemMedChem*, *ChemSusChem*, *ChemCatChem*, *ChemPlusChem* and *ChemistryOpen*.

COVER PICTURE

The cover picture shows how single-stranded dinuclear lanthanide helicates (green) survive immersion into a drop of less polar solvent (e.g. CH_2Cl_2) and their eventual self-organization into a liquid-crystalline material. For alternative triple-stranded lanthanide helicates (red), drastic solvation effects lead to complete dissociation. Details are discussed in the article by E. Terazzi, C. Piguet et al. on p. 3323ff. For more on the story behind the cover research, see the Cover Profile.

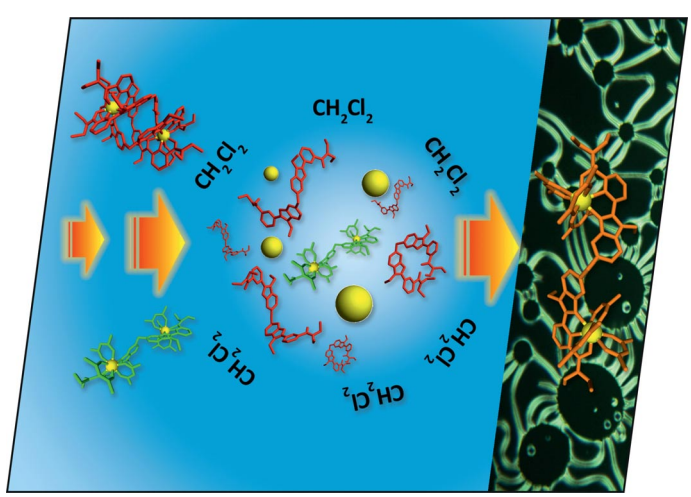

EurJIC European Journal of Inorganic Chemistry

ChemPubSoc Europe

FULL PAPER

DOI:10.1002/ejic.201300176

Implementing Liquid-Crystalline Properties in Single-Stranded Dinuclear Lanthanide Helicates

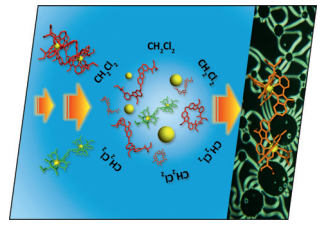

COVER PICTURE

Emmanuel Terazzi,*[a] Amir Zaïm,[a] Bernard Bocquet,[a] Johan Varin,[a] Laure Guénée,[b] Thibault Dutronc,[a] Jean-François Lemonnier,[a] Sébastien Floquet,[c] Emmanuel Cadot,[c] Benoît Heinrich,[d] Bertrand Donnio,[d] and Claude Piguet*[a]

Keywords: Liquid crystals / Metallomesogens / Polynuclear complexes / Amphiphiles / Helical structures / Lanthanides

The connection of flexible protodendritic wedges to the bis-tridentate rigid polyaromatic ligand **L1** provides amphiphilic receptors **L5** and **L6**; their reduced affinities for complexing trivalent lanthanides (Ln = La, Y, Lu) in organic solvent (by fifteen orders of magnitude!) prevent the formation of the expected dinuclear triple-stranded helicates $[Ln_2(\mathbf{L}\boldsymbol{k})_3]^{6+}$. This limitation could be turned into an advantage because **L1** or **L6** can be treated with $[Ln(hfac)_3]$ (Hhfac = 1,1,1,5,5,5-hexafluoro-2,4-pentanedione) to give neutral single-stranded $[Ln_2(\mathbf{L}\boldsymbol{k})(hfac)_6]$ complexes with no trace of higher-order helicates. Whereas ligands **L1** and **L5** are not liquid crystals, **L6** can be melted above room temperature (41 °C) to give a nematic mesophase, and its associated dinuclear helical complex $[Y_2(\mathbf{L6})(hfac)_6]$ self-organises at the same temperature into a fluidic smectic mesophase.

Introduction

For a long time, lanthanide supramolecular chemistry focused on the design and on the thermodynamic rationalisation of discrete sophisticated polynuclear molecular architectures such as helicates,[1] cages,[2] clusters[3] and grids.[4] Owing to the remarkable magnetic and optical properties associated with the 4f-centred open-shell electronic configurations, these compounds were approached for overcoming modern technological limitations, but the exploitation of their intrinsic properties for lighting, sensing and switching further requires specific patterns gained by the self-organisation of amphiphilic receptors connected to the inorganic cores.[5,6] When the organic coating induces liquid-crystalline properties, the resulting metal-containing liquid crystals are referred to as metallomesogens,[7] or more specifically, as lanthanidomesogens for those that incorporate metallic cations with $[Xe]4f^n$ configurations.[8] Roughly speaking, most thermotropic liquid crystals (i.e., liquid crystals that self-organise with temperature) are produced by connecting long and flexible aliphatic chains to various rigid polarisable aromatic cores.[9] Optimisation of the intermolecular interactions in the crystalline state results in a microsegregation process, in which the rigid cores are packed together, whereas the less polarisable flexible alkyl chains fill the residual voids of the structure.[10] Upon heating, the decorrelation between the flexible alkyl chains produces a molten continuum (assigned to the melting process), with the residual interactions between aromatics ensuring the stability of the liquid-crystalline phase. At higher temperature, the interactions between the aromatic units become smaller than the thermal energy and a classical liquid is obtained (assigned to the isotropisation process). This standard two-step melting model satisfyingly predicts the thermal behaviour of low-molecular-weight amphiphilic organic molecules that possess considerable anisometric shapes.[10,11] In metallomesogens, the isotropic three-dimensional expansion brought by the coordination spheres of the metals usually disrupts the microsegregation and destabilises the liquid-crystalline phase. Except for complexes with linear or square-planar arrangements that are reminiscent of the molecular shapes found in purely organic liquid crystals,[7,12] common coordination geometries are difficult to combine with the structural anisotropy required for inducing mesomorphism and liquid-crystalline phases are not formed. In this context, only a few metallomesogens contain a tetrahedral[13] or an octahedral metal centre,[14] and

[a] Department of Inorganic and Analytical Chemistry, University of Geneva,
30 quai E. Ansermet, 1211 Geneva 4, Switzerland
E-mail: Emmanuel.Terazzi@unige.ch
Claude.Piguet@unige.ch
Homepage: http://www.unige.ch/sciences/chiam/piguet/Welcome.html
[b] Laboratory of Crystallography, University of Geneva,
24 quai E. Ansermet, 1211 Geneva 4, Switzerland
[c] Institut Lavoisier de Versailles, UMR 8180,
University of Versailles Saint-Quentin,
45 av. des Etats-Unis, 78035 Versailles, France
[d] Institut de Physique et Chimie des Matériaux de Strasbourg (IPCMS), UMR 7504 (CNRS – Université de Strasbourg),
23 rue du Loes, BP43, 67034 Strasbourg cedex 2, France

Supporting information for this article is available on the WWW under http://dx.doi.org/10.1002/ejic.201300176.

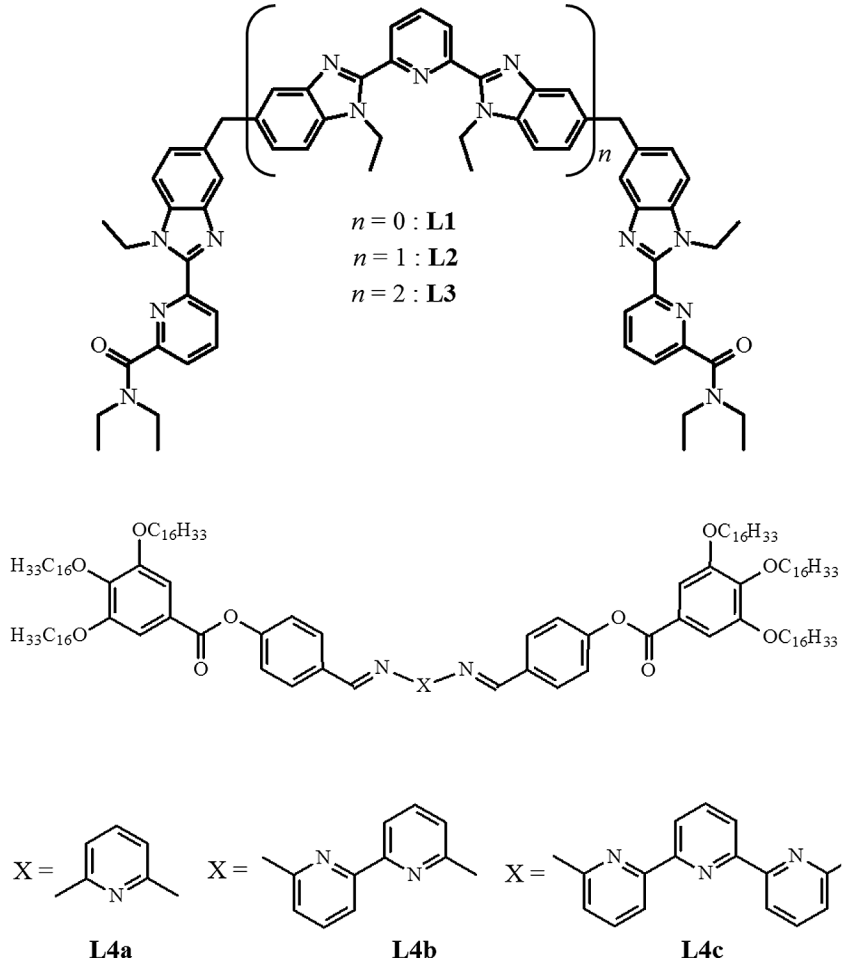

L4a **L4b** **L4c**

those with coordination number (CN) 7–12, typical of large lanthanide cations, have remained challenging for some time.[5,15] Pioneering work dedicated to fullerodendrimers[16] established that mesomorphism could be induced when the bulky spherical cores were coated with divergent polarised dendritic architectures, a strategy that led to the preparation of a unique discotic dinuclear lanthanidomesogen.[15d] To the best of our knowledge, there is no other report of multinuclear mesomorphic analogues despite a rich catalogue of polynuclear linear triple-stranded helicates such as $[Ln_2(\mathbf{L1})_3]^{6+}$, $[Ln_3(\mathbf{L2})_3]^{9+}$ and $[Ln_4(\mathbf{L3})_3]^{12+}$, the cylindrical rigid cores of which make them ideal for the design of calamitic metallomesogens.[1]

However, by following this strategy, lipophilic dinuclear helicates with d-block metals $[Cu_2(\mathbf{L4}n)_2]^{2+}$ (n = a, b, c) have been shown to self-organise into columnar mesophases.[13b,17] Interestingly, the connection of the long lipophilic and diverging alkyl chains to the cylindrical core drastically limited the stability of these complexes in solution, an observation that might explain the paucity of helical scaffolds in metallomesogens. To extend this approach to magnetically and optically active 4f-block cations, we connect here two different lipophilic protomesomorphic dendrons perpendicularly to the helical axis in **11** through ether links (**L5**) or ester bonds (**L6**) (Scheme 1). The conditions required for the preparation of stable dinuclear lanthanidomesogens are explored together with their liquid-crystalline properties.

Results and Discussion

Synthesis of Ligands L*k* (*k* = 5, 6) and Formation of the Triple-Stranded Complexes $[Ln_2(L\mathit{k})_3(CF_3SO_3)_6]$ (Ln = La, Y, Lu; *k* = 5, 6) in Solution

Alkylation of intermediate **11** with **15** gave the target ligand **L5**, whereas esterification with **16**[15i] yielded **L6** (Scheme 1 and Appendix 1 in the Supporting Information).

The five different ^{1}H NMR spectroscopic signals detected for the aromatic protons Hb–Hf in L*k* (*k* = 5, 6), combined with the observation of a singlet for the protons Ha and of a quartet for the protons Hm, confirmed the existence of dynamically averaged C_{2v} symmetries for the free ligands in solution (see Scheme 1 for numbering). The lack of a nuclear Overhauser enhancement (NOE) effect between the ethyl residues of the benzimidazole rings and the protons connected at the 3-positions of the pyridine rings agreed with a standard *trans* arrangement of the N-donor atoms borne by the adjacent aromatic rings. This arrangement was confirmed by analysis of the solid-state structure

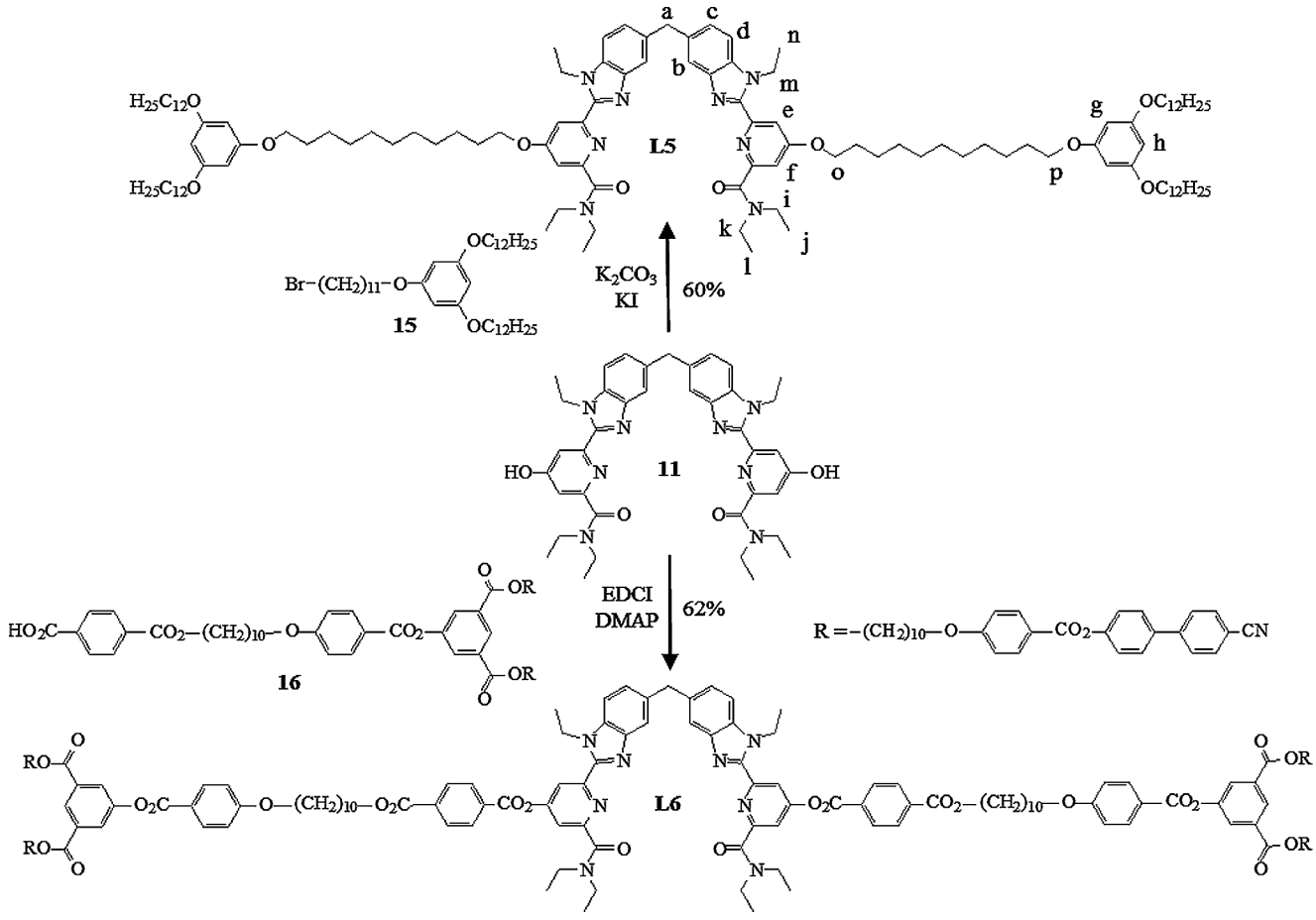

Scheme 1. Synthesis and structures of bis-tridentate ligands **L5** and **L6**, derived from **11** (with numbering scheme for NMR spectra).

of intermediate **10** (Appendix 1 in the Supporting Information). Reaction of the bis-tridentate ligand **L6** (3 equiv.) with $[Y(CF_3SO_3)_3]\cdot 4H_2O$ (1 equiv.) in CD_2Cl_2 provided a temperature-independent broad ^1H NMR spectrum (Figure S2a in the Supporting Information) that indicates weak interactions between the binding unit and the central diamagnetic Y^{3+} cation, which leads to the formation of intricate mixtures of complexes in intermediate exchange on the NMR spectroscopic timescale. The use of more polar solvents ($CDCl_3$, CD_3NO_2, $[D_8]$THF; Figure S2b) did not improve the situation and the ESI-MS spectrum of the colourless mixture only showed the presence of the protonated free ligand $[\mathbf{L6} + H]^+$. Since the bis-tridentate ligand **L1** is known to produce very stable triple-helical complexes $[Ln_2(\mathbf{L1})_3](CF_3SO_3)_6$ in acetonitrile [log ($\beta_{2,3}^{\mathbf{L1}}$ ≅ 25)],[18] this deleterious effect can be tentatively assigned to the considerable lipophilicity of **L6**, which is efficiently solvated in organic solvents. Upon reaction of the less lipophilic ligand **L5** (3 equiv.) with $[Y(CF_3SO_3)_3]\cdot 4H_2O$ (1 equiv.) in CD_2Cl_2/CD_3CN = 1:4, the six metal-shifted ^1H NMR spectroscopic signals observed for the aromatic protons Hb–Hh were diagnostic for overall threefold symmetry.[19] The helical arrangement of the strands was substantiated by the detection of pseudo-sextets [ABX_3 spin systems for which $^2J = 2\cdot(^3J)$] for the diastereomeric methylene protons of the ethyl residues (Hm), whereas the singlet (A_2 spin system) observed for the enantiotopic methylene protons (Ha) of the diphenylmethane spacer points to the existence of three twofold axes perpendicular to the threefold axis in line with the regular D_3-symmetrical triple-helical arrangement of the expected triple-stranded helicate $[Y_2(\mathbf{L5})_3]^{6+}$ (Figure 1, a). Upon addition of increasing amounts of CD_2Cl_2, the signals of the complex were broadened because of partial ligand dissociation and slow exchange processes (Figure 1b–h and Figure S3 in the Supporting Information), a trend that was confirmed by the decreasing ratio of the peaks detected by ESI-MS spectra for $[Y_2(\mathbf{L5})_3(CF_3SO_3)_n]^{(6-n)+}$ and $[\mathbf{L5} + H]^+$, respectively. We conclude that the reduced lipophilicity in **L5** limits the solvation of the free ligand to such an extent that $[Y_2(\mathbf{L5})_3]^{6+}$ can be obtained in polar organic solvents at millimolar concentrations [see Equilibrium (1) below].

If we take the integral I_{gh} of the ^1H NMR spectral singlet recorded for the peripheral aromatic protons Hg,Hh as a probe for calibrating the total ligand concentration in each mixture ($|\mathbf{L5}|_{tot} = |\mathbf{L5}| + 3|[Y_2(\mathbf{L5})_3]|$), the stability constants $\beta_{2,3}^{Ln,\mathbf{L5}}$ for Equilibrium (1) can be estimated by integration

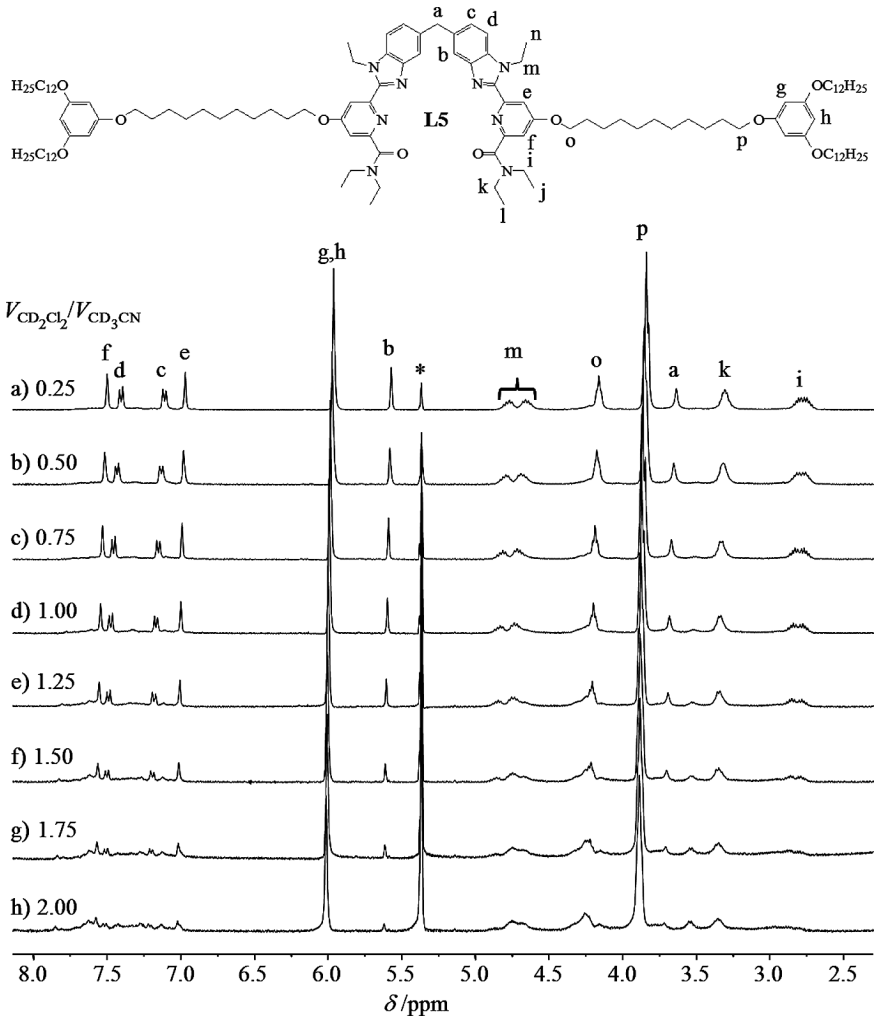

Figure 1. ^{1}H NMR spectra with numbering scheme of the diamagnetic triple-stranded helicate $[Y_2(\mathbf{L5})_3]^{6+}$ at different $V_{CD_2Cl_2}/V_{CD_3CN}$ volume; * = $CDHCl_2$ (total ligand concentration $|\mathbf{L5}|_{Tot}$ ≅ 0.01 M, 298 K).

of the signals recorded for proton b (I_b) in each solvent mixture (Table 1).

$$3\mathbf{L5} + 2Ln(CF_3SO_3)_3 \rightleftharpoons [Ln_2(\mathbf{L5})_3](CF_3SO_3)_6 \ \beta_{2,3}^{Ln,\mathbf{L5}} \quad (1)$$

The stability constants estimated for $[Ln_2(\mathbf{L5})_3](CF_3SO_3)_6$ are more than fifteen orders of magnitude smaller than those found for the parent nonlipophilic complexes $[Ln_2(\mathbf{L1})_3](CF_3SO_3)_6$ in pure acetonitrile (Figures S4–S9 in the Supporting Information).[18] These thermodynamic data unambiguously demonstrate that the efficient solvation of ligand **L*k*** (k = 5, 6) in organic solvents severely limits their affinity for trivalent lanthanides, but the presence of a significant amount of CH_2Cl_2 is crucial for the solubilisation of these ligand. These two conflicting requirements prevent the isolation of pure triple-stranded lipophilic helical lanthanide complexes, which results from the successive

Table 1. Experimental cumulative formation constants $\log(\beta_{2,3}^{Ln,\mathbf{L5}})$ obtained by ^{1}H NMR spectroscopy according to Equilibrium (1) (Ln = La, Y and Lu; total concentration of ligand $|\mathbf{L5}|_{tot}$ = 0.01 M).[a]

$V_{CD_2Cl_2}/V_{CD_3CN}$	$\log(\beta_{2,3}^{La,\mathbf{L5}})$ $[La_2(\mathbf{L5})_3](CF_3SO_3)_6$	$\log(\beta_{2,3}^{Y,\mathbf{L5}})$ $[Y_2(\mathbf{L5})_3](CF_3SO_3)_6$	$\log(\beta_{2,3}^{Lu,\mathbf{L5}})$ $[Lu_2(\mathbf{L5})_3](CF_3SO_3)_6$
0.25	8.8(1)	10.1(1)	9.5(2)
0.50	8.3(1)	9.8(2)	8.4(1)
0.75	7.4(1)	9.6(2)	7.7(1)
1.00	7.1(2)	9.1(1)	7.1(2)
1.25	6.4(4)	8.9(1)	6.5(4)
1.50	5(1)	8.3(1)	4.4(4)
1.75	_[b]	7.3(2)	5.9(8)
2.00	_[b]	7.1(3)	_[b]

[a] The standard deviations are calculated for integration uncertainties of 5%. [b] The signals of the complexes are too weak to be detected.

fixation of three tridentate binding unit about each metal. However, this drawback can be turned into an advantage with the lipophilic ligand **L6**, which possesses the structural criteria for designing lanthanidomesogens. Indeed, the replacement of poorly coordinating triflate anions with hexafluoroacetylacetonate (hfac) anions should strictly limit the affinity of the central metal to a single tridentate binding unit, as found in [Ln(**L*k***)(hfac)$_3$] (*k* = 7, 8),[20] thus leading to the formation of the single-stranded [Ln$_2$(**L6**)(hfac)$_6$] complexes with no possible mixing with higher-order helicates.

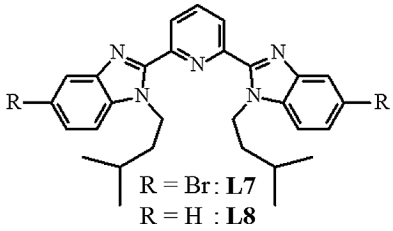

Synthesis and Structure of the Single-Stranded Complexes [Ln$_2$(L*k*)(hfac)$_6$] (*k* = 1, 6; Ln = Y, Lu)

Reaction of the C_{2v}-symmetrical bis-tridentate ligand **L1** (1 equiv.) with [Lu(hfac)$_3$(diglyme)] (2 equiv.) in acetonitrile followed by the slow diffusion of diethyl ether yielded small colourless crystals suitable for X-ray analysis (Tables S4–S6 in the Supporting Information). No standard hydrogen bonds or intermolecular stacking interactions could be found, and the molecular structure confirmed the coordination of one Lu^{III} ion to each *cis–cis* tridentate segment of ligand **L1**, thus leading to an intramolecular intermetallic Lu···Lu separation of 12.533(1) Å (Figure 2). Each Lu^{III} cation is almost held within the equatorial plane defined by the three donor atoms of each tridentate binding unit (O1, N1, N3 for Lu1 and O2, N5, N7 for Lu2; deviations of the Lu atom from the planes: 0.009 and 0.018 Å, respectively). Each coordination sphere is completed with three didentate hfac anions, with two of them being located on both sides of the equatorial plane and the third roughly perpendicular (81.4–84.1°) to the latter plane. This results in pseudo-C_{2v} symmetry around the lutetium ion, an arrangement that is compatible with the description of the nine-coordinate coordination spheres as distorted mono-capped square antiprisms with N1 (Lu1) or N5 (Lu2) occupying the capping positions (Figure S10 and Tables S7–S8 in the Supporting Information). The average distances Lu1–O = 2.34(5) Å, Lu1–N = 2.477(4) Å, Lu2–O = 2.35(5) Å and Lu2–N = 2.502(8) Å (Table S5 in the Supporting Information) are close to those found in the mononuclear analogues [Lu(**L*k***)(hfac)$_3$] (*k* = 7, 8),[20] an observation that is corroborated by the calculated bond valences (Table S9 in the Supporting Information).[21] The helicity of the diphenylmethane spacer, defined as a five-atom crooked line (C15–C14–C20–C21–C27) amounts to *H* = 0.55,[22] a value that is in line with *H* = 0.76 reported for the analogous single-stranded complex [Eu$_2$(**L1**)(NO$_3$)$_6$(H$_2$O)$_2$].[23]

Monitoring the titration of **L6** with [Y(hfac)$_3$(diglyme)] in CDCl$_3$ by using ^{1}H NMR spectroscopy showed the stepwise formation of the complexes [Y(**L6**)(hfac)$_3$] and [Y$_2$(**L6**)(hfac)$_6$] according to Equilibria (2) and (3) (Figures S11–S17 in the Supporting Information). The broadened ^{1}H NMR spectroscopic signals implied the operation of intermolecular exchange processes with an intermediate rate on the NMR spectroscopic timescale but the concomitant observation of a singlet for the protons of the three complexed hfac anions indicated fast intramolecular exchange between axial and meridional positions in [Y(**L6**)(hfac)$_6$] and [Y$_2$(**L6**)(hfac)$_6$].

$$\mathbf{L6} + [Y(hfac)_3(diglyme)] \rightleftharpoons [Y(\mathbf{L6})(hfac)_3] + diglyme \quad \beta_{1,1}^{Y(hfac)_3,\mathbf{L6}} \tag{2}$$

$$\mathbf{L6} + 2[Y(hfac)_3(diglyme)] \rightleftharpoons [Y_2(\mathbf{L6})(hfac)_6] + 2\,diglyme \quad \beta_{2,1}^{Y(hfac)_3,\mathbf{L6}} \tag{3}$$

A thorough analysis of the ^{1}H NMR spectroscopic signals for the Y^{III}/**L6** = 2.0 ratio in chloroform revealed the

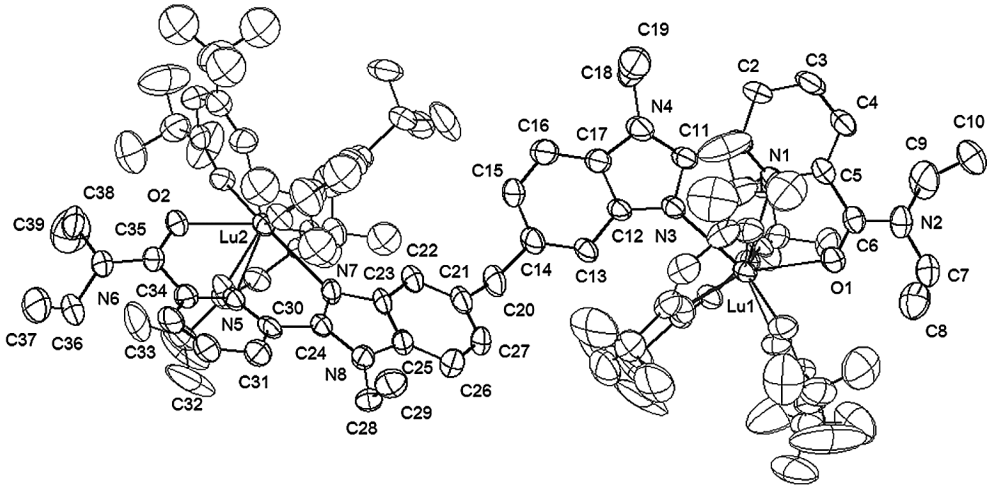

Figure 2. Perspective view with numbering scheme of the molecular structure of [Lu$_2$(**L1**)(hfac)$_6$]. Ellipsoids are represented at 50% probability level. The labels for hfac and the hydrogen atoms are omitted for clarity.

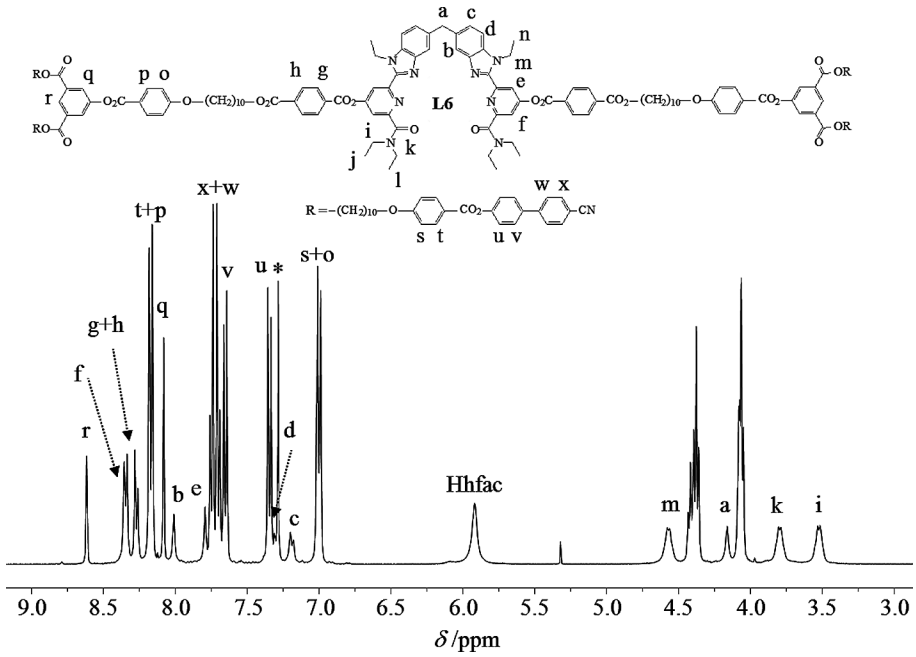

Figure 3. ^{1}H NMR spectrum with numbering scheme of the diamagnetic complex [Y_2(**L6**)(hfac)$_6$] ($CDCl_3$, 298 K); * = $CHCl_3$.

existence of a single complex in solution with a pattern of five signals for the aromatic protons Hb–Hf (twofold symmetry) and the presence of a singlet for the enantiotopic methylene protons Ha (planar symmetry) that are diagnostic of an average C_{2v}-symmetrical arrangement of the coordinated ligand strand in [Y_2(**L6**)(hfac)$_6$] (Figure 3).

Nonlinear least-squares fit[24] of the dynamically averaged ^{1}H NMR spectroscopic titration data provided complete sets of chemical shifts for [Y(**L6**)(hfac)$_6$] and [Y_2(**L6**)(hfac)$_6$] (Table S10 in the Supporting Information) together with cumulative stability constants $\log[\beta_{1,1}^{Y(hfac)_3,\mathbf{L6}}]$ = 6(2) and $\log[\beta_{2,1}^{Y(hfac)_3,\mathbf{L6}}]$ = 11(2), which agreed with $\log[\beta_{1,1}^{Ln(hfac)_3,\mathbf{Lk}}] \geq 5.7$ estimated for the mononuclear complexes [Ln(**L*k***)(hfac)$_3$] (*k* = 7, 8; Ln = La, Eu, Lu, Y) in $CDCl_3$.[20] The pure single-stranded dinuclear [Y_2(**L6**)-(hfac)$_6$]·29H_2O complex could be eventually obtained by treating **L6** (1 equiv.) with [Y(hfac)$_3$(diglyme)] (2 equiv.) in $CHCl_3$ followed by precipitation with hexane (Table S1 in the Supporting Information).

Liquid-Crystalline Organisation of Ligand L6 and Its Complex [Y_2(L6)(hfac)$_6$]

The thermal behaviours of ligand **L6** and its yttrium complex [Y_2(**L6**)(hfac)$_6$] were studied by a combination of polarised optical microscopy (POM), thermogravimetric analysis (TGA) and differential scanning calorimetry (DSC) measurements (Figure 4, Table 2 and Figures S18–20 in the Supporting Information). Temperature-dependent POM observations (20–250 °C temperature range) showed the formation of fluid birefringent textures for **L6** and [Y_2(**L6**)(hfac)$_6$] upon heating (Figure S18) that are typical of the occurrence of liquid-crystalline organisations, whereas ligand **L5** did not show any birefringence in solid

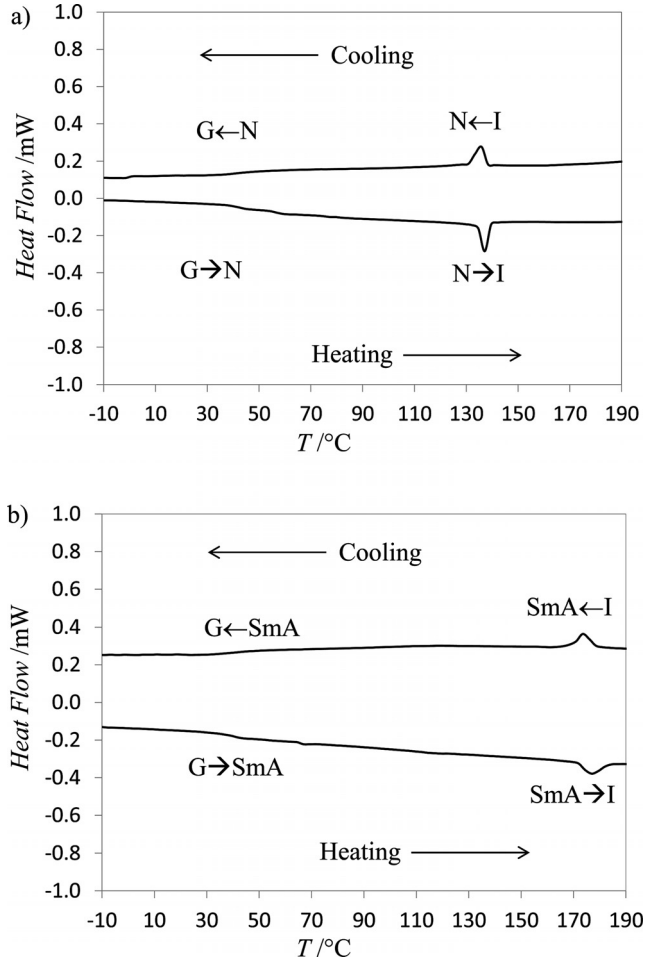

Figure 4. (a) DSC trace of the ligand **L6** at 5 °C min^{-1}; (b) DSC trace of complex [Y_2(**L6**)(hfac)$_6$] at 5 °C min^{-1} (second heating and cooling).

or in liquid states. The optical defects observed in the liquid-crystalline texture of ligand **L6** were typical of a nematic phase (N) (Figure S18a), whereas the observation of homeotropic zones for $[Y_2(\mathbf{L6})(hfac)_6]$ suggested the formation of a more ordered smectic A (SmA) phase (Figure S18b).

Table 2. Temperatures, enthalpy and entropy changes of the phase transitions observed for ligands **L*k*** (*k* = 5, 6) and complex $[Y_2(\mathbf{L6})(hfac)_6]$.

Compound	Phase sequence[a]	Transition temp. *T* [°C]	ΔH [kJ mol^{-1}]	ΔS [J mol^{-1} K^{-1}]
L5	G → I	–30	–	–
L6[b]	G → N	41	–	–
	N → I	134	16.2	39.8
$[Y_2(\mathbf{L6})(hfac)_6]$[b]	G → SmA	40	–	–
	SmA → I	172	15.8	35.5

[a] G = glassy state, N = nematic phase, SmA = smectic A phase, I = isotropic fluid. [b] The liquid-crystalline phases were identified from their optical textures by POM and from small angle (SA) XRD studies. Temperatures are given for the onset of the peaks observed during the second heating processes.

DSC measurements confirmed these observations. Ligand **L5** transformed directly through a low-temperature glass transition into an isotropic liquid, which was then stable up to 350 °C (Table 2 and Figure S19 in the Supporting Information). For ligand **L6** and its dinuclear complex $[Y_2(\mathbf{L6})(hfac)_6]$, glass transitions (centred around 40 °C for both compounds) led to the mesophases, which were then transformed into isotropic liquid through first-order transitions at higher temperature (Figure 4, Table 2). After the first heating, during which co-crystallised molecules of water were lost (Figure S20 in the Supporting Information), these two mesomorphic compounds showed a good thermal stability (i.e., no weight loss is observed by TGA and the complex remained unchanged by POM) together with a reversible thermal behaviour over several heating/cooling cycles (5 °C min^{-1} under N_2).

Temperature-dependent SAXRD patterns were recorded for **L6** and $[Y_2(\mathbf{L6})(hfac)_6]$ in the 20–200 °C range (Figures S21–25 in the Supporting Information). In both cases, the presence of a large and diffuse signal at approximately 4.5 Å, which was associated with the liquidlike lateral ordering of the molten chains and mesogenic cores, confirmed the fluidlike nature of the mesophases. No sharp small-angle reflection could be detected for **L6**, only a broad scattering, that, along POM observation, corroborated the induction of the nematic liquid-crystalline phase. The diffractogram collected at 120 °C for $[Y_2(\mathbf{L6})(hfac)_6]$, taken as a representative example, showed two sharp small-angle reflections in the ratio 1:2, which was characteristic of 1D lamellar ordering (the reflections were indexed with the 001 and 002 Miller indices), and the position of which gave a weakly temperature-dependent periodicity of d = 105 Å. This periodicity in $[Y_2(\mathbf{L6})(hfac)_6]$ is shorter (i) than the total length of **L6** in its extended conformation (estimated to be about 130 Å; see Figure S26 in the Supporting Information) and (ii) than the periodicity previously reported for the SmA phases ($d \approx 120$ Å) produced by the related mononuclear dendritic complexes $[Ln_2(\mathbf{L9})(NO_3)_6]$ and $[Ln_2(\mathbf{L10})(NO_3)_6]$ (see Figure S26).[15i–15j]

The abnormal intensity profile displayed by the two reflections (Figures S22–S24 in the Supporting Information) with a relatively weak (001) reflection with respect to (002) involves the alternation of several high-electronic density sublayers, hence the central metallic fragment and the branching and peripheral mesogens, with low-electronic density sublayers associated with the C10 aliphatic spacers (Figure 5). The relative intensity ratio indeed depends on the respective thickness ratios of these sublayers and from the sharpness of the various interfaces (i.e., the quality of the microsegregation). A rough estimation of the volume of the rodlike yttrium complex at 120 °C, obtained by addition of partial volume $\{V_{mol} = V(\mathbf{L6}) + 2V([Y(hfac)_3]) \approx 6200 + 1800 = 8000$ Å$^2\}$,[25] gives a molecular area of $A_{mol} = V_{mol}/d = 76$ Å^2 (e.g., a value that corresponds to an area per cyanobiphenyl of 38 Å^2), which is significantly larger than the cross-section of an aliphatic chain (22.5 Å^2). Altogether, the shorter lamellar periodicity and the larger molecular area can be traced back to a considerable tilt angle of the peripheral and internal mesogens and consequently to the undulation of the layers at the mesogen–mesogen interface. A possible model for the supramolecular organisation of the complexes into a lamellar structure would consist of their lateral arrangement primarily induced by the segregation of the chelating part to form the central sublayer. On either side of that sublayer are first disposed a mixed stratum including aliphatic spacers and branching mesogen, followed by terminal cyanobiphenyls. The large surface area is compensated by large undulations of the layer, which is equivalent at the molecular level to an average important

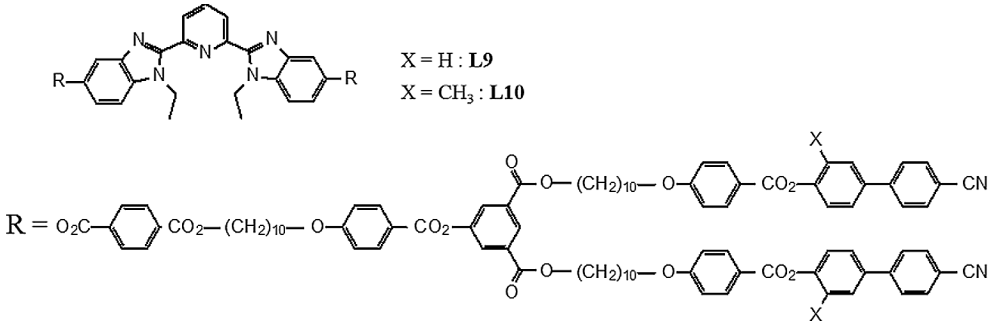

tilt angle of the mesogens to reach the 38 Å^2 target area for a terminal cyanobiphenyl.

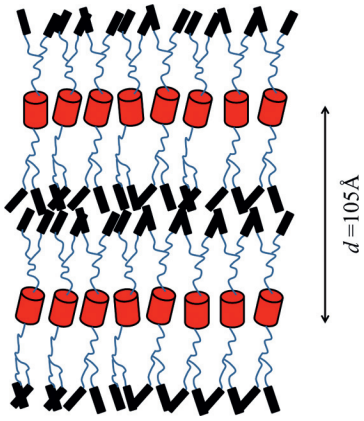

Figure 5. Proposed SmA-like organisation for $[Y_2(\mathbf{L6})(hfac)_6]$. The red cylinders are the metallic cores of the complexes, the blue lines are the dendritic spacer and the black rectangles are the terminal cyanobiphenyl mesogens.

Further insight into the organisation of the cyanobiphenyl units at the interface can be gained by monitoring the C≡N stretching vibration (ν_{CN}) during the crystal–liquid to isotropic liquid phase transitions.[26] Interestingly, ν_{CN} is particularly sensitive to changes in intermolecular CN···CN interactions that occur at the phase transitions[27] but the temperature dependence (20–200 °C) of both frequency (ν_{CN} [cm^{-1}]) and integrated intensities (I_{CN} in the 2200 to 2250 cm^{-1} range)[28] of the CN stretching band in $[Y_2(\mathbf{L6})(hfac)_6]$ during the isotropisation process shows no abrupt variation (Figures S27 and S28 in the Supporting Information) except during the first heating, in which cocrystallised water molecules are expulsed (Figures S29–32 in the Supporting Information). We conclude that, as expected from the large molecular area estimated at the interface, the terminal cyano groups are not significantly involved in the stabilisation of the SmA phase in $[Y_2(\mathbf{L6})(hfac)_6]$. On the contrary, a significant and abrupt change of ν_{CN} was measured for ligand **L6** at the N→I transition (Figures S33 and S34 in the Supporting Information). The weaker constraints in the nematic phase of **L6** make the CN groups of the ligand free enough to interact with neighbouring groups, thus contributing to the stabilisation of the mesophase.

Conclusion

The drastic decrease in stability previously reported for lipophilic d-block liquid-crystalline helicates $[Cu_2(\mathbf{L4}n)_2]^{2+}$ (n = a, b, c)[17] is strictly mirrored by f-block helicates. The special anchoring of the dendrimeric residues perpendicular to the helical axis excludes the operation of significant repulsive interstrand steric effects, and the instability of the lipophilic complexes $[Ln_2(\mathbf{L5})_3](CF_3SO_3)_6$ (Ln = La, Y, Lu) and $[Y_2(\mathbf{L6})_3](CF_3SO_3)_6$ in CD_2Cl_2/CD_3CN can be unambiguously assigned to the efficient solvation of the lipophilic receptors **L**k (k = 5, 6) in organic solvents. With this in mind, the limited stability of multistranded complexes can be exploited for the alternative selective preparation of the dinuclear single-stranded complex $[Y_2(\mathbf{L6})(hfac)_6]$ in the absence of higher-order helicates. The rigid metallic core modelled by $[Y_2(\mathbf{L1})(hfac)_6]$ (helicity index = 0.55) has a cylindrical shape with a 50–80 Å^2 cross-section and 25 Å length (Figure S36 in the Supporting Information). Its dendritic lipophilic version found in $[Y_2(\mathbf{L6})(hfac)_6]$ self-organises just above room temperature to give a SmA-type liquid-crystalline phase. To the best of our knowledge, $[Y_2(\mathbf{L6})(hfac)_6]$ is the first reported rodlike dinuclear lanthanidomesogen.

Experimental Section

General: Chemicals were purchased from Acros, Alfa Aesar and Aldrich, and used without further purification unless otherwise stated. The trifluoromethanesulfonate $[Ln(CF_3SO_3)_3]\cdot xH_2O$[29] and hexafluoroacetylacetonate $[Ln(hfac)_3(diglyme)]$[30] salts were prepared from the corresponding oxide (Aldrich, 99.99%). The Ln contents of solid salts were determined by complexometric titrations with Titriplex III (Merck) in the presence of urotropine and xylene orange.[31] Acetonitrile and dichloromethane were distilled from calcium hydride. Methanol was distilled from $Mg(OCH_3)_2$. Silica gel plates Merck 60 F254 were used for thin-layer chromatography (TLC) and Fluka silica gel 60 (0.04–0.063 mm) was used for preparative column chromatography.

Preparation of L5: Anhydrous K_2CO_3 (0.12 g, 0.87 mmol) and a catalytic amount of KI (50 mg) were added to a solution of **11** (0.10 g, 0.15 mmol) and **15** (0.24 g, 0.35 mmol) in DMF (20 mL). The reaction mixture was stirred at 60 °C for 24 h under a nitrogen atmosphere. The reaction mixture was evaporated to dryness and the resulting oily mixture was partitioned between CH_2Cl_2/half-saturated NaCl (100 mL:100 mL). The organic phase was separated, dried with anhydrous $MgSO_4$, filtered and the solvents were evaporated to dryness. The product was purified by column chromatography [silica gel (50 g), CH_2Cl_2/MeOH 100:0, 99.5:0.5, 99:1 and 98.5:1.5] and dried for 24 h under vacuum at 80 °C to yield **L5** (0.170 g, 8.68×10^{-5} mol, 60%) as a white oil that solidified after several days. ^{1}H NMR (400 MHz, $CDCl_3$): δ = 0.90 (t, ^3J = 6.8 Hz, 12 H), 1.10 (t, ^3J = 7.1 Hz, 6 H), 1.23–1.52 (m, 112 H), 1.72–1.89 (m, 16 H), 3.38 (q, ^3J = 7.1 Hz, 4 H), 3.61 (q, ^3J = 7.1 Hz, 4 H), 3.92 (t, ^3J = 6.6 Hz, 12 H), 4.12–4.12 (br., 4 H), 4.30 (s, 2 H), 4.77 (q, ^3J = 6.8 Hz, 4 H), 6.08 (s, 6 H), 7.07 (d, ^4J = 2.0 Hz, 2 H), 7.24 (d, ^3J = 8.0 Hz, 2 H), 7.37 (d, ^3J = 8.0 Hz, 2 H), 7.72 (s, 2 H), 7.89 (s, 2 H) ppm. ESI-MS (CH_2Cl_2/MeOH, 9:1): m/z = 960.5 $[M + 2H]^{2+}$, 1919.9 $[M + H]^+$. $C_{121}H_{192}N_8O_{10}$ (1918.90): calcd. C 75.61, H 9.95, N 8.39; found C 75.74, H 10.09, N 8.34.

Preparation of L6: 1-Ethyl-3-(3-dimethylaminopropyl)carbodiimide hydrochloride (EDCI·HCl; 0.033 g, 1.74×10^{-4} mol), and 4-dimethylaminopyridine (DMAP; catalytic) were added to a solution of **16** (0.145 g, 9.58×10^{-5} mol) in CH_2Cl_2 (40 mL) under an inert atmosphere. The solution was stirred at room temp. for 5 min and compound **10** (0.030 g, 4.36×10^{-5} mol) was added. The reaction mixture was heated at reflux for 12 h [the progression of the reaction was monitored by TLC (CH_2Cl_2/MeOH, 98:2)]. The reaction mixture was then diluted to 100 mL with CH_2Cl_2, washed with a half-saturated aqueous solution of NaCl (3×50 mL), dried with anhydrous Na_2SO_4, filtered and the solvents evaporated to dryness. The crude product was purified by column chromatography [silica gel (75 g), CH_2Cl_2/MeOH 100:0, 99.5:0.5, 99:1]. Finally, the product

was dissolved in CH_2Cl_2 (2 mL) and this solution was then poured into MeOH (50 mL). The precipitate was filtered using a membrane (45 μm porosity), washed with MeOH and dried under vacuum at 80 °C for 12 h to yield **L6** (0.099 g, 2.70×10^{-5} mol, 62%) as a white solid. ^{1}H NMR (400 MHz, $CDCl_3$): δ = 1.15 (t, ^3J = 7.0 Hz, 6 H), 1.31 (t, ^3J = 7.1 Hz, 6 H), 1.33–1.54 (m, 78 H), 1.75–1.88 (m, 24 H), 3.44 (q, ^3J = 7.0 Hz, 4 H), 3.64 (q, ^3J = 7.1 Hz, 4 H), 4.06 (t, ^3J = 6.5 Hz, 8 H), 4.07 (t, ^3J = 6.5 Hz, 4 H), 4.30 (s, 2 H), 4.37 (t, ^3J = 6.8 Hz, 8 H), 4.39 (t, ^3J = 6.8 Hz, 4 H), 4.81 (q, ^3J = 7.2 Hz, 4 H), 7.00 (d, ^3J = 9.1 Hz, 8 H),7.01 (t, ^3J = 9.1 Hz, 4 H), 7.26 (dd, ^3J = 8.5 Hz, ^4J = 1.5 Hz, 2 H), 7.34 (d, ^3J = 8.9 Hz, 8 H), 7.39 (d, ^3J = 8.5 Hz, 2 H), 7.58 (d, ^4J = 2.2 Hz, 2 H), 7.65 (d, ^3J = 9.1 Hz, 8 H), 7.69–7.72 (m, 10 H), 7.74–7.77 (m, 8 H), 8.08 (d, ^4J = 1.5 Hz, 4 H), 8.17 (d, ^3J = 9.1 Hz, 4 H), 8.18 (d, ^3J = 9.1 Hz, 8 H), 8.21 (d, ^3J = 8.8 Hz, 4 H), 8.28 (d, ^3J = 8.8 Hz, 4 H), 8.38 (d, ^4J = 2.2 Hz, 2 H), 8.61 (t, ^4J = 1.5 Hz, 2 H) ppm. ESI-MS (CH_2Cl_2/MeOH, 9:1): *m/z* = 3681.4 $[M + H]^+$. $C_{225}H_{232}N_{12}O_{36}$·18.01, H_2O: calcd. C 67.48, H 6.75, N 4.20; found C 67.48, H 6.75, N 4.20. The hydration was confirmed by TGA (Figure S20a in the Supporting Information).

Preparation of Complex [Y_2(L6)(hfac)$_6$]: Ligand **L6** (30 mg, 8.15×10^{-6} mol; 1 equiv.) was treated with anhydrous [Y(hfac)$_3$(diglyme)] (2.0 equiv.) in $CHCl_3$ (2 mL) at room temperature. After 1 h stirring, hexane (4 mL) was added and a white precipitate formed. The suspension was centrifuged (5000 rpm, 10 min) and the solvent was removed. This procedure was repeated twice. The white solid was dried under vacuum at 80 °C for 12 h, thereby quantitatively yielding the expected [Y_2(**L6**)(hfac)$_6$] complex (Table S1 in the Supporting Information).

Spectroscopic and Analytical Measurements: ^{1}H and ^{13}C NMR spectra were recorded at 298 K with a Bruker Avance 400 MHz spectrometer. Chemical shifts are given in ppm with respect to TMS. Pneumatically assisted electrospray (ESI-MS) mass spectra were recorded from 10^{-4} M solutions with an Applied Biosystems API 150EX LC/MS System equipped with a Turbo Ionspray source. Elemental analyses were performed by K. L. Buchwalder of the University of Geneva. The variable-temperature FTIR spectra were recorded with an IRTF Nicolet iS10 spectrometer in diffuse reflectance mode by using a high-temperature diffuse reflectance environmental chamber. The samples were diluted into a KBr matrix and the resulting mixtures that contained about 10% of compound were ground before being heated at 200 °C for a few minutes. After cooling to room temperature, the FTIR spectra were recorded in the 20–200 °C and 200–20 °C temperature ranges by using a heating or cooling rate of 2 °C min^{-1}. The spectra were recorded with a resolution of 0.4 cm^{-1}. TGA was performed with a Seiko TG/DTA 320 thermogravimetric balance (under N_2). DSC traces were obtained with a Mettler Toledo DSC1 Star Systems differential scanning calorimeter from 3 to 5 mg samples (5 °C min^{-1} under N_2). Characterisation of the mesophases was performed with a Leitz OrthoplanPol polarising microscope with a Leitz LL 20×/0.40 polarising objective and equipped with a Linkam THMS 600 variable-temperature stage. The SAXRD patterns were obtained with three different experimental setups, and in all cases the crude powder was filled in Lindemann capillaries that were 1 mm in diameter: (1) A STOE STADI P transmission powder diffractometer system using a focused monochromatic Cu-$K_{\alpha 1}$ beam obtained from a curved germanium monochromator (Johann-type) and collected on a curved image-plate position-sensitive detector. A calibration with silicon and copper laurate standards for high- and low-angle domains, respectively, was performed preliminarily. Sample capillaries were placed in the high-temperature attachment for measurements in the range of desired temperatures (from 20 to 160 °C), for which the sample temperature was controlled within 0.05 °C. (2) An image plate. The cell parameters were calculated from the position of the reflection at the smallest Bragg angle, which was in all cases the most intense. Periodicities up to 150 Å could be measured, and the sample temperature was controlled within a temperature range of 0.3 °C. The exposure times were varied from 2 to 6 h, depending on the specific reflections sought (weaker reflections clearly taking longer exposure times). (3) An SAXS system from Molecular Metrology equipped with a Cu-$K_{\alpha 1}$ Bede microsource conditioned with confocal MaxFluxTM optics and a two-dimensional multiwire gas detector. A modified temperature stage from Linkham was used to control the temperatures. The computational analysis was performed with MatLab-based open-source software from Molecular Metrology.

X-ray Crystallography: Summary of crystal data, intensity measurements and structure refinements for **10** and [Lu_2(**L1**)(hfac)$_6$] are collected in Tables S2 and S4 (in the Supporting Information). Crystals were mounted on a quartz fibre with protection oil. Cell dimensions and intensities were measured at 180 K with a Stoe IPDS diffractometer with graphite-monochromated Mo-K_α radiation (λ = 0.71073 Å) for **10** and at 180 K with a Supernova (Agilent) diffractometer using mirror-monochromated Cu-K_α radiation (λ = 1.5418 Å) for [Lu_2(**L1**)(hfac)$_6$]. Data were corrected for Lorentz and polarisation effects and for absorption. The structure was solved by direct methods (SIR97)[32] or SHELXS;[33] all other calculation were performed with SHELXL97[33] and ORTEP[34] software.

CCDC-905224 (for **10**) and -905225 (for [Lu_2(**L1**)(hfac)$_6$]) contain the supplementary crystallographic data for this paper. These data can be obtained free of charge from The Cambridge Crystallographic Data Centre via www.ccdc.cam.ac.uk/data_request/cif.

Comments on the Crystal Structure of 10: Precursory ligand **10** crystallised in a monoclinic system (space group *C*2/*c*) with one independent molecule in the asymmetric unit (Z = 8). There was one additional nitromethane solvent molecule. Atoms C17, C16 and C26 were disordered and refined over two sites with occupancy factors of 0.52/0.48, 0.61/0.39 and 0.47/0.53, respectively, and with constrained isotropic displacement parameters. The positions of hydrogen atoms were calculated and refined with restraints on bond lengths and bond angles. Intermolecular π stacking were observed (1) between planar aromatic benzimidazole rings related by an inversion centre (d = 3.615Å, shift distance = 0.863Å) and (2) between a phenyl ring and a benzimidazole ring (d = 3.67Å, angle between planes = 4.69°). There were three intermolecular π-stacking interactions per molecule (Figure S1b in the Supporting Information).

Comments on the Crystal Structure of [Lu_2(L1)(hfac)$_6$]: Crystallisation of complex [Lu_2(**L1**)(hfac)$_6$] in the triclinic $P\bar{1}$ space group gave small colourless prismatic crystals. The measured small crystal is a two nonmerohedral twin (the ratio of the twin components is 0.47:0.53). No solvate molecules were found in the structure. Some CF_3 groups of the coordinated hfac counterions were disordered (rotation about the threefold axes) and therefore displayed large anisotropic ellipsoids. The three most disordered CF_3 groups were refined by splitting each F atom on two sites with restraints on bond lengths and on bond angles. Their displacement parameters were refined isotropically and constrained to be equal. Occupancy factors were refined and converge to values of around 0.5. Hydrogen atoms were calculated and refined with restraints on bond lengths and bond angles.

Supporting Information (see footnote on the first page of this article): This includes Schemes S1 and S2, Figures S1–S36 and Tables S1–S11.

Acknowledgments

Financial support from the Swiss National Science Foundation is gratefully acknowledged. S. F. acknowledges the Centre National de la Recherche Scientifique (CNRS), the Ministère de l'Enseignement Supérieur et de la Recherche (MESR) and C'Nano Ile de France through the project ECOPOMs 2009 for financial support.

[1] a) C. Piguet, J.-C. G. Bünzli, G. Bernardinelli, G. Hopfgartner, A. F. Williams, *J. Am. Chem. Soc.* **1993**, *115*, 8197–8206; b) N. Martin, J.-C. G. Bünzli, V. McKee, C. Piguet, G. Hopfgartner, *Inorg. Chem.* **1998**, *37*, 577–589; c) S. Floquet, N. Ouali, B. Bocquet, G. Bernardinelli, D. Imbert, J.-C. G. Bünzli, G. Hopfgartner, C. Piguet, *Chem. Eur. J.* **2003**, *9*, 1860–1875; d) K. Zeckert, J. Hamacek, J.-M. Senegas, N. Dalla-Favera, S. Floquet, G. Bernardinelli, C. Piguet, *Angew. Chem.* **2005**, *117*, 8168; *Angew. Chem. Int. Ed.* **2005**, *44*, 7954–7958; e) C. Piguet, J.-C. G. Bünzli, in *Handbook on the Physics and Chemistry of Rare Earths*, Vol. 40 (Eds.: K. A. Gschneidner Jr, J.-C. G. Bünzli, V. K. Pecharsky), Elsevier Science, Amsterdam, **2009**, pp. 301–553; f) C. Lincheneau, F. Stomeo, S. Comby, T. Gunnlaugsson, *Aust. J. Chem.* **2011**, *64*, 1315–1326; g) S. Zebret, C. Besnard, G. Bernardinelli, J. Hamacek, *Eur. J. Inorg. Chem.* **2012**, 2409–2417; h) H.-F. Li, P.-F. Yan, P. Chen, Y. Wang, H. Xu, G.-M. Li, *Dalton Trans.* **2012**, *41*, 900–907.

[2] a) M. P. Oude Wolbers, F. C. J. M. van Veggel, F. G. A. Peters, E. S. E. van Beelen, J. W. Hofstraat, F. A. J. Geurts, D. N. Reinhoudt, *Chem. Eur. J.* **1998**, *4*, 772–780; b) J. Hamacek, G. Bernardinelli, Y. Filinchuk, *Eur. J. Inorg. Chem.* **2008**, 3419–3422; c) B. El Aroussi, L. Guénée, P. Pal, J. Hamacek, *Inorg. Chem.* **2011**, *50*, 8588–8597; d) J. Xu, T. M. Corneillie, E. G. Moore, G.-L. Law, N. G. Butlin, K. N. Raymond, *J. Am. Chem. Soc.* **2011**, *133*, 19900–19910; e) J. Hamacek, D. Poggiali, S. Zebret, B. El Aroussi, M. W. Schneider, M. Mastarlez, *Chem. Commun.* **2012**, *48*, 1281–1283.

[3] a) J. Xu, K. N. Raymond, *Angew. Chem.* **2000**, *112*, 2857; *Angew. Chem. Int. Ed.* **2000**, *39*, 2745–2747; b) Z. Zheng, *Chem. Commun.* **2001**, 2251–2259; c) D. Chapon, P. Delangle, C. Lebrun, *J. Chem. Soc., Dalton Trans.* **2002**, 68–74; d) S. Delagrange, C. Gateau, D. Chapon, C. Lebrun, P. Delangle, P. Vottéro, *Eur. J. Inorg. Chem.* **2002**, 2991–2998; e) D. Chapon, J.-P. Morel, P. Delangle, C. Gateau, J. Pécaut, *Dalton Trans.* **2003**, 2745–2749; f) N. Ouali, J.-P. Rivera, D. Chapon, P. Delangle, C. Piguet, *Inorg. Chem.* **2004**, *43*, 1517–1529; g) T. Kajiwara, H. Wu, T. Ito, N. Iki, S. Miyano, *Angew. Chem.* **2004**, *116*, 1868; *Angew. Chem. Int. Ed.* **2004**, *43*, 1832–1835; h) X. Yng, R. A. Jones, *J. Am. Chem. Soc.* **2005**, *127*, 7686–7687; i) O. Mamula, M. Lama, H. Stoeckli-Evans, S. Shova, *Angew. Chem.* **2006**, *118*, 5062; *Angew. Chem. Int. Ed.* **2006**, *45*, 4940–4944; j) X.-Y. Chen, Y. Bretonnière, J. Pécaut, D. Imbert, J.-C. G. Bünzli, M. Mazzanti, *Inorg. Chem.* **2007**, *46*, 625–637.

[4] M. A. Anwar, L. K. Thompson, L. N. Dave, F. Habib, M. Murugesu, *Chem. Commun.* **2012**, *48*, 4576–4578.

[5] a) D.-J. Qian, K.-Z. Yang, H. Nakahara, K. Fukuda, *Langmuir* **1997**, *13*, 5925–5932; b) K. Binnemans, C. Görller-Walrand, *Chem. Rev.* **2002**, *102*, 2303–2346; c) C. Piguet, J.-C. G. Bünzli, B. Donnio, D. Guillon, *Chem. Commun.* **2006**, 3755–3768; d) M. Burnworth, D. Knapton, S. J. Rowan, C. Weder, *J. Inorg. Organomet. Polym. Mater.* **2007**, *17*, 91–103; e) B. Donnio, S. Buathong, I. Bury, D. Guillon, *Chem. Soc. Rev.* **2007**, *36*, 1495–1513; f) K. Binnemans, *J. Mater. Chem.* **2009**, *19*, 448–453; g) K. Binnemans, *Chem. Rev.* **2009**, *109*, 4283–4374; h) B. M. McKenzie, R. J. Wojtecki, K. A. Burke, C. Zhang, A. Jakli, P. T. Mather, S. J. Rowan, *Chem. Mater.* **2011**, *23*, 3525–3533.

[6] R. L. Carrol, C. B. Gorman, *Angew. Chem. Int. Ed.* **2002**, *41*, 4379–4400.

[7] a) A. M. Giroud-Godquin, P. M. Maitlis, *Angew. Chem.* **1991**, *103*, 370; *Angew. Chem. Int. Ed. Engl.* **1991**, *30*, 375–402; b) D. W. Bruce, *J. Chem. Soc., Dalton Trans.* **1993**, 2983–2989; c) S. A. Hudson, P. M. Maitlis, *Chem. Rev.* **1993**, *93*, 861–885; d) J. L. Serrano, *Metallomesogens, Synthesis Properties and Applications*, VCH, Weinheim, Germany, **1996**; e) P. Espinet, M. A. Esteruelas, L. A. Oro, J.-L. Serrano, E. Sola, *Coord. Chem. Rev.* **1992**, *117*, 215–274; f) B. Donnio, D. W. Bruce, *Struct. Bonding (Berlin)* **1999**, *95*, 194–247; g) B. Donnio, D. Guillon, R. Deschenaux, D. W. Bruce, in *Comprehensive Coordination Chemistry* (Eds.: J. A. McCleverty, T. J. Meyer), Elsevier, Oxford, U.K. **2003**, vol. 7, chapter 79.

[8] K. Binnemans, in: *Handbook on the Physics and Chemistry of Rare Earths*, vol. 43 (Eds.: J.-C. G. Bünzli, V. K. Pecharsky), Elsevier BV, Burlington, **2013**, chapter 254, p. 1–158.

[9] *Handbook of Liquid Crystals* (Eds.: D. Demus, J. W. Goodby, G. W. Gray, H.-W. Spiess, V. Vill), Wiley-VCH, Weinheim, Germany, **1998**.

[10] A. Skoulios, D. Guillon, *Mol. Cryst. Liq. Cryst.* **1988**, *165*, 317–332.

[11] K. J. Toyne, *Thermotropic Liquid Crystals* (Ed.: G. W. Gray), Critical Reports on Applied Chemistry, Wiley, Chichester, UK, **1987**, vol. 22, pp. 28–63.

[12] R. W. Date, E. Fernandez Iglesias, K. E. Rowe, J. M. Elliott, D. W. Bruce, *Dalton Trans.* **2003**, 1914–1931.

[13] a) F. Neve, M. Ghedini, G. De Munno, A. M. Levelut, *Chem. Mater.* **1995**, *7*, 688–693; b) L. Douce, A. El-ghayouri, A. Skoulios, R. Ziessel, *Chem. Commun.* **1999**, 2033–2034; c) R. Gimenez, A. B. Manrique, S. Uriel, J. Barbera, J. L. Serrano, *Chem. Commun.* **2004**, 2064–2065; d) E. Cavero, S. Uriel, P. Romero, J. L. Serrano, R. Gimenez, *J. Am. Chem. Soc.* **2007**, *129*, 11608–11618; e) R. Ziessel, G. Pickaert, F. Camerel, B. Donnio, D. Guillon, M. Cesario, T. Prange, *J. Am. Chem. Soc.* **2004**, *126*, 12403–12413; f) E. D. Baranoff, J. Voignier, T. Yasuda, V. Heitz, J.-P. Sauvage, T. Kato, *Angew. Chem.* **2007**, *119*, 4764; *Angew. Chem. Int. Ed.* **2007**, *46*, 4680–4683; g) D. Pucci, I. Aiello, A. Bellusci, A. Crispini, M. Ghedini, M. La Deda, *Eur. J. Inorg. Chem.* **2009**, 4274–4281.

[14] a) G. Lattermann, S. Schmidt, R. Kleppinger, J. H. Wendorf, *Adv. Mater.* **1992**, *4*, 30–33; b) S. Schmidt, G. Lattermann, R. Kleppinger, J. H. Wendorff, *Liq. Cryst.* **1994**, *16*, 693–702; c) H. Zheng, T. M. Swager, *J. Am. Chem. Soc.* **1994**, *116*, 761–762; d) X.-H. Liu, M. N. Abser, D. W. Bruce, *J. Organomet. Chem.* **1998**, *551*, 271–280; e) G. H. Walf, R. Benda, F. J. Litterst, U. Stebani, S. Schmidt, G. Lattermann, *Chem. Eur. J.* **1998**, *4*, 93–99; f) K. E. Rowe, D. W. Bruce, *J. Chem. Soc., Dalton Trans.* **1996**, 3913–3915; g) S. Morrone, D. Guillon, D. W. Bruce, *Inorg. Chem.* **1996**, *35*, 7041–7048; h) F. Camerel, R. Ziessel, B. Donnio, D. Guillon, *New J. Chem.* **2006**, *30*, 135–139; i) A. M. Prokhorov, A. Santoro, J. A. G. Williams, D. W. Bruce, *Angew. Chem.* **2012**, *124*, 99; *Angew. Chem. Int. Ed.* **2012**, *51*, 95–98; j) Y. Galyametdinov, V. Ksenofontov, A. Prosvirin, I. Ovchinnikov, G. Ivanova, P. Gütlich, W. Haase, *Angew. Chem.* **2001**, *113*, 4399; *Angew. Chem. Int. Ed.* **2001**, *40*, 4269–4271; k) F. Camerel, J. Barberá, J. Otsuki, T. Tokimoto, Y. Shimazaki, L.-Y. Chen, S.-H. Liu, M.-S. Lin, C.-C. Wu, R. Ziessel, *Adv. Mater.* **2008**, *20*, 3462–3467; l) T. Cardinaels, J. Ramaekers, K. Driesen, P. Nockemann, K. Van Hecke, L. Van Meervelt, B. Goderis, K. Binnemans, *Inorg. Chem.* **2009**, *48*, 2490–2499; m) S. Frein, M. Auzias, A. Sondenecker, L. Vieille-Petit, B. Guintchin, N. Maringa, G. Süss-Fink, J. Barbera, R. Deschenaux, *Chem. Mater.* **2008**, *20*, 1340–1343; n) E. Terazzi, C. Bourgogne, R. Welter, J.-L. Gallani, D. Guillon, G. Rogez, B. Donnio, *Angew. Chem.* **2008**, *120*, 500; *Angew. Chem. Int. Ed.* **2008**, *47*, 490–495.

[15] a) E. Terazzi, S. Torelli, G. Bernardinelli, J.-P. Rivera, J.-M. Bénech, C. Bourgogne, B. Donnio, D. Guillon, D. Imbert, J.-C. G. Bünzli, A. Pinto, D. Jeannerat, C. Piguet, *J. Am. Chem.*

Soc. **2005**, *127*, 888–903; b) K. Binnemans, K. Lodewyckx, B. Donnio, D. Guillon, *Eur. J. Inorg. Chem.* **2005**, 1506–1513; c) H. Nozary, S. Torelli, L. Guénée, E. Terazzi, G. Bernardinelli, B. Donnio, D. Guillon, C. Piguet, *Inorg. Chem.* **2006**, *45*, 2989–3003; d) K. Binnemans, K. Lodewyckx, T. Cardinaels, T. N. Parac-Vogt, C. Bourgogne, D. Guillon, B. Donnio, *Eur. J. Inorg. Chem.* **2006**, 150–157; e) Y. Yang, K. Driesen, P. Nockemann, K. Van Hecke, L. Van Meervelt, K. Binnemans, *Chem. Mater.* **2006**, *18*, 3698–3704; f) E. Terazzi, L. Guénée, P.-Y. Morgantini, G. Bernardinelli, B. Donnio, D. Guillon, C. Piguet, *Chem. Eur. J.* **2007**, *13*, 1674–1691; g) A. Escande, L. Guénée, H. Nozary, G. Bernardinelli, F. Gumy, A. Aebischer, J.-C. G. Bünzli, B. Donnio, D. Guillon, C. Piguet, *Chem. Eur. J.* **2007**, *13*, 8696–8713; h) T. Cardinaels, K. Driesen, T. N. Parac-Vogt, B. Heinrich, C. Bourgogne, D. Guillon, B. Donnio, K. Binnemans, *Chem. Mater.* **2005**, *17*, 6589–6598; i) E. Terazzi, B. Bocquet, S. Campidelli, B. Donnio, D. Guillon, R. Deschenaux, C. Piguet, *Chem. Commun.* **2006**, 2922–2924; j) T. B. Jensen, E. Terazzi, B. Donnio, D. Guillon, C. Piguet, *Chem. Commun.* **2008**, 181–183; k) A. A. Knyazev, Y. G. Galyametdinov, B. Goderis, K. Driesen, K. Goossens, C. Görller-Walrand, K. Binnemans, T. Cardinaels, *Eur. J. Inorg. Chem.* **2008**, 756–761; l) T. B. Jensen, E. Terazzi, K.-L. Buchwalder, L. Guénée, H. Nozary, K. Schenk, B. Heinrich, B. Donnio, D. Guillon, C. Piguet, *Inorg. Chem.* **2010**, *49*, 8601–8619.

[16] B. Dardel, D. Guillon, B. Heinrich, R. Deschenaux, *J. Mater. Chem.* **2001**, *11*, 2814–2831.

[17] a) A. El-ghayoury, L. Douce, A. Skoulios, R. Ziessel, *Angew. Chem.* **1998**, *110*, 2327; *Angew. Chem. Int. Ed.* **1998**, *37*, 2205–2208; b) R. Ziessel, L. Douce, A. El-ghayoury, A. Harriman, A. Skoulios, *Angew. Chem.* **2000**, *112*, 1549; *Angew. Chem. Int. Ed.* **2000**, *39*, 1489–1493.

[18] K. Zeckert, J. Hamacek, J.-P. Rivera, S. Floquet, A. Pinto, M. Borkovec, C. Piguet, *J. Am. Chem. Soc.* **2004**, *126*, 11589–11601.

[19] a) C. Piguet, G. Bernardinalli, G. Hopfgartner, *Chem. Rev.* **1997**, *97*, 2005–2062; b) M. Albrecht, *Chem. Rev.* **2001**, *101*, 3457–3497.

[20] A. Zaïm, H. Nozary, L. Guénée, C. Besnard, J.-F. Lemonnier, S. Petoud, C. Piguet, *Chem. Eur. J.* **2012**, *18*, 7155–7168.

[21] a) A. Escande, L. Guénée, K.-L. Buchwalder, C. Piguet, *Inorg. Chem.* **2009**, *48*, 1132–1147; b) I. D. Brown, D. Altermatt, *Acta Crystallogr., Sect. B* **1985**, *41*, 244–247; c) N. E. Breese, M. O'Keeffe, *Acta Crystallogr., Sect. B* **1991**, *47*, 192–197; d) I. D. Brown, *Acta Crystallogr., Sect. B* **1992**, *48*, 553–572; e) I. D. Brown, *The Chemical Bond in Inorganic Chemistry*, Oxford University Press, UK, **2002**; f) I. D. Brown, *Chem. Rev.* **2009**, *109*, 6858–6919; g) A. Trzesowska, R. Kruszynski, T. J. Bartczak, *Acta Crystallogr., Sect. B* **2004**, *60*, 174–178; h) A. Trzesowska, R. Kruszynski, T. J. Bartczak, *Acta Crystallogr., Sect. B* **2005**, *61*, 429–434; i) F. J. Zocchi, *Mol. Struct. A* **2007**, *805*, 73–78.

[22] $H = 6\sqrt{3}\pi\frac{LA}{D^3}$ with L = 4.06 Å is the end-to-end distance of the helix taken as the C15···C27 contact distance. A = 0.80 Å^2 is the area of the quadrangle produced by the projection of the five atoms of the diphenylmethane spacer onto a plane perpendicular to the main helical axis defined as the line passing through the two terminal atoms of the chain. Finally, D = 5.78 Å is the length of the crooked line: J. H. Brewster, *Top. Curr. Chem.* **1974**, *46*, 29–71.

[23] N. Dalla Favera, L. Guénée, G. Bernardinelli, C. Piguet, *Dalton Trans.* **2009**, 7625–7638.

[24] *HypNMR-2008 software*: a) C. Frassineti, S. Ghelli, P. Gans, A. Sabatini, M. S. Moruzzi, A. Vacca, *Anal. Biochem.* **1995**, *231*, 374–382; b) C. Frassineti, L. Alderighi, P. Gans, A. Sabatini, A. Vacca, S. Ghelli, *Anal. Bioanal. Chem.* **2003**, *376*, 1041–1052.

[25] The volume of [Y(hfac)$_3$] was estimated from that of [Y(acac)$_3$], see: J. A. Cunningham, D. E. Sands, W. F. Wagner, *Inorg. Chem.* **1967**, *6*, 499–503.

[26] K. Hori, M. Kuribayashi, M. Iimuro, *Phys. Chem. Chem. Phys.* **2000**, *2*, 2863–2868, and references cited therein.

[27] P. A. Wood, S. J. Borwick, D. J. Watkin, W. D. S. Motherwell, F. H. Allen, *Acta Crystallogr., Sect. B* **2008**, *64*, 393–396.

[28] D. Steele, in: *Handbook of Vibrational Spectroscopy*, vol. 1 (Eds.: J. M. Chalmers, P. R. Griffiths), Wiley, Chichester, UK, **2002**, chapter 3.

[29] J. F. Desreux, in: *Lanthanide Probes in Life, Chemical and Earth Sciences* (Eds.: J.-C. G. Bünzli, G. R. Choppin), Elsevier, Amsterdam, **1989**, chapter 2, p. 43.

[30] a) W. J. Evans, D. G. Giarikos, M. A. Johnston, M. A. Greci, J. W. Ziller, *J. Chem. Soc., Dalton Trans.* **2002**, 520–526; b) G. Malandrino, R. Lo Nigro, I. L. Fragala, C. Benelli, *Eur. J. Inorg. Chem.* **2004**, 500–509.

[31] G. Schwarzenbach, *Complexometric Titrations*, Chapman & Hall, London, **1957**, p. 8.

[32] A. Altomare, M. C. Burla, M. Camalli, G. Cascarano, C. Giacovazzo, A. Guagliardi, G. Moliterni, G. Polidori, R. Spagna, *J. Appl. Crystallogr.* **1999**, *32*, 115–119.

[33] SHELXL97, G. M. Sheldrick, *Acta Crystallogr. A* **2008**, *A64*, 112–122.

[34] *ORTEP-III for Windows*, J. L. Farrugia, *J. Appl. Crystallogr.* **1997**, *30*, 565.

Received: February 4, 2013
Published Online: April 22, 2013

Implementing Liquid Crystalline Properties in Single-Stranded Dinuclear Lanthanide Helicates

---

Emmanuel Terazzi,*[a] Amir Zaïm,[a] Bernard Bocquet,[a] Johan Varin,[a] Laure Guénée,[b] Thibault Dutronc,[a] Jean-François Lemonnier,[a] Sébastien Floquet,[c] Emmanuel Cadot,[c] Benoît Heinrich,[d] Bertrand Donnio,[d] Claude Piguet,*[a]

[a] Dr E. Terazzi, A. Zaïm, , B. Bocquet, J. Varin, T. Dutronc, Dr J.-F. Lemonnier, Prof. Dr C. Piguet. Department of Inorganic and Analytical Chemistry, University of Geneva, 30 quai E. Ansermet, CH-1211 Geneva 4, Switzerland.

[b] Dr L. Guénée. Laboratory of Crystallography, University of Geneva, 24 quai E. Ansermet, CH-1211 Geneva 4, Switzerland.

[c] Dr S. Floquet, Dr E. Cadot. Institut Lavoisier de Versailles, UMR 8180, University of Versailles Saint-Quentin, 45 av. des Etats-Unis, 78035 Versailles, France.

[d] Dr B. Donnio, Dr B. Heinrich. Institut de Physique et Chimie des Matériaux de Strasbourg (IPCMS), UMR 7504 (CNRS-Université de Strasbourg), 23 rue du Loes, BP43, 67034 Strasbourg cedex 2, France.

E-mail: Emmanuel.Terazzi@unige.ch, Claude.Piguet@unige.ch

Supporting Information

(44 pages)

Appendix 1: Preparation and characterization of intermediates **11** and **15**

Synthesis of intermediates 11 and 15

The key intermediate **11** was synthesized in eleven steps starting from diethyloxalate and ortho-nitrochlorobenzene (Scheme S1).[1]-[4] The dicatenar compound **15** was obtained in four steps through the mono-acylation of phloroglucinol,[5] followed by Williamson etherification, hydrolysis and Mitsunobu reaction (Scheme S2).

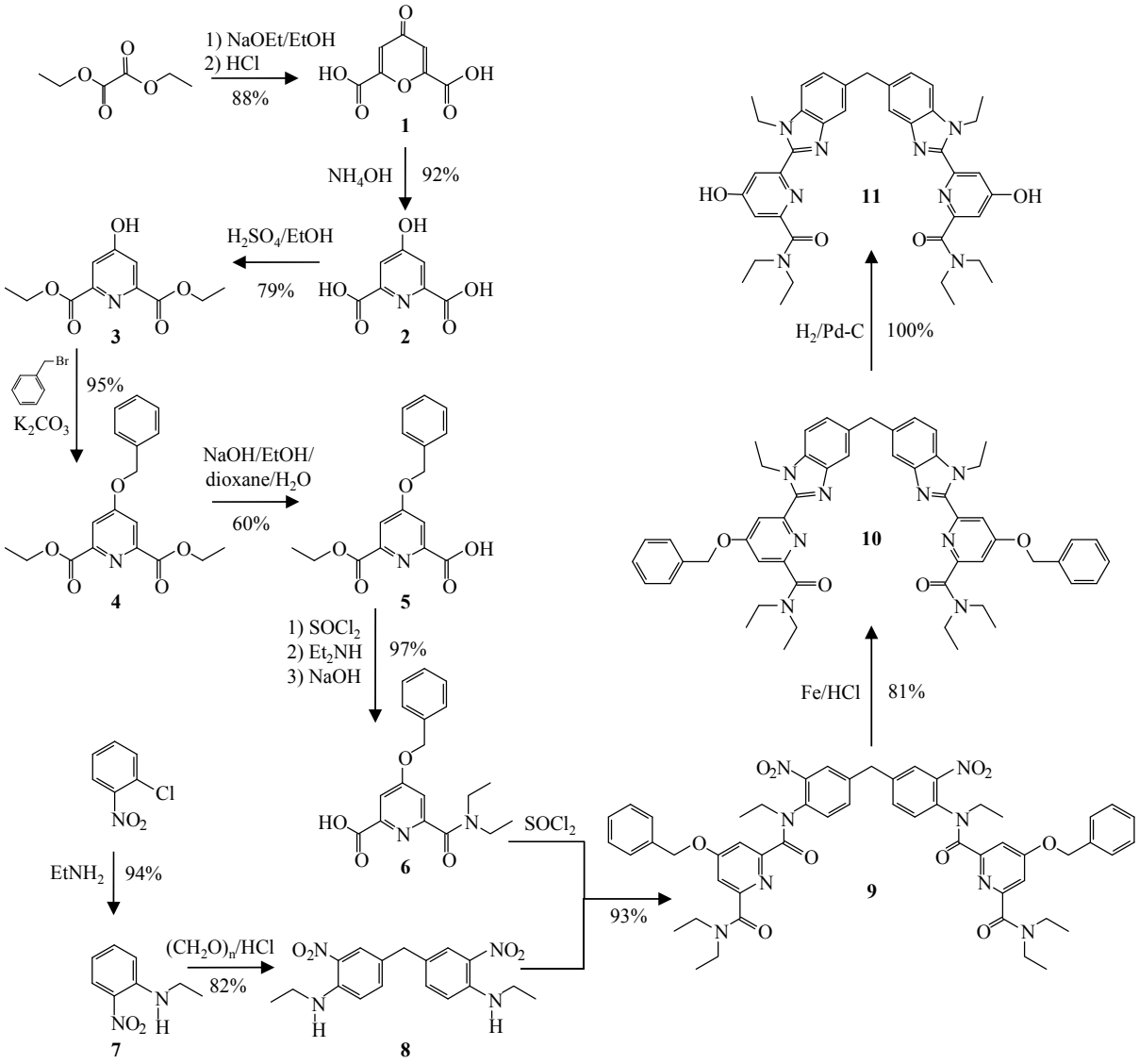

Scheme S1 Synthesis of the precursor **11**.

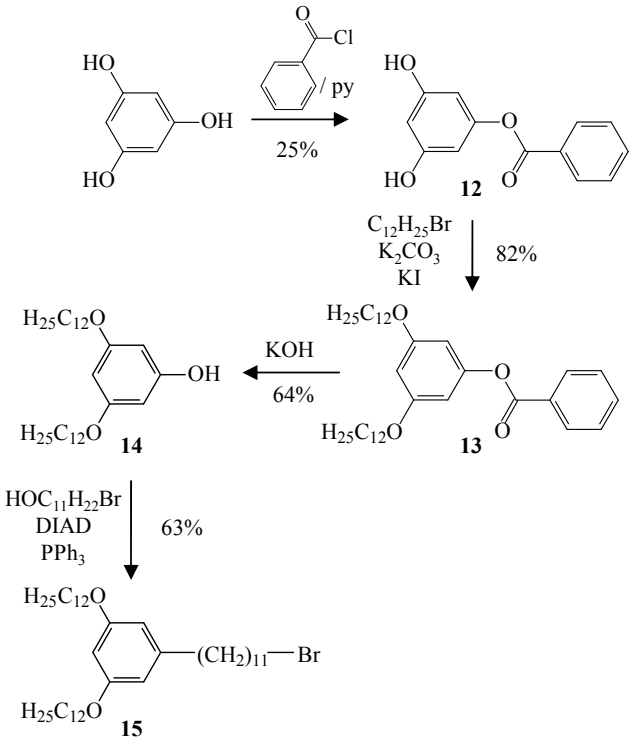

Scheme S2 Synthesis of the dicatenar **15**.

Preparation of chelidonic acid (1).[1] Sodium (23.5 g, 1.02 mol) was dissolved in 360 mL of dry ethanol. A mixture of 29.0 g (38 mL, 0.5 mol) of dry acetone and 155.0 g (144 mL, 1.06 mol) of diethyloxalate were added in 15 min.. During the addition, a yellow precipitate was formed. The reaction mixture was kept at 60°C for one hour to complete the reaction. Then, 200 ml of 37% aqueous HCl and 100 mL of water were added, ant the solution was stirred at 50°C for one day. About 450 mL of aqueous ethanol was removed under reduced pressure. 300 mL of water and 50 ml of 37% aqueous HCl were then added to this mixture and stirring was continued until a silica gel TLC (eluent : 3/7 (v/v) 10% aqueous NaCl/ethanol) showed only one spot (R_f = 0.65) for **1** (about three days). After cooling down, the precipitated crystals were filtered off, washed first with water then with cold acetone. The crude product was recrystallized from boiling water (2.5 L) using charcoal to give 81.0 g (88%) of pure **1** as a white microcrystalline powder. ^{1}H NMR (400 MHz, D_2O): δ=7.04 (s, 2H); ESIMS (DMSO): *m/z*: 185.1 $[M+H]^+$, 207.1 $[M+Na]^+$.

Preparation of chelidamic acid (2).[1] To compound **1** (50.0 g , 248 mmol) was dropwise added 500 mL of 25% aqueous NH_3 solution at 0°C. The resulting white suspension was stirred at room temperature for two days (after five hours, the suspension became orange). Excess of aqueous ammonia solution was removed under reduced pressure and the residue was boiled with 500 mL of water using 10 g of charcoal and filtered. The cold solution was acidified with 37% aqueous HCl to about pH = 1. The white crystals were filtered off, washed three times with ice-cold water and dried under vacuum at 150°C for 24 hours to give 49.9 g (92%) of **2**. R_f = 0.35 (silica gel TLC, 3/7 (v/v) 10% aqueous NaCl/ethanol). ^{1}H NMR (400 MHz, D_2O): δ=7.11 (s, 2H); ESIMS (DMSO): *m/z*: 184.1 $[M+H]^+$, 206.1 $[M+Na]^+$, 367.2 $[2M+H]^+$.

Preparation of 3.[2] Concentrated sulphuric acid (15 ml) was added was added to compound **2** (7.0 g, 38.23 mmol) in ethanol (200 mL). The solution was heated at reflux for 4 hours and slowly neutralized with a saturated aqueous solution of $NaHCO_3$ (pH = 7). Ethanol was evaporated, and the residual aqueous solution was extracted with CH_2Cl_2 (6 x 100 ml). PH was stepwise adjusted to pH=3 between each extractions with HCl 1M (i.e. 6, 5, 4 and then 3). The combined organic layers were dried over anhydrous $MgSO_4$, filtered, evaporated to dryness and dried under vacuum at 80°C for 24 h to provide 7.21 g (79%) of **3** as a solid. This compound was crystallized from hot hexane/ethanol 9:1 mixture to provide white crystals. ^{1}H NMR (400 MHz, $CDCl_3$): δ=1.43 (t, ^3J= 7.2 Hz, 6H), 4.48 (q, ^3J= 7.2 Hz, 4H), 7.38 (s, 2H); ESIMS (CH_2Cl_2/MeOH 9:1): *m/z*: 240.2 $[M+H]^+$, 479.5 $[2M+H]^+$.

Preparation of 4.[1] Benzyl bromide, (1.29 g , 7.52 mmol) and anhydrous K_2CO_3 (1.30 g, 9.41 mmol) were added to compound **3** (1.50 g , 6.27 mmol) dissolved in 15 mL of DMF. The suspension was heated at 60°C for one day, then evaporated to dryness. The crude mixture was partitioned between CH_2Cl_2/H_2O 1:1 (100 mL). The aqueous phase was extracted with CH_2Cl_2 (3 x 50 mL). The combined organic phases were dried over anhydrous $MgSO_4$, filtered and evaporated to dryness. The resulting pale yellow oil was triturated and sonicated in 50 mL hexane until a white

precipitate formed. The precipitate was filtered, washed with cold hexane and dried under vacuum. Finally, the crude product was filtered over silica gel (CH_2Cl_2/EtOH 100:0; 99:1; 98.5:1.5; 98:2) and dried under vacuum at 80°C for 24 h, to give 1.96 g (95%) of **4** as a white crystalline powder. ^{1}H NMR (400 MHz, $CDCl_3$): δ=1.44 (t, ^3J= 7.2 Hz, 6H), 4.46 (t, ^3J= 7.2 Hz, 4H); 5.21(s, 2H), 7.34-7.45 (m, 5H), 7.86 (s, 2H); ESIMS (CH_2Cl_2/MeOH 9:1): *m/z*: 330.4 $[M+H]^+$, 352.4 $[M+Na]^+$, 659.7 $[2M+H]^+$, 676.7 $[2M+NH_4]^+$.

Preparation of 5. 0.87 g (21.7 mmol) of NaOH in 4.0 mL H_2O was added to intermediate **4** (7.24 g, 22.0 mmol) dissolved in 360 mL of EtOH/dioxane 1:1. After 30 min the reaction was over(TLC, CH_2Cl_2/MeOH 80:20). The pH of the reaction was found to be 5, and the solution was acidified with an excess of glacial acetic acid (20 mL). The reaction mixture was poured into 1.2 L of water with the formation of a transcient white precipitate. CH_2Cl_2 (600 mL) were added and the biphasic mixture was stirred until the complete dissolution of the precipitate (about 15 min). Sometimes, a larger excess of glacial acetic acid is needed to completely dissolve the precipitate. The layers were separated and the aqueous phase was extracted with CH_2Cl_2 (3 x 200 mL). The combined organic phases were dried over anhydrous $MgSO_4$, filtered and evaporated to dryness. The colourless oil was dissolved in 50 mL of CH_2Cl_2/Et_2O 1:1 and evaporated. This last operation was repeated until a white powder was obtained. The white solid (6.47 g) was dried under vacuum for 24 h, to provide a mixture of **4** and **5** (TLC CH_2Cl_2/MeOH 80:20 R_f(**4**) = 0.9 and R_f(**5**) = 0.6 for a concentrated spot). Intermediate **5** was purified by column chromatography (silica gel (100 g), CH_2Cl_2/EtOH 100:0; 99.7:0.3 and then 99.5:0.5) to give 3.98 g (13.2 mmol, yield: 60%) of **5** as a white crystalline solid. ^{1}H NMR of **5** (400 MHz, [D_6]DMSO): δ=1.35 (t, ^3J=7.2 Hz, 3H), 4.37 (q, ^3J=7.2 Hz, 2H), 5.37 (s, 2H), 7.34-7.52 (m, 5H), 7.79-7.81 (m, 2H); ^{13}C NMR (100 MHz, [D_6]DMSO): δ=14.58 (C_{prim}); 62.03, 70.58 (C_{sec}); 114.58, 114.71, 128.37, 128.75, 129.04 (C_{tert}); 136.05, 150.00, 151.10, 164.68, 166.04, 166.58 (C_{quat}); ESIMS of **5** (CH_2Cl_2/EtOH 9:1): *m/z*: 601.6 $[2M-H]^-$.

Preparation of 6. $SOCl_2$ (11.18 g, 94.0 mmol) and a catalytic amount of DMF (50 µL) were added to compound **5** (2.83 g, 9.4 mmol in dry CH_2Cl_2 (50 mL). The reaction mixture was refluxed for 1 hour under N_2. The resulting solution was evaporated to dryness and the solid residue was dried under vacuum at 80°C for 1 h. This activated intermediate was dissolved in dry CH_2Cl_2 (50 mL) and a large excess of diethylamine (6.87 g, 94.0 mmol) was added. The reaction mixture was refluxed for 1 h. , then stirred at r.t. for 12 h under N_2. The pale brown reaction mixture was diluted with 100 mL CH_2Cl_2, and washed with a solution of half-saturated NaCl in water (3 x 50 mL). The CH_2Cl_2 phase was dried over anhydrous $MgSO_4$, filtered and evaporated to dryness. The resulting brown oil was dissolved in EtOH/H_2O 1:1 (200 mL) and NaOH (5.0 g, 105.0 mmol) in water (4 mL) were added. The reaction mixture was stirred at r.t. for 30 min and the pH was adjusted to 2 with 37% HCl. The reaction mixture was evaporated until **6** precipitated. After about 12 h at 4°C, the crystals were filtered, washed with cold water (100 mL) and dried under vacuum for 12 h at 80°C to give 2.99 g (9.10 mmol, yield: 97%) of **6** as a white solid. In case of contamination, compound **6** can be purified by column chromatography (silica gel (100 g), CH_2Cl_2/EtOH 100:0 and then 98:2). ^{1}H NMR of **6** (400 MHz, [D_6]DMSO): δ=1.08 (t, ^3J=7.0 Hz, 3H), δ=1.17 (t, ^3J=7.0 Hz, 3H), 3.20 (q, ^3J=7.0 Hz, 2H), 3.44 (q, ^3J=7.0 Hz, 2H), 5.32 (s, 2H), 7.33-7.51 (m, 6H), 7.65 (d, ^4J=2.4 Hz, 1H); ^{13}C NMR (100 MHz, [D_6]DMSO): δ=13.22, 14.44 (C_{prim}); 39.85, 43.19, 70.40 (C_{sec}); 111.93, 112.63, 128.35, 128.68, 129.02 (C_{tert}); 136.18, 149.63, 156.97, 166.20, 166.38, 167.40 (C_{quat}); ESIMS of **6** (CH_2Cl_2/MeOH 9:1): *m/z*: 329.4 $[M+H]^+$, 657.7 $[2M+H]^+$, 986.1 $[3M+H]^+$.

Preparation of 9. The reaction was carried out under nitrogen atmosphere. $SOCl_2$ (4.35 g, 36.50 mmol) and a catalytic amount of DMF (50 µL) were added to **6** (1.20 g, 3.65 mmol) dissolved in dry CH_2Cl_2 (60 mL). The reaction mixture was refluxed for 1 h. The resulting solution was evaporated to dryness and the white solid residue was dried under vacuum at 80°C for 1 h. This activated intermediate was dissolved in dry CH_2Cl_2 (60 mL) and **8** (0.50 g, 1.46 mmol) was added

as a solid. The solution was refluxed for 24 h., whereby neither starting material nor mono-substituted intermediate remained (TLC: CH_2Cl_2/MeOH 98:2). The pH of the reaction was adjusted to 7 by addition of *N*,*N*'-diisopropylethylamine, and the reaction mixture was evaporated and dried under vacuum. The yellow solid was purified by column chromatography (silica gel (100 g), CH_2Cl_2/MeOH 100:0; 99.5:0.5; 99.2:0.8; and then 99:1) to give 1.30 g (1.35 mmol, yield: 93%) of **9** as a yellow voluminous solid. ESIMS (CH_2Cl_2/MeOH 9:1): *m/z*: 966.1 $[M+H]^+$.

Preparation of 10. Compound **9** (1.20 g, 1.24 mmol) was dissolved in a EtOH/H_2O solvent mixture (505/125 mL) and activated iron powder (2.08 g, 37.30 mmol) was added. The reaction mixture was heated to 90°C and HCl 37 % was slowly added until the reaction started to bubble (10 mL). The colorless reaction mixture was then refluxed for 24 h under an N_2 atmosphere. The progression of the reaction was followed by TLC (TLC: CH_2Cl_2/MeOH 90:10). After completion of the reaction, the pale pink solution was filtered in order to remove the excess of metallic iron. The EtOH was evaporated and a yellow precipitate formed. H_2O (200 mL) and CH_2Cl_2 (300 ml) were added leading to a limpid biphasic solution. A solution of Na_4EDTA (40 g) in H_2O (150 mL) was added and the pH adjusted to 8.0-8.5 with an aqueous NH_4OH 25% solution. H_2O_2 (4 mL) was slowly added and the pH was checked in order to remain constant during the addition. The biphasic solution was stirred for 30 minutes and the organic layer was separated. The aqueous dark red phase was further extracted with CH_2Cl_2 (3 x 200 mL). The combined organic layers were dried over anhydrous $MgSO_4$, filtered and evaporated to dryness. The pale yellow solid was purified by column chromatography (silica gel (100 g), CH_2Cl_2/MeOH 100:0; 99:1; 98.5:1.5 and 98:2 at the end of the column) to yield 0.87 g (1.00 mmol, yield: 81%) of **10** as a white solid. ^{1}H NMR (400 MHz, $CDCl_3$): δ=1.07 (t, ^3J=7.2 Hz, 6H), 1.29 (t, ^3J=7.1 Hz, 6H), 1.46 (t, ^3J=7.1 Hz, 6H), 3.37 (q, ^3J=7.1 Hz, 4H), 3.61 (q, ^3J=7.1 Hz, 4H), 4.31 (s, 2H), 4.77 (q, ^3J=7.2 Hz, 4H), 5.27 (s, 4H), 7.14 (d, ^4J=2.4 Hz, 2H), 7.26 (dd, ^3J=8.5 Hz, ^4J=1.3 Hz, 2H), 7.34-7.49 (m, 12H), 7.73 (s, 2H), 8.02 (d, ^4J=2.4 Hz, 2H); ^{13}C NMR (100 MHz, $CDCl_3$): δ=12.79, 14.28, 15.38 (C_{prim}); 39.48, 40.59, 42.23,

42.77, 70.32 (C_{sec}); 110.05, 110.24, 110.60, 119.97, 124.98, 127.59, 128.43, 128.74 (C_{tert}); 134.86, 135.37, 136.51, 142.92, 149.42, 151.36, 156.05, 166.17, 168.42 (C_{quat}); ESIMS (CH_2Cl_2/MeOH 9:1): *m/z*: 870.1 $[M+H]^+$, 1739.2 $[2M+H]^+$.

Preparation of 11. Pd/C 10% (50 mg) dispersed in MeOH (10 mL) were added to ligand **10** (0.25 g, 0.29 mmol) in CH_2Cl_2 (20 mL). The reaction mixture was stirred for 6 h. at r.t. under an hydrogen atmosphere (1 atm.). The progression of the reaction was monitored by TLC (CH_2Cl_2/MeOH 90:10). The reaction mixture was filtered through a filter paper, then through a membrane (45 μm porosity), evaporated, and dried under vacuum at 80°C for 12 h. to yield 0.20 g (0.29 mmol, yield: 100%) of **11** as a white solid. ^{1}H NMR (400 MHz, $CDCl_3$): δ=1.06 (t, ^3J=7.0 Hz, 6H), 1.25 (t, ^3J=7.2 Hz, 6H), 1.39 (t, ^3J=7.0 Hz, 6H), 3.33 (q, ^3J=7.0 Hz, 4H), 3.57 (q, ^3J=7.0 Hz, 4H), 4.20 (s, 2H), 4.59 (q, ^3J=7.2 Hz, 4H), 7.04 (s, 2H), 7.23 (d, ^3J=8.3 Hz, 2H), 7.31 (d, ^3J=8.3 Hz, 2H), 7.56 (s, 2H), 7.85 (s, 2H); ESIMS (CH_2Cl_2/MeOH 9:1): *m/z*: 689.8 $[M+H]^+$, 1378.7 $[2M+H]^+$, 2067.5 $[3M+H]^+$. The ^{13}C NMR spectrum was not registered for solubility reasons.

Preparation of 13. A mixture containing **12** (2.82 g, 12.20 mmol), anhydrous K_2CO_3 (10.12 g, 73.20 mmol) and a catalytic amount of KI (50 mg) in acetone (200 mL) was refluxed, and a solution of 1-bromododecane (9.12 g, 36.60 mmol) was then added. The reaction mixture was refluxed for 4 days and evaporated to dryness. The resulting mixture was partitioned between CH_2Cl_2/H_2O 1:1 (500 mL). The organic layer was separated and the aqueous layer was extracted with CH_2Cl_2 (3 x 100 ml). The gathered organic layers were dried over anhydrous $MgSO_4$, filtered and evaporated to dryness. Ethanol (200 mL) was added to the crude oily product to give a white precipitate which was cooled to 0°C, filtered and washed with cold ethanol. The product was dried for 24 h under vacuum at 50°C to give 5.67 g (10.00 mmol, yield: 82%) of **13**, as a white solid. ^{1}H NMR (400 MHz, $CDCl_3$): δ=0.91 (t, ^3J=6.8 Hz, 6H), 1.22-1.50 (m, 36H), 1.77 (q, ^3J=6.5 Hz, 4H), 3.95 (t, ^3J=6.5 Hz, 4H); 6.39 (s, 3H), 7.53 (t, ^3J=7.6 Hz, 2H), 7.66 (t, ^3J=7.5 Hz, 1H), 8.21 (d, ^3J=7.9 Hz, 2H); ^{13}C NMR (100 MHz, $CDCl_3$): δ= 14.13 (C_{prim}); 22.71, 26.04, 29.19, 29.37, 29.39, 29.59,

29.62, 29.66, 29.68, 31.94, 68.26 (C_{sec}); 99.27, 100.63, 128.54, 130.16, 133.52 (C_{tert}); 129.64, 152.40, 160.72, 165.01(C_{quat}); ESIMS (CH_2Cl_2/MeOH 9:1): *m/z*: 567.9 $[M+H]^+$, 1151.8 $[2M+NH_4]^+$, 1718.7 $[3M+NH_4]^+$.

Preparation of 14. A solution of KOH (1.23 g, 22.05 mmol) in H_2O (4 mL) was added to **13** (2.50 g, 4.41 mmol) dissolved in EtOH/THF (100/100 mL), and the solution was stirred for 60 minutes at 25°C. The pH was adjusted to 5 with 37% HCl. A precipitate formed and the reaction mixture was evaporated to dryness. The resulting mixture was partitioned between CH_2Cl_2/H_2O 1:1 (400 mL). The organic layer was separated and the aqueous layer was extracted with CH_2Cl_2 (3 x 100 ml). The gathered organic layers were dried over anhydrous Na_2SO_4, filtered and evaporated to dryness. The crude product was purified by column chromatography (silica gel (200 g), CH_2Cl_2/MeOH 100:0 and 99:1 at the end of the column). The product was dried for 24 h under vacuum to give 1.30 g (2.82 mmol, yield: 64%) of **14**, as a white solid. ^{1}H NMR (400 MHz, $CDCl_3$): δ=0.91 (t, ^3J=6.8 Hz, 6H), 1.23-1.50 (m, 36H), 1.77 (q, ^3J=6.5 Hz, 4H), 3.91 (t, ^3J=6.6 Hz, 4H), 6.02 (d, ^4J=1.5 Hz, 2H), 6.09 (t, ^3J=1.5 Hz, 1H); ^{13}C NMR (100 MHz, $CDCl_3$):): δ=14.12 (C_{prim}); 22.71, 26.04, 29.21, 29.37, 29.41, 29.60, 29.63, 29.66, 29.69, 31.94, 68.12 (C_{sec}); 94.20, 94.64 (C_{tert}); 157.24, 161.11 (C_{quat}); ESIMS (CH_2Cl_2/MeOH 9:1): *m/z*: 463.8 $[M+H]^+$, 926.5 $[2M+H]^+$.

Preparation of 15. 11-bromo-1-undecanol (0.31 g, 1.23 mmol), triphenylphosphine (0.48 g, 1.85 mmol) and DIAD (diisopropylazodicarboxylate) (0.37 g, 1.85 mmol) in anhydrous THF (50 mL, 0°C), was added dropwise to **14** (0.57 g, 1.23 mmol). The reaction mixture was stirred at 0°C for 1 h, then at room temperature for 12 h. The solvent was removed and the residue was purified by column chromatography (silica gel (100 g), CH_2Cl_2). The product was dried for 24 h under vacuum to give 0.54 g (0.78 mmol, yield: 63%) of **15**, as a colourless oil. ^{1}H NMR (400 MHz, $CDCl_3$): δ=0.91 (t, ^3J=6.8 Hz, 6H), 1.24-1.51 (m, 46H), 1.77 (q, ^3J=7.3 Hz, 6H), 1.88 (q, ^3J=7.3 Hz, 2H), 3.43 (t, ^3J=6.9 Hz, 2H), 3.92 (t, ^3J=6.6 Hz, 6H), 6.08 (s, 3H); ^{13}C NMR (100 MHz, $CDCl_3$): δ= 14.14 (C_{prim}); 22.72, 26.07, 26.09, 28.21, 28.79, 29.29, 29.39, 29.43, 29.44, 29.49, 29.54, 29.62,

29.64, 29.67, 29.70, 31.96, 32.87, 33.90, 67.95, 67.99 (C_{sec}); 93.78 (C_{tert}); 160.97 (C_{quat}); ESIMS (CH_2Cl_2/MeOH 9:1): *m/z*: 696.7 $[M+H]^+$.

Solid state structure of intermediate 10

Slow evaporation of a CH_2Cl_2/CH_3NO_2 solution of the protected precursor **10** gives colourless prisms, from which a X-ray crystal structure could be obtained (Table S2). The solid state structure confirms the *trans* arrangement of the nitrogen donors in the ligand (Figure S1a), a geometry which minimizes the global electric dipole momentum (N1 is *trans* to N3 and N5 is in *trans* to N7). The oxygen atoms of the terminal carboxamide functions are also found to be in *trans* arrangement with respect to the pyridine N-donors atoms (N1 is *trans* to O2 and N7 is in trans to O3) in agreement with similar *trans*-*trans* arrangements previously reported for 2,6-disubstituted pyridine units in ligands **L1**-**L3.**[6] Bond lengths and bond angles are standard (Table S3)[7] and the ligand possesses a pseudo-twofold axis passing through C27. No classical hydrogen bond was found in the structure and two kinds of intermolecular stacking interactions operate in the unit cell (see Figure S1b and the comments on the structure of **10** in the experimental part).

Tables and Figures

Table S1 Elemental Analysis for Ligands **L*k*** (*k* = 5, 6) and Complex $[Y_2(\mathbf{L6})(hfa)_6]$.

Compound	%C found	%H found	%N found	%C calcd	%H calcd	%N calcd
L6·18.01 H_2O[a]	67.48	6.75	4.20	67.48	6.75	4.20
$[Y_2(\mathbf{L6})(hfa)_6]$·29.25 H_2O[a]	54.44	5.42	2.93	54.42	5.31	2.99
L5	75.61	9.95	8.39	75.74	10.09	8.34

[a] The hydration found by elemental analysis was confirmed by TGA (see Figure S20)

Table S2 Summary of Crystal Data, Intensity Measurement and Structure Refinement for **10**.

Compound	(**10**)	
Empirical formula	$C_{54}H_{59}N_9O_6$	
Formula weight	930.10	
Temperature	180(2) K	
Wavelength	0.71073 Å	
Crystal system	Monoclinic	
Space group	*C* 2/c	
Unit cell dimensions	*a* = 39.714(3) Å	α= 90°.
	b = 6.5535(4) Å	β= 93.244(7)°.
	c = 37.438(3) Å	γ = 90°.
Volume	9728.2(13) Å^3	
Z	8	
Density (calculated)	1.270 g/cm^3	
Absorption coefficient	0.085 mm^{-1}	
F(000)	3952	
Crystal size	0.355 x 0.136 x 0.100 mm^3	
Theta range for data collection	1.45 to 25.68°.	
Index ranges	-48<=*h*<=48, -7<=*k*<=7, -45<=*l*<=45	
Reflections collected	26978	
Independent reflections	8893 [*R*(int) = 0.0471]	
Completeness to theta = 25.68°	96.7 %	
Absorption correction	Numerical	
Max. and min. transmission	0.9920 and 0.9808	
Refinement method	Full-matrix least-squares on F^2	
Data / restraints / parameters	8893 / 0 / 629	
Goodness-of-fit on F^2	1.024	
Final *R* indices [*I*>2sigma(*I*)]	*R*1 = 0.0716, *wR*2 = 0.1897	
R indices (all data)	*R*1 = 0.1097, *wR*2 = 0.2112	
Largest diff. peak and hole	0.434 and -0.526 e.Å^{-3}	

Table S3 Selected Least-Squares Planes Data for **10**.

Least-Squares Planes

Least-squares planes description	Abbreviation	Max. deviation/Å	Atom
Phenyl 1	Ph1		
C1 C2 C3 C4 C5 C6		0.016(1)	C1
Pyridine 1	Py1		
N1 C8 C9 C10 C11 C12		0.015(1)	C10
Benzimidazole 1	Bz1		
C18 N4 C19 C20 C21 C22 C23 C24 N3		0.026(1)	N3
Benzimidazole 2	Bz2		
C28 C29 C30 N5 C31 N6 C32 C33 C34		0.009(1)	C33
Pyridine 2	Py2		
C37 C38 C39 C40 C41 N7		0.011(1)	C41
Phenyl 2	Ph2		
C48 C49 C50 C51 C52 C53		0.005(1)	C53

Interplanar angles (°) (esd < 0.1°)

	Py1	Bz1	Bz2	Py2	Ph2
Ph1	77.7	72.2	4.8	29.0	54.7
Py1		45.4	78.9	48.9	88.7
Bz1			74.0	82.3	46.0
Bz2				30.0	59.1
Py2					65.1

Table S4 Summary of Crystal Data, Intensity Measurement and Structure Refinement for $[Lu_2(\mathbf{L1})(hfac)_6]$.

Empirical formula	$C_{69}H_{50}F_{36}Lu_2N_8O_{14}$	
Formula weight	2249.11	
Diffractometer	Supernova Cu	
Temperature	180.0 K	
Wavelength	1.5418 Å	
Crystal system	Triclinic	
Space group	*P*-1	
Unit cell dimensions	a = 12.6357(4) Å	α= 83.577(3)°.
	b = 17.6457(5) Å	β= 89.254(3)°.
	c = 18.3732(6) Å	γ = 88.667(2)°.
Volume	4069.6(2) Å^3	
Z	2	
Density (calculated)	1.835 g/cm^3	
Absorption coefficient	5.888 mm^{-1}	
F(000)	2196	
Crystal size	0.2881 x 0.1708 x 0.0562 mm	
Theta range for data collection	2.52 to 79.77°.	
Index ranges	-15<=*h*<=15, -21<=*k*<=21, -22<=*l*<=22	
Reflections collected	24565	
Independent reflections	24565 [*R*(int) = 0.0000]	
Completeness to theta = 68.00°	99.2 %	
Absorption correction	Analytical	
Max. and min. transmission	0.735 and 0.431	
Refinement method	Full-matrix least-squares on F^2	
Data / restraints / parameters	24565 / 18 / 1143	
Goodness-of-fit on F^2	1.020	
Final R indices [*I*>2sigma(*I*)]	*R*1 = 0.0606, *wR*2 = 0.1655	
R indices (all data)	*R*1 = 0.0694, *wR*2 = 0.1742	
Largest diff. peak and hole	1.785 and -1.463 e.Å^{-3}	

Table S5 Selected Bond Distances (Å), Bond Angles (°) in $[Lu_2(\mathbf{L1})(hfac)_6]$.

Bond distances (Å)

Atom 1	Atom 2	Distance	Atom 1	Atom 2	Distance
Lu(1)	O(8)	2.266(4)	Lu(1)	O(7)	2.381(4)
Lu(1)	O(1)	2.284(4)	Lu(1)	O(3)	2.394(4)
Lu(1)	O(5)	2.326(4)	Lu(1)	N(1)	2.474(5)
Lu(1)	O(6)	2.354(4)	Lu(1)	N(3)	2.479(5)
Lu(1)	O(4)	2.375(5)	Lu(1)	Lu(2)	12.533 (1)
Lu(2)	O(10)	2.279(4)	Lu(2)	O(14)	2.388(4)
Lu(2)	O(2)	2.296(4)	Lu(2)	O(13)	2.395(4)
Lu(2)	O(11)	2.339(4)	Lu(2)	N(5)	2.496(5)
Lu(2)	O(12)	2.360(5)	Lu(2)	N(7)	2.507(5)
Lu(2)	O(9)	2.379(4)			

Angles (°)

At. 1	At. 2	At. 3	angle	At. 1	At. 2	At. 3	angle
O(8)	Lu(1)	O(1)	139.66(17)	O(6)	Lu(1)	O(3)	134.53(15)
O(8)	Lu(1)	O(5)	100.86(17)	O(4)	Lu(1)	O(3)	69.23(16)
O(1)	Lu(1)	O(5)	76.42(17)	O(7)	Lu(1)	O(3)	138.70 (16)
O(8)	Lu(1)	O(6)	140.86(16)	O(8)	Lu(1)	N(1)	128.34(17)
O(1)	Lu(1)	O(6)	77.73(15)	O(1)	Lu(1)	N(1)	65.27(17)
O(5)	Lu(1)	O(6)	72.92(15)	O(5)	Lu(1)	N(1)	130.76(16)
O(8)	Lu(1)	O(4)	70.02(17)	O(6)	Lu(1)	N(1)	69.76(14)
O(1)	Lu(1)	O(4)	70.77(16)	O(4)	Lu(1)	N(1)	117.89(17)
O(5)	Lu(1)	O(4)	73.30(16)	O(7)	Lu(1)	N(1)	123.82(16)
O(6)	Lu(1)	O(4)	138.06(16)	O(3)	Lu(1)	N(1)	64.77(15)
O(8)	Lu(1)	O(7)	72.25(16)	O(8)	Lu(1)	N(3)	76.25(17)
O(1)	Lu(1)	O(7)	137.18(15)	O(1)	Lu(1)	N(3)	129.64(16)
O(5)	Lu(1)	O(7)	68.12(16)	O(5)	Lu(1)	N(3)	142.45(16)
O(6)	Lu(1)	O(7)	69.65(13)	O(6)	Lu(1)	N(3)	85.94(15)
O(4)	Lu(1)	O(7)	118.28(16)	O(4)	Lu(1)	N(3)	135.67(16)
O(8)	Lu(1)	O(3)	73.60(17)	O(7)	Lu(1)	N(3)	75.60(15)
O(1)	Lu(1)	O(3)	84.44(17)	O(3)	Lu(1)	N(3)	74.31(16)
O(5)	Lu(1)	O(3)	141.71(17)	N(1)	Lu(1)	N(3)	64.38(16)
O(10)	Lu(2)	O(2)	141.33(16)	O(12)	Lu(2)	O(13)	119.47(16)
O(10)	Lu(2)	O(11)	100.34(15)	O(9)	Lu(2)	O(13)	139.68(15)
O(2)	Lu(2)	O(11)	75.26(16)	O(14)	Lu(2)	O(13)	69.17(14)
O(10)	Lu(2)	O(12)	70.32(16)	O(10)	Lu(2)	N(5)	128.13(15)
O(2)	Lu(2)	O(12)	71.73(17)	O(2)	Lu(2)	N(5)	65.02(16)
O(11)	Lu(2)	O(12)	73.12(16)	O(11)	Lu(2)	N(5)	131.41(15)
O(10)	Lu(2)	O(9)	73.81(15)	O(12)	Lu(2)	N(5)	116.30(16)
O(2)	Lu(2)	O(9)	85.19(16)	O(9)	Lu(2)	N(5)	64.52(15)

O(11)	Lu(2)	O(9)	139.86(16)	O(14)	Lu(2)	N(5)	70.67(14)
O(12)	Lu(2)	O(9)	67.50(16)	N(13)	Lu(2)	N(5)	124.23(15)
O(10)	Lu(2)	O(14)	140.84(14)	O(10)	Lu(2)	N(7)	76.63(15)
O(2)	Lu(2)	O(14)	75.78(16)	O(2)	Lu(2)	N(7)	129.02(15)
O(11)	Lu(2)	O(14)	73.45(15)	O(11)	Lu(2)	N(7)	143.79(15)
O(12)	Lu(2)	O(14)	138.02(16)	O(12)	Lu(2)	N(7)	135.12(16)
O(9)	Lu(2)	O(14)	135.20(14)	O(9)	Lu(2)	N(7)	74.80(16)
O(10)	Lu(2)	O(13)	72.61(15)	O(14)	Lu(2)	N(7)	86.32(16)
O(2)	Lu(2)	O(13)	135.10(16)	O(13)	Lu(2)	N(7)	76.29(15)
O(11)	Lu(2)	O(13)	68.59(15)	N(5)	Lu(2)	N(7)	64.03(15)

Table S6 Selected Least-Squares Planes Data for $[Lu_2(\mathbf{L1})(hfac)_6]$.

Least-Squares Planes

Least-squares planes description	Abbreviation	Atom	Max. deviation (Å)
Lu1 part of the complex			
Pyridine N1, C1, C2, C3, C4, C5	Py1	N1	0.011(1)
Benzimidazole C11, C12, C13, C14, C15, C16, C17, N3, N4	Bz1	C14	0.049(1)
Hexafluoroacetylacetonate O6, C50, C51, C52, O7, Lu1	Hfa1	C50	0.019(1)
Hexafluoroacetylacetonate O4, C45, C46.C47, O5, Lu1	Hfa2	C46	0.007(1)
Hexafluroacetylacetonate O4, C42, C41, C40, O8, Lu1	Hfa3	C40	0.028(1)
Lu2 part of the complex			
Pyridine N5, C34, C33, C32, C31, C30	Py2	C34	0.010(1)
Benzimidazole N8, C24, N7, C25, C26, C27, C21, C22, C23	Bz2	C21	0.044(1)
Hexafluoroacetylacetonate O12, C60, C61, C62, O11, Lu2	Hfa4	C61	0.008(1)
Hexafluoroacetylacetonate O9, C55, C56, C57, O10, Lu2	Hfa5	C57	0.019(1)
Hexafluroacetylacetonate O13, C65, C66, C67, O14, Lu2	Hfa6	C67	0.021(1)

Interplanar angles (°) (esd < 0.1°)

	Bz1	Py1	Bz2	Py2	Hfa1	Hfa2	Hfa3	Hfa4	Hfa5
Py1	4.8								
Bz2	60.7	59.1							
Py2	72.9	71.9	14.5						
Hfa1	107.8	111.1	79.4	66.6					
Hfa2	101.8	97.5	59.1	59.4	105.0				
Hfa3	118.4	122.2	90.7	77.3	12.4	107.1			
Hfa4	115.2	110.8	69.8	67.5	100.9	13.4	100.3		
Hfa5	103.6	106.7	73.6	61.0	5.9	102.3	18.2	99.4	

Hfa6	110.0	113.0	76.8	63.6	13.9	5.3	99.8	95.6	6.4

Table S7 Deviations of the Coordinating Atoms from the Upper and Lower Planes in the two Coordination Sites of Complex $[Lu_2(\mathbf{L1})(hfac)_6]$ in a Monocaped Pseudo-Tetragonal Anti-prismatic Geometry.

Atom	Deviation [Å]	Atome	Déviation [Å]
Upper plane		Lower plane	
	Lu1		
O1	0.048	O7	0.123
O6	-0.045	O8	-0.122
N3	0.045	O4	0.119
O3	-0.047	O5	-0.120
	Lu2		
O2	0.064	O13	0.141
O14	-0.061	O11	-0.139
N7	0.059	O10	-0.141
O9	-0.062	O12	0.139

Table S8 Selected Geometrical Parameters [a] in $[Lu_2(\mathbf{L1})(hfac)_6]$.

Compound		θ (R^1-Lu-R^2) /°	Φ /°	ω /°
$[Lu_2(\mathbf{L1})(hfa)_6]$	Lu1	60.42	177.7	44(2)
	Lu2	116.99	179.1	43(2)

[a] (O1, O6, N3, O3) and (O7, O8, O4, O5) respectively define the upper and lower planes around Lu1, whereas (O2, O14, N7, O2) and (O13, O11, O10, O12) define the upper and lower planes around Lu2. The N1 and N5 coordinating atoms of the two pyridines are the pertinent capping atoms. For the definition of θ, Φ and ω in a monocaped pseudo-tetragonal anti-prism, see Figure S10. R^1(Lu1) = Lu1-O1 + Lu1-O3 + Lu1-O6 + Lu1-N3, R^2(Lu1) = Lu1-O4 + Lu1-O5 + Lu1-O7 + Lu1-O8 and R^1(Lu2) = Lu2-O2 + Lu2-O11 + Lu2-O14 + Lu2-N7, R^2(Lu2) = Lu2-O10 + Lu2-O12 + Lu2O13 + Lu2-O15. Proj[X*i*] (X = O, N) is the projection of X*i* along the R^1-R^2 direction onto a perpendicular plane passing through the metal atom.

Table S9 Bond Distances ($\delta_{\mathrm{Lu},j}$) Bond Valences ($\nu_{\mathrm{Ln},j}$)[a] and Total Atom Valence (V_{Lu})[b] in the Crystal Structure of $[Lu_2(\mathbf{L1})(hfac)_6]$.

Atom[c]	Donor type	$\delta_{\mathrm{Lu},j}$	$\nu_{\mathrm{Lu},j}$	
		Lu1		
Lu1-N3	Bzim	2.479	0.310	Average N-heterocyclic
Lu1-N1	Py	2.474	0.315	0.312(3)
Lu1-O1	Amide	2.284	0.402	
Lu1-O3	Hfa	2.394	0.299	
Lu1-O8	Hfa	2.266	0.422	
Lu1-O4	Hfa	2.375	0.315	
Lu1-O5	Hfa	2.326	0.359	
Lu1-O6	Hfa	2.354	0.333	Average O-hfac
Lu1-O7	Hfa	2.381	0.309	0.35(5)
		V_{Lu1}	**3.064**	
		Lu2		
Lu2-N7	Bzim	2.507	0.288	Average N-heterocyclic
Lu2-N5	Py	2.496	0.296	0.29(1)
Lu2-O2	Amide	2.296	0.389	
Lu2-O11	Hfa	2.339	0.347	
Lu2-O12	Hfa	2.360	0.328	
Lu2-O9	Hfa	2.379	0.311	
Lu2-O10	Hfa	2.279	0.408	
Lu2-O13	Hfa	2.395	0.298	Average O-hfac
Lu2-O14	Hfa	2.388	0.304	0.34(4)
		V_{Lu2}	**2.968**	

[a] $\nu_{\mathrm{Lu},j} = e^{\left[\left(R_{\mathrm{Lu},j} - \delta_{\mathrm{Lu},j}\right)/b\right]}$ where $\delta_{\mathrm{Lu},j}$ is the bond lenght, $R_{\mathrm{Lu},j}$ corresponds to the bond valence parameters and b =0.37 Å is a universal scalling constant) [4]. [b] $V_{\mathrm{Lu}} = \sum_j \nu_{\mathrm{Lu},j}$.

Table S10 Computed ^{1}H NMR Chemical Shifts for **L6**, [Y(**L6**)(hfac)$_3$] and [Y$_2$(**L6**)(hfac)$_6$]

Proton	δ **L6** /ppm	δ [Y(**L6**)(hfac)$_3$] /ppm	δ [Y$_2$(**L6**)(hfac)$_6$] /ppm
Hf	8.3900(53)	8.3649(53)	8.3400(53)
Hm	8.2800(53)	8.3085(53)	8.3500(53)
Hn	8.2100(53)	8.2401(53)	8.2700(53)
Hb	7.5900(53)	7.7266(53)	7.7800(53)
Hd	7.3900(53)	7.3945(53)	7.3200(53)
Hc	7.2700(53)	7.2167(53)	7.1900(53)
Ha	4.3000(53)	4.2504(53)	4.1600(53)
Hk	3.6400(53)	3.6987(53)	3.7700(53)
Hi	3.4300(53)	3.4628(53)	3.5300(53)

Table S11 Indexation at a Given Temperature for the Reflections Detected in the Liquid-crystalline Phases by SA-XRD for Complex [Y$_2$(**L6**)(hfac)$_6$].

T /°C	$d_{hkl\ (mes)}$ /Å	*I* /a.u.	*00l*	$d_{hkl\ (calc)}$ /Å	
25°C	97.1	VS(Sh)	001	97.4	*d* = 97.4 Å
[Y$_2$(**L6**)(hfa)$_6$]	48.8	VS(Sh)	002	48.7	
	4.5	S(Br)	-	-	
40°C	99.3	VS(Sh)	001	99.2	*d* = 99.2 Å
[Y$_2$(**L6**)(hfa)$_6$]	49.5	VS(Sh)	002	49.6	
	4.5	S(Br)	-	-	
120°C	105.2	VS(Sh)	001	105.5	*d* = 105.5 Å
[Y$_2$(**L6**)(hfa)$_6$]	52.9	VS(Sh)	002	52.8	
	4.5	S(Br)	-	-	

$d_{hkl\ (mes)}$ and $d_{hkl\ (calc)}$ are the measured and calculated diffraction spacing ; *d* is the lattice parameter of the smectic phase ; *I* corresponds to the intensity of the reflections (VS : very strong, S : strong ; br and sh stand for broad and sharp) ; The $d_{001\ (calc)}$ are calculated according the formula : $<d_{001}>_{(calc)} = ½\ (d_{001(exp)} + 2d_{002\ (exp)})$.

a)

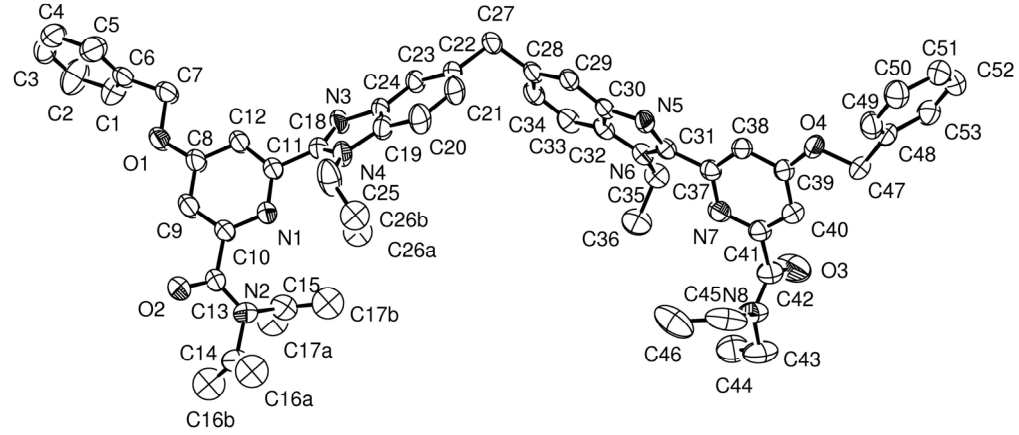

b)

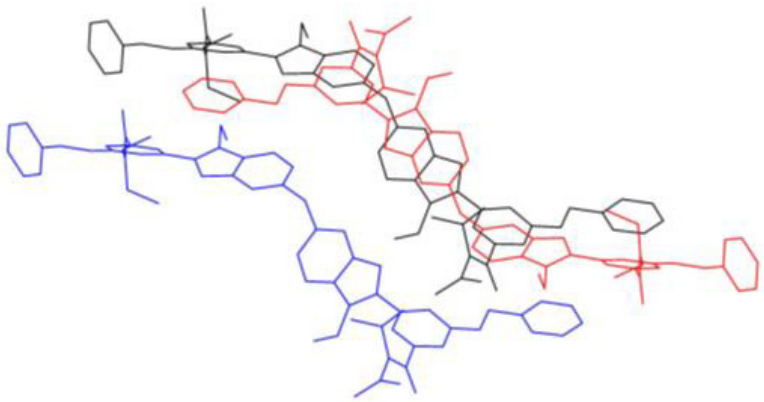

Figure S1 a) View of the crystal structure of **10**, the protected precursor of **11**, with scheme numbering. Ellipsoids are represented at the 50% probability level. The hydrogen atoms and solvent molecules are omitted for clarity. b) View of the intermolecular stacking interactions in the precursory ligand **10**. See Comments on the crystal structure of **10** for details.

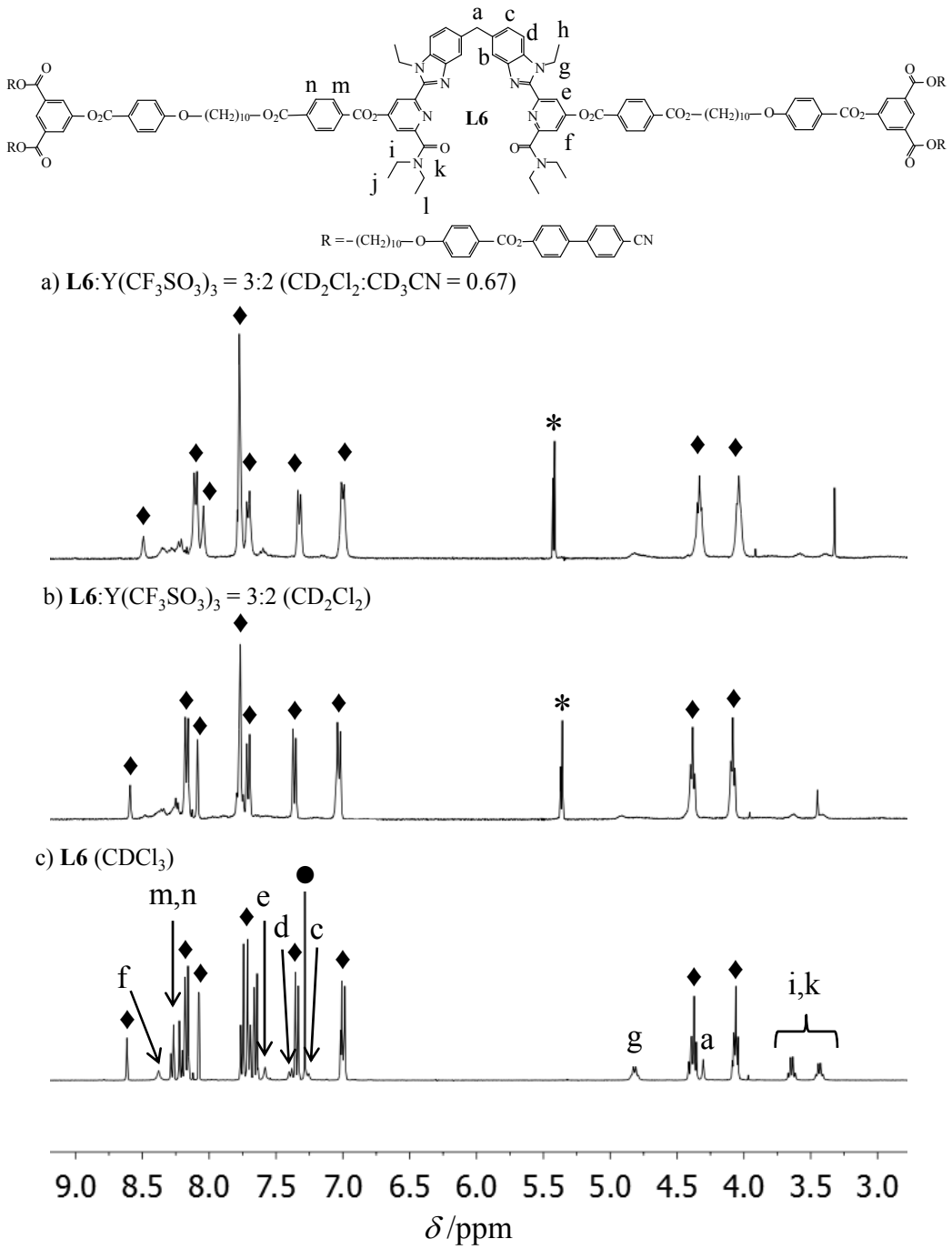

Figure S2 ^{1}H NMR spectra with numbering scheme of the titration of **L6** with diamagnetic $Y(CF_3SO_3)_3$ at 298 K.* = CH_2Cl_2 and $CDHCl_2$, ● = $CHCl_3$ and ♦ = Signals of the peripheral dendritic part of the ligand **L6** (total ligand concentration $|\mathbf{L6}|_{Tot} \cong 0.01$ M).

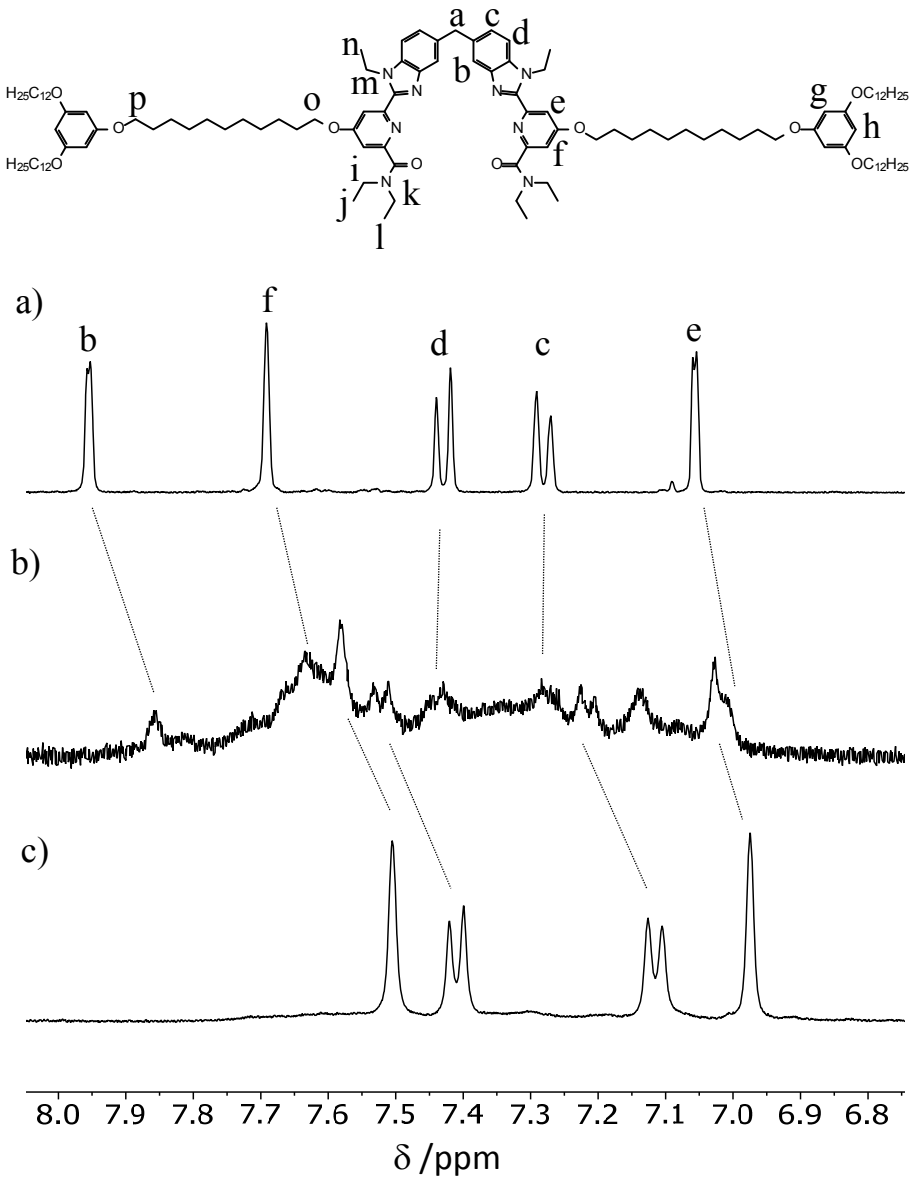

Figure S3 ^{1}H NMR spectra with numbering scheme (aromatic region) of a) the ligand **L5** in CD_2Cl_2, b) the complex **[**Y_2(**L5**)$_3$](CF$_3$SO$_3$)$_6$ in CD_2Cl_2 and c) the complex **[**Y_2(**L5**)$_3$](CF$_3$SO$_3$)$_6$ in $V_{CD_2Cl_2} / V_{CD_3CN}$ = 0.25 (298 K, total ligand concentration $|\mathbf{L5}|_{tot} \cong 0.01$ M).

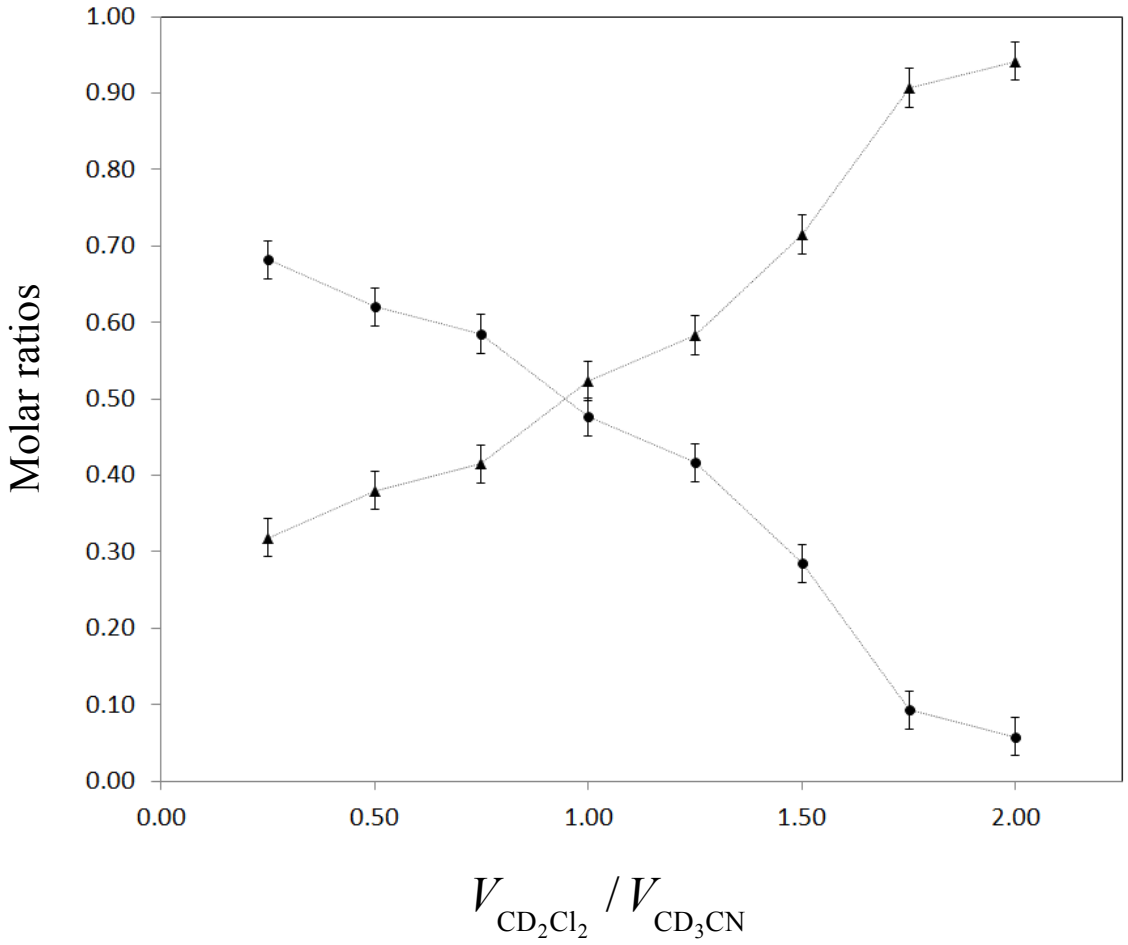

Figure S4 Molar ratios of ligand involved in the complex $[Y_2(\mathbf{L5})_3](CF_3SO_3)_6$ (●) and of free ligand **L5** (▲) at different $V_{CD_2Cl_2} / V_{CD_3CN}$ ratios.

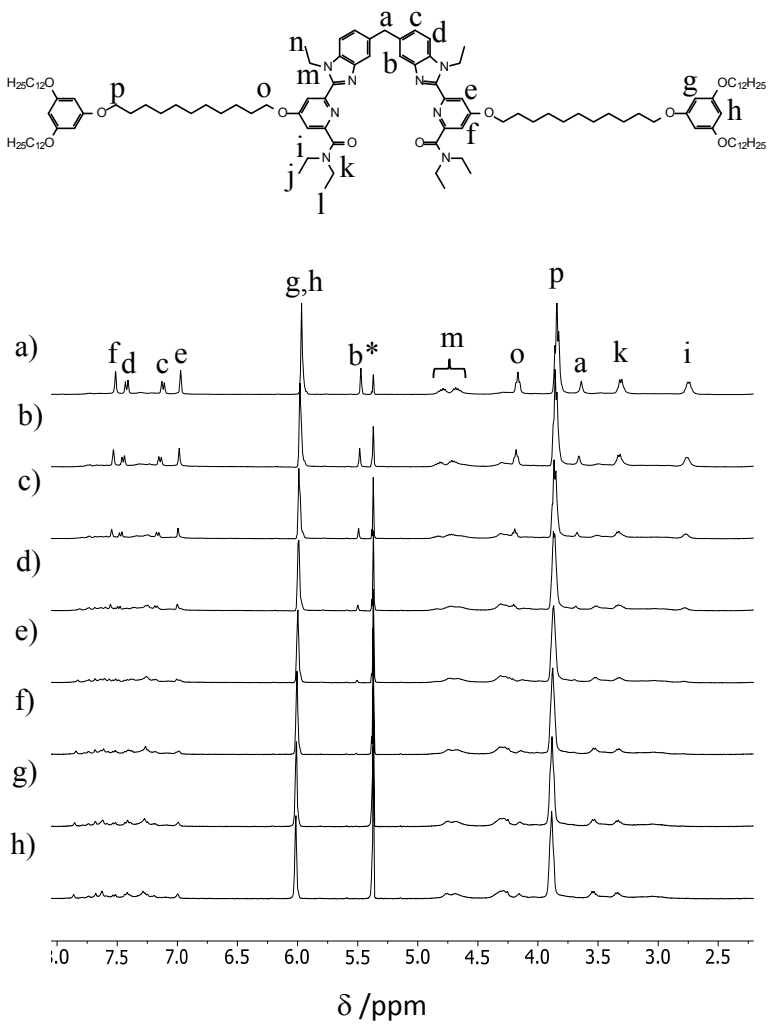

Figure S5 ^{1}H NMR spectra with numbering scheme of the diamagnetic complex **[**Lu_2(**L5**)$_3$](CF$_3$SO$_3$)$_6$ at different $V_{CD_2Cl_2}/V_{CD_3CN}$ ratios a) $V_{CD_2Cl_2}/V_{CD_3CN}$ = 0.25, b) $V_{CD_2Cl_2}/V_{CD_3CN}$ = 0.50, c) $V_{CD_2Cl_2}/V_{CD_3CN}$ = 0.75, d) $V_{CD_2Cl_2}/V_{CD_3CN}$ = 1.00 e) $V_{CD_2Cl_2}/V_{CD_3CN}$ = 1.25, f) $V_{CD_2Cl_2}/V_{CD_3CN}$ = 1.50 g) $V_{CD_2Cl_2}/V_{CD_3CN}$ = 1.75 and h) $V_{CD_2Cl_2}/V_{CD_3CN}$ = 2.00. * = CH_2Cl_2 and $CDHCl_2$ (298 K, total ligand concentration $|\mathbf{L5}|_{tot} \cong 0.01$ M).

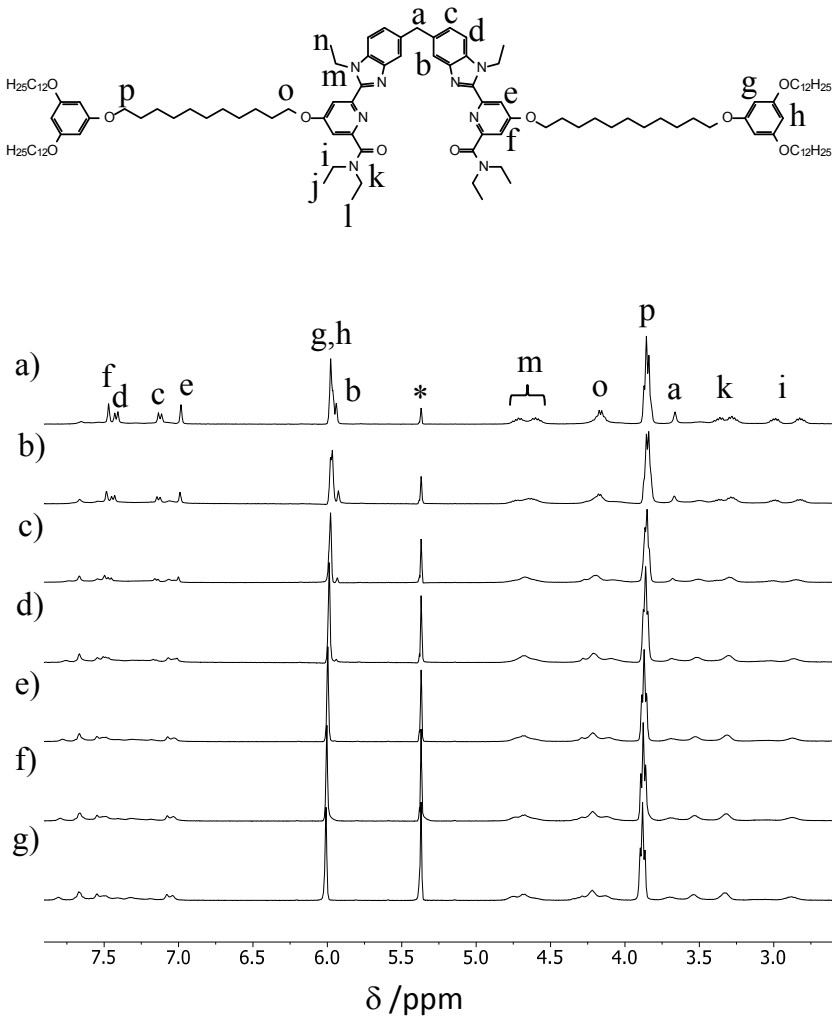

Figure S6 ^{1}H NMR spectra with numbering scheme of the diamagnetic complex **[**La_2(**L5**)$_3$](
$CF_3SO_3)_6$ at different $V_{CD_2Cl_2} / V_{CD_3CN}$ ratios a) $V_{CD_2Cl_2} / V_{CD_3CN}$ = 0.25, b) $V_{CD_2Cl_2} / V_{CD_3CN}$ = 0.50, c) $V_{CD_2Cl_2} / V_{CD_3CN}$ = 0.75, d) $V_{CD_2Cl_2} / V_{CD_3CN}$ = 1.00 e) $V_{CD_2Cl_2} / V_{CD_3CN}$ = 1.25, f) $V_{CD_2Cl_2} / V_{CD_3CN}$ = 1.50 and g) $V_{CD_2Cl_2} / V_{CD_3CN}$ = 1.75. * = CH_2Cl_2 and $CDHCl_2$(298 K, total ligand concentration $|\mathbf{L5}|_{tot} \cong 0.01$ M).

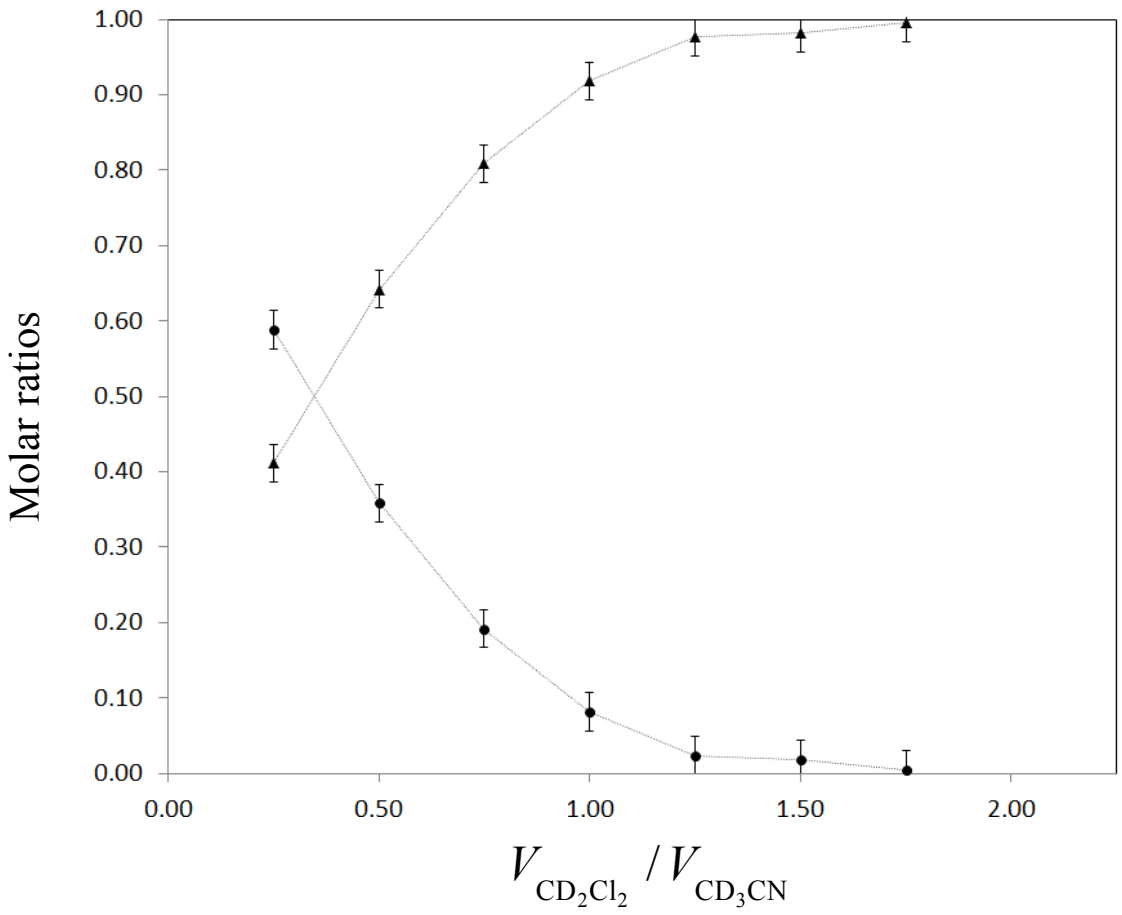

Figure S7 Molar ratios of ligand involved in the complex **[**Lu_2(**L5**)$_3$](CF$_3$SO$_3$)$_6$ (●) and of free ligand **L5** (▲) at different $V_{CD_2Cl_2} / V_{CD_3CN}$ ratios.

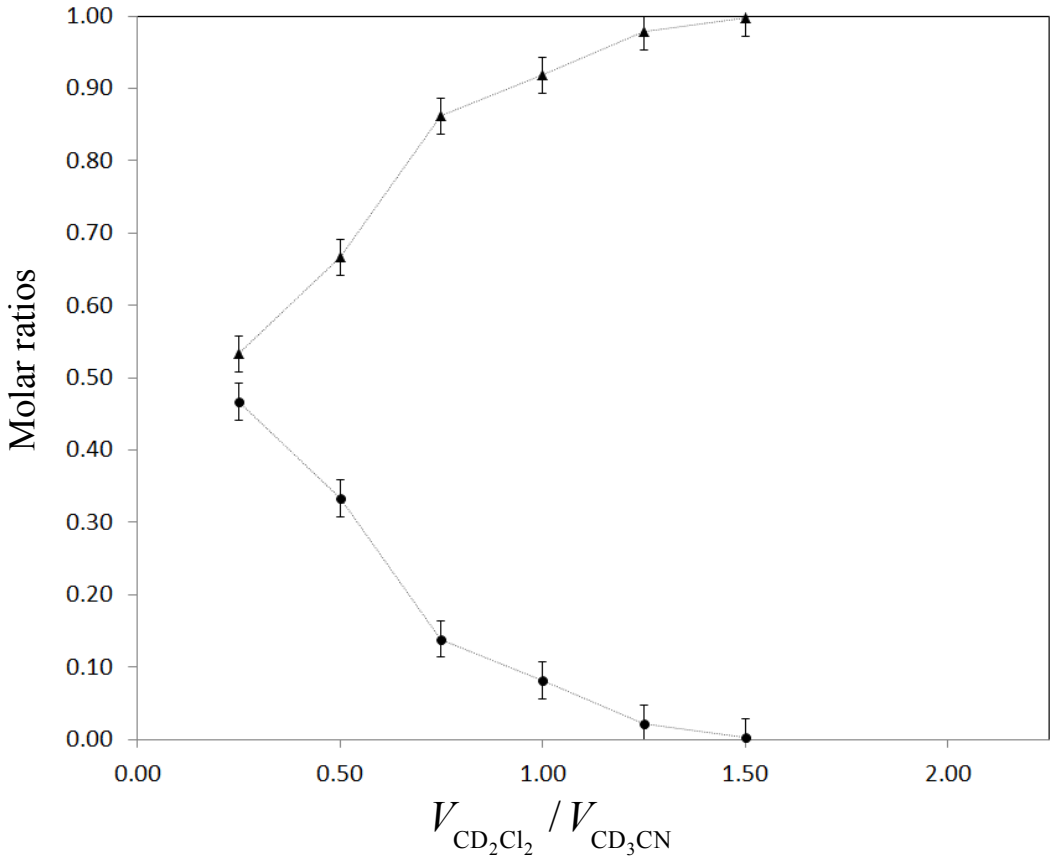

Figure S8 Molar ratios of ligand involved in the complex **[**La_2(**L5**)$_3$](CF$_3$SO$_3$)$_6$ (●) and of free ligand **L5** (▲) at different $V_{CD_2Cl_2} / V_{CD_3CN}$ ratios.

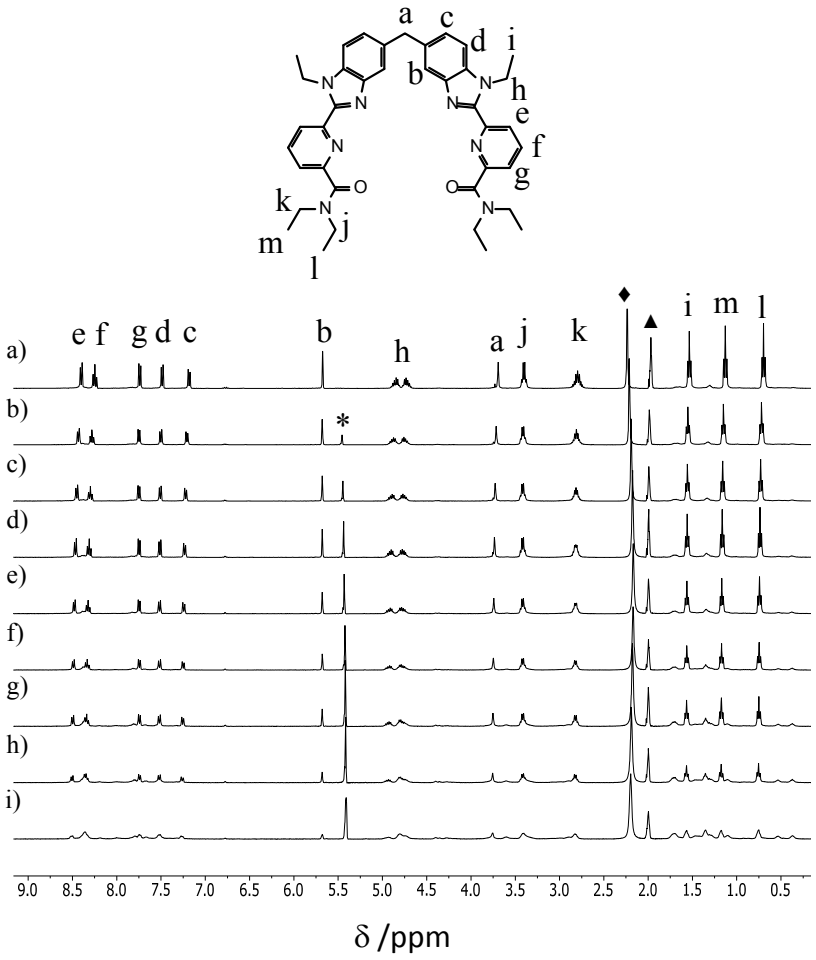

Figure S9 ^{1}H NMR spectra with numbering scheme of the diamagnetic complex **[**Y_2(**L1**)$_3$](
$CF_3SO_3)_6$ at different $V_{CD_2Cl_2}/V_{CD_3CN}$ ratios a) $V_{CD_2Cl_2}/V_{CD_3CN}$ = 0.25, b) $V_{CD_2Cl_2}/V_{CD_3CN}$ = 0.50, c) $V_{CD_2Cl_2}/V_{CD_3CN}$ = 0.75, d) $V_{CD_2Cl_2}/V_{CD_3CN}$ = 1.00 e) $V_{CD_2Cl_2}/V_{CD_3CN}$ = 1.25, f) $V_{CD_2Cl_2}/V_{CD_3CN}$ = 1.50, g) $V_{CD_2Cl_2}/V_{CD_3CN}$ = 1.75, h) $V_{CD_2Cl_2}/V_{CD_3CN}$ = 2.00, i) $V_{CD_2Cl_2}/V_{CD_3CN}$ = 2.25. * = CH_2Cl_2 and $CDHCl_2$, ▲= CH_3CN, CDH_2CN and CD_2HCN, ♦ = H_2O (298 K, total ligand concentration $|\mathbf{L1}|_{tot} \cong 0.01$ M).

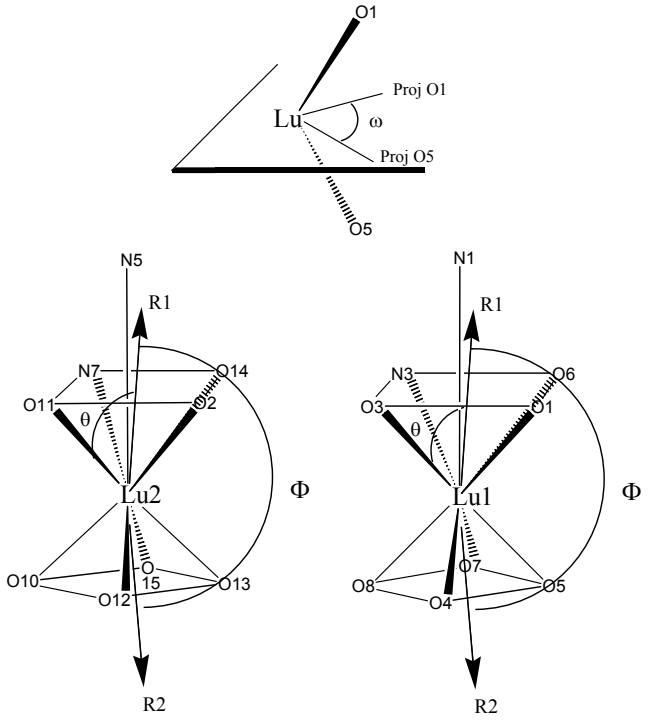

Figure S10 Definitions of angles θ, Φ and ω for the Lu1 and Lu2 coordination spheres in the crystal structure of $[Lu_2(\mathbf{L1})(hfac)_6]$.

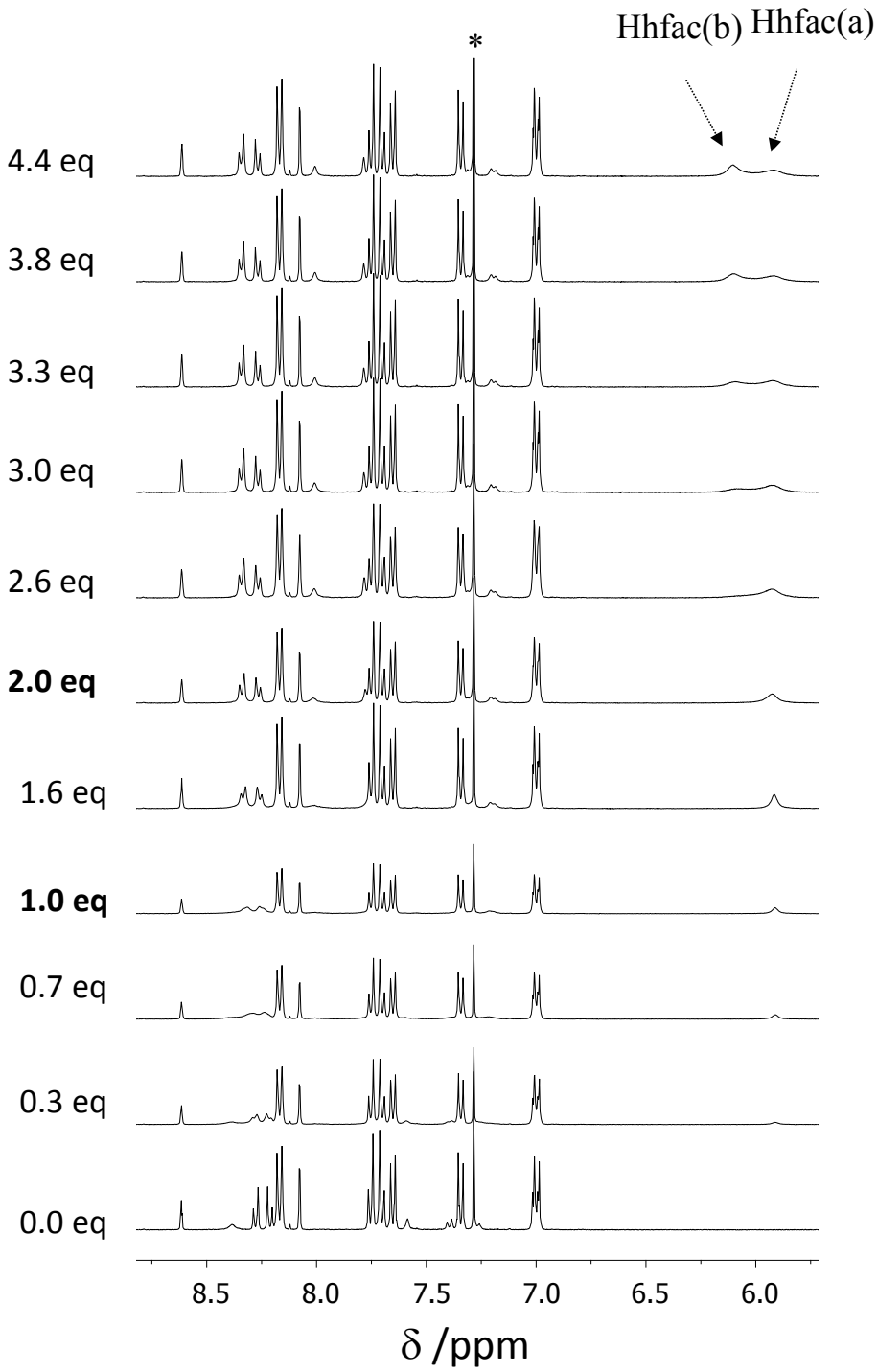

Figure S11 Variation of the ^{1}H NMR spectra (aromatic region) for the titration of **L6** with0.1-4.4 eqs of [Y(hfac)$_3$diglyme] (total ligand concentration $\left|\mathbf{L6}\right|_{tot} \cong 0.005$ M, $CDCl_3$, 298K). * = $CHCl_3$.

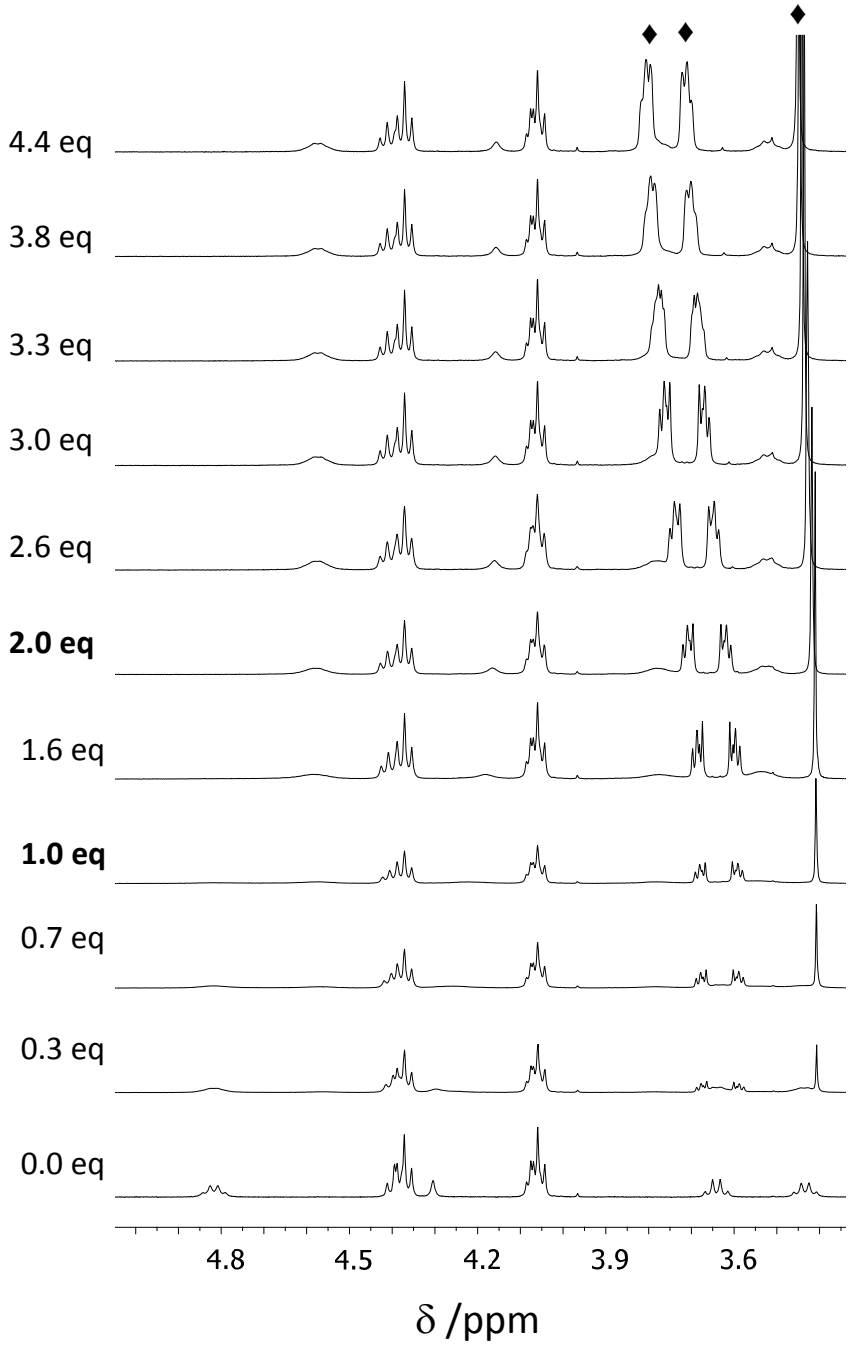

Figure S12 Variation of the ^{1}H NMR spectra (aliphatic) for the titration of **L6** with 0.1-4.4 eqs of [Y(hfac)$_3$diglyme] (total ligand concentration $\left|\mathbf{L6}\right|_{tot} \cong 0.005$ M, $CDCl_3$, 298K). * = $CHCl_3$, ♦ = diglyme.

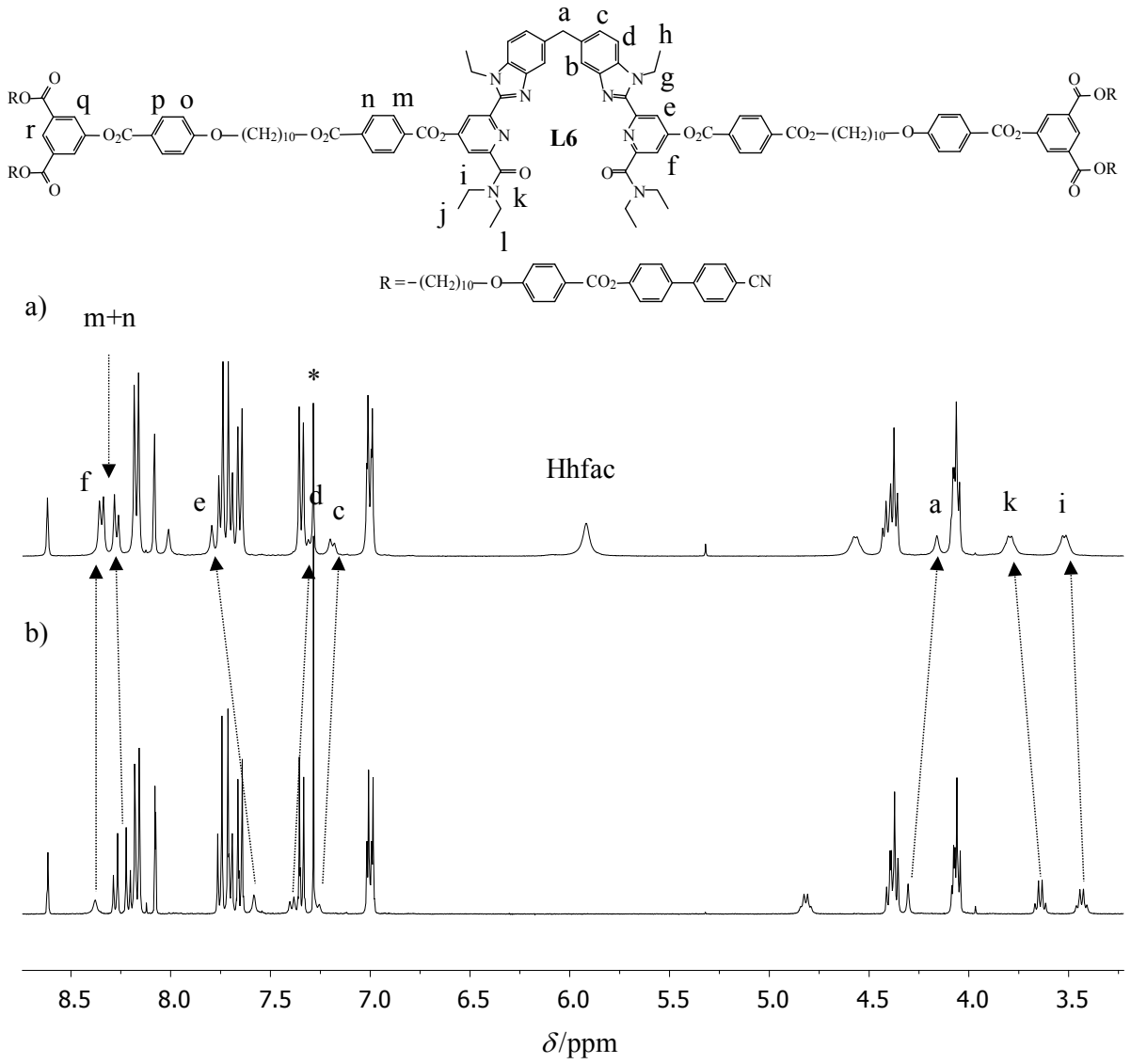

Figure S13 ^{1}H NMR spectrum with numbering scheme of a) the diamagnetic complex $[Y_2(\mathbf{L6})(hfac)_6]$ and b) the ligand **L6** ($CDCl_3$, 298K). * = $CHCl_3$. The labelled signals are those used for the determination of the cumulative formation constants β_1 and β_2.

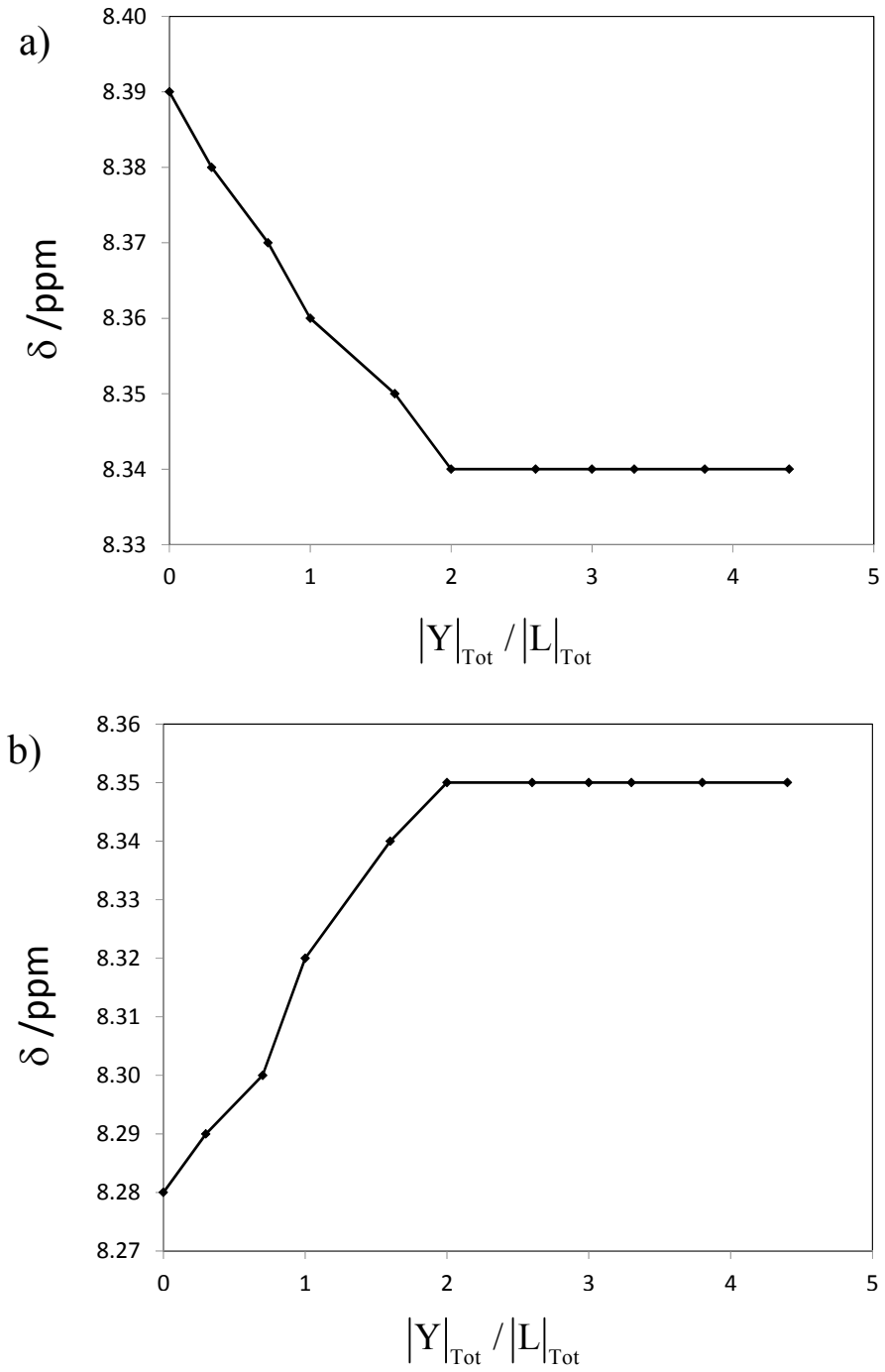

Figure S14 Variation of the ^{1}H NMR chemical shifts for the titration of **L6** with [Y(hfac)$_3$diglyme], a) Hf and b) Hm. (For numbering, see Figure S13)

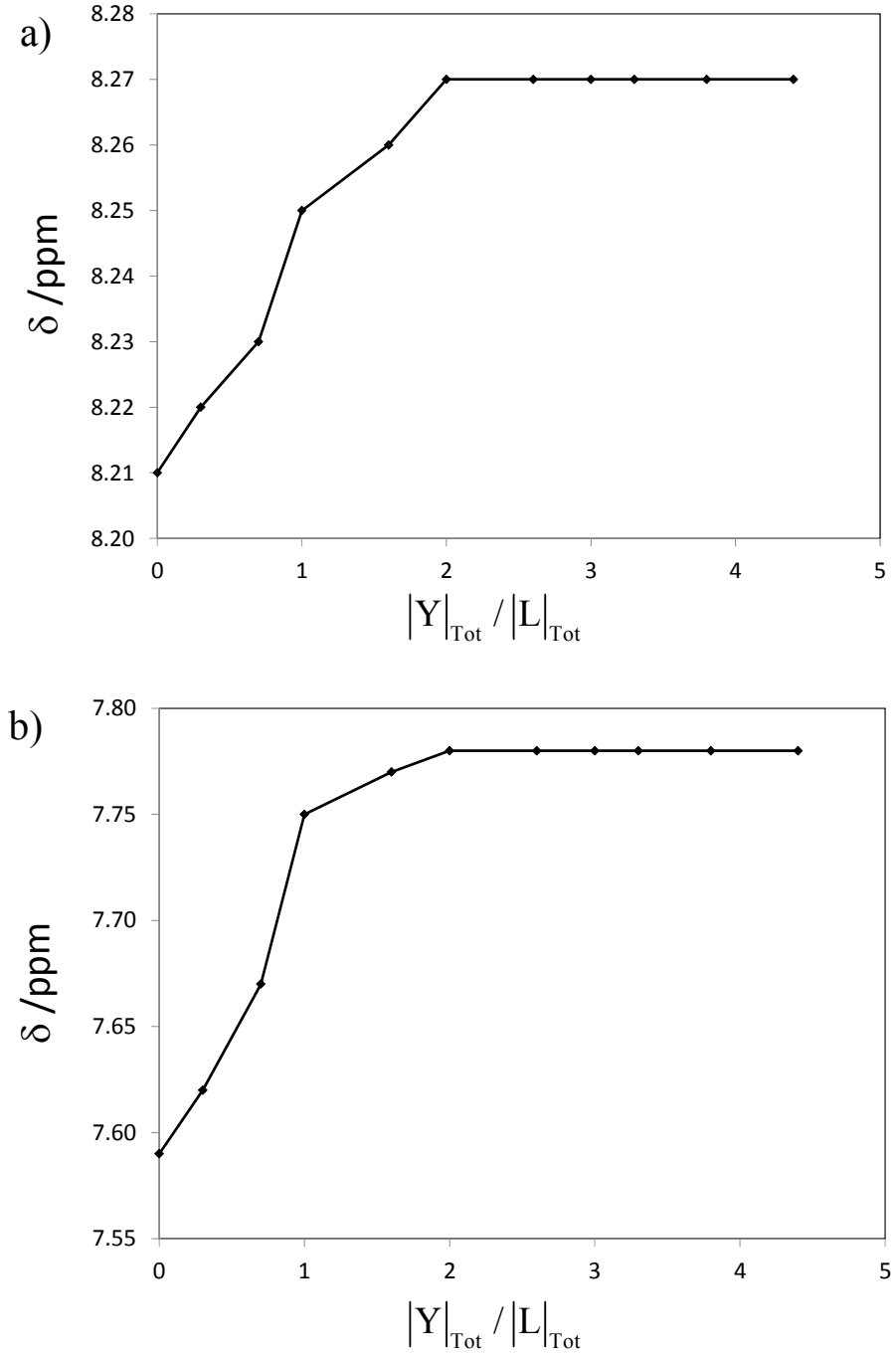

Figure S15 Variation of the ^{1}H NMR chemical shifts for the titration of **L6** with [Y(hfac)$_3$diglyme], a) Hn and b) He. (For numbering, see Figure S13)

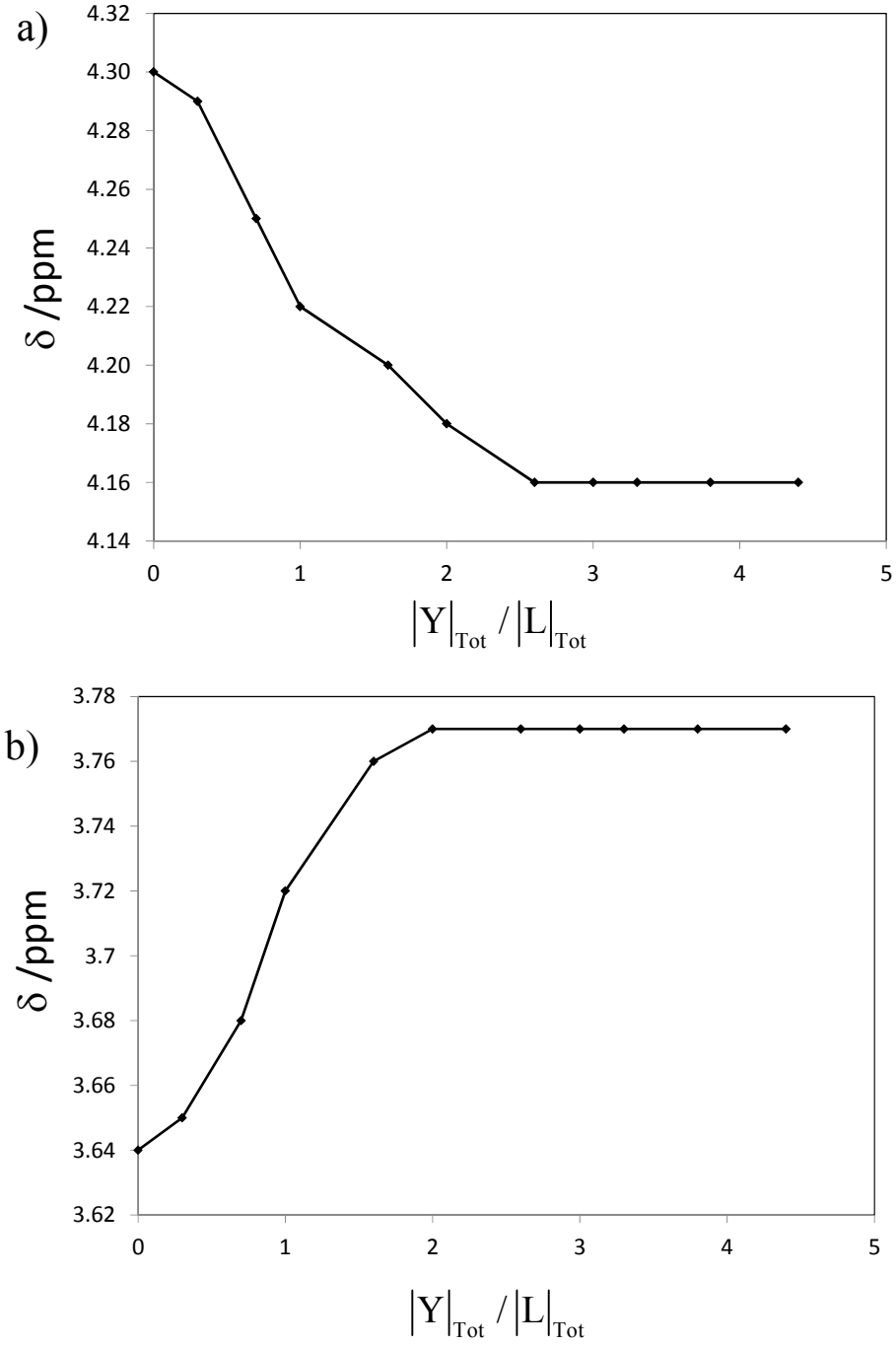

Figure S16 Variation of the ^{1}H NMR chemical shifts for the titration of **L6** with [Y(hfac)$_3$diglyme], a) Ha and b) Hk. (For numbering, see Figure S13)

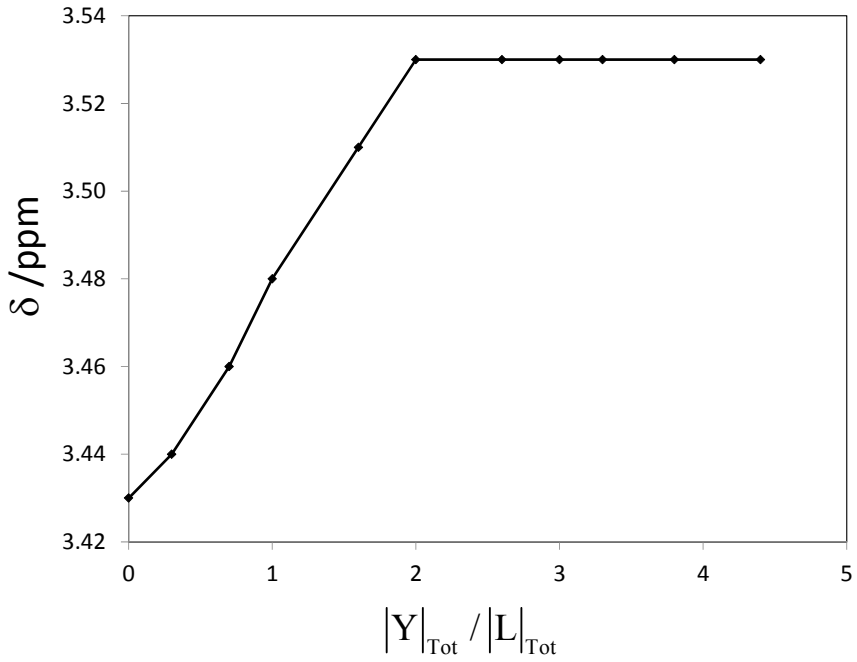

Figure S17 Variation of the ^{1}H NMR chemical shifts for the titration of **L6** with [Y(hfac)$_3$diglyme], proton Hi. (For numbering, see Figure S13)

a)

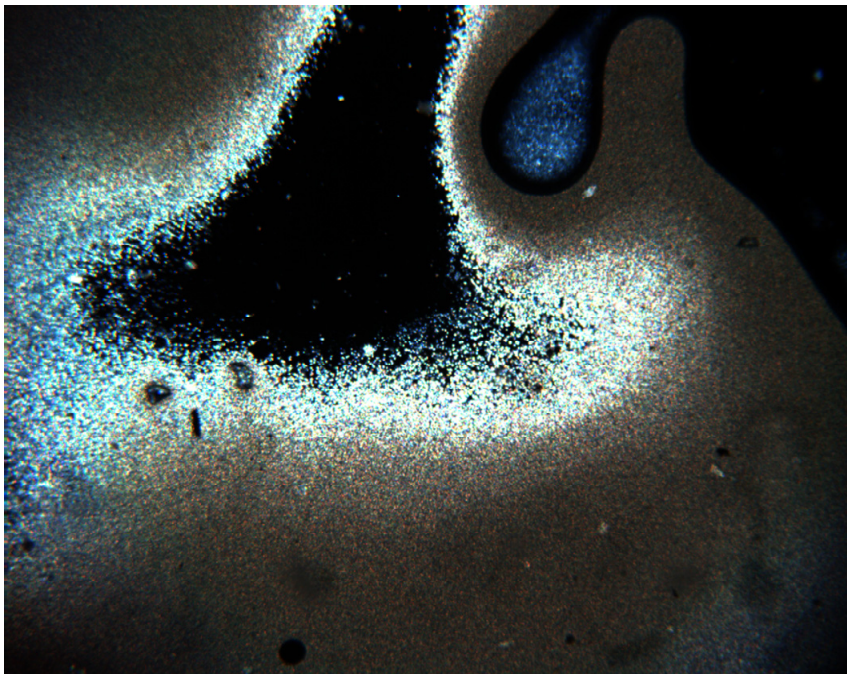

b)

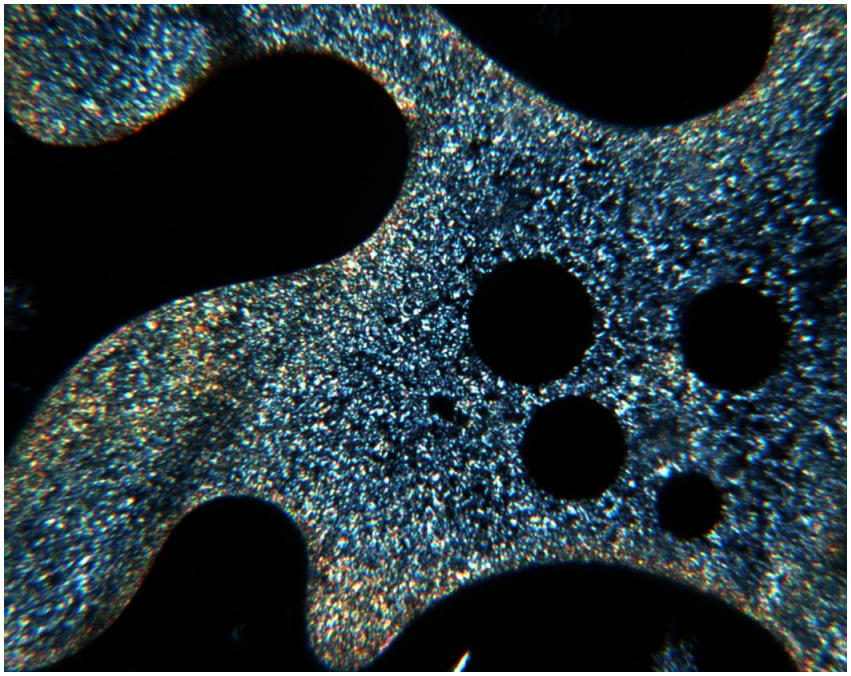

Figure S18 a) Optical texture observed by POM for Ligand **L6** in the N mesophase at 135°C after cooling from the isotropic liquid and b) optical texture observed by POM for the complex $[Y_2(\mathbf{L6})(hfac)_6]$ in the SmA mesophase at 175°C after cooling from the isotropic liquid.

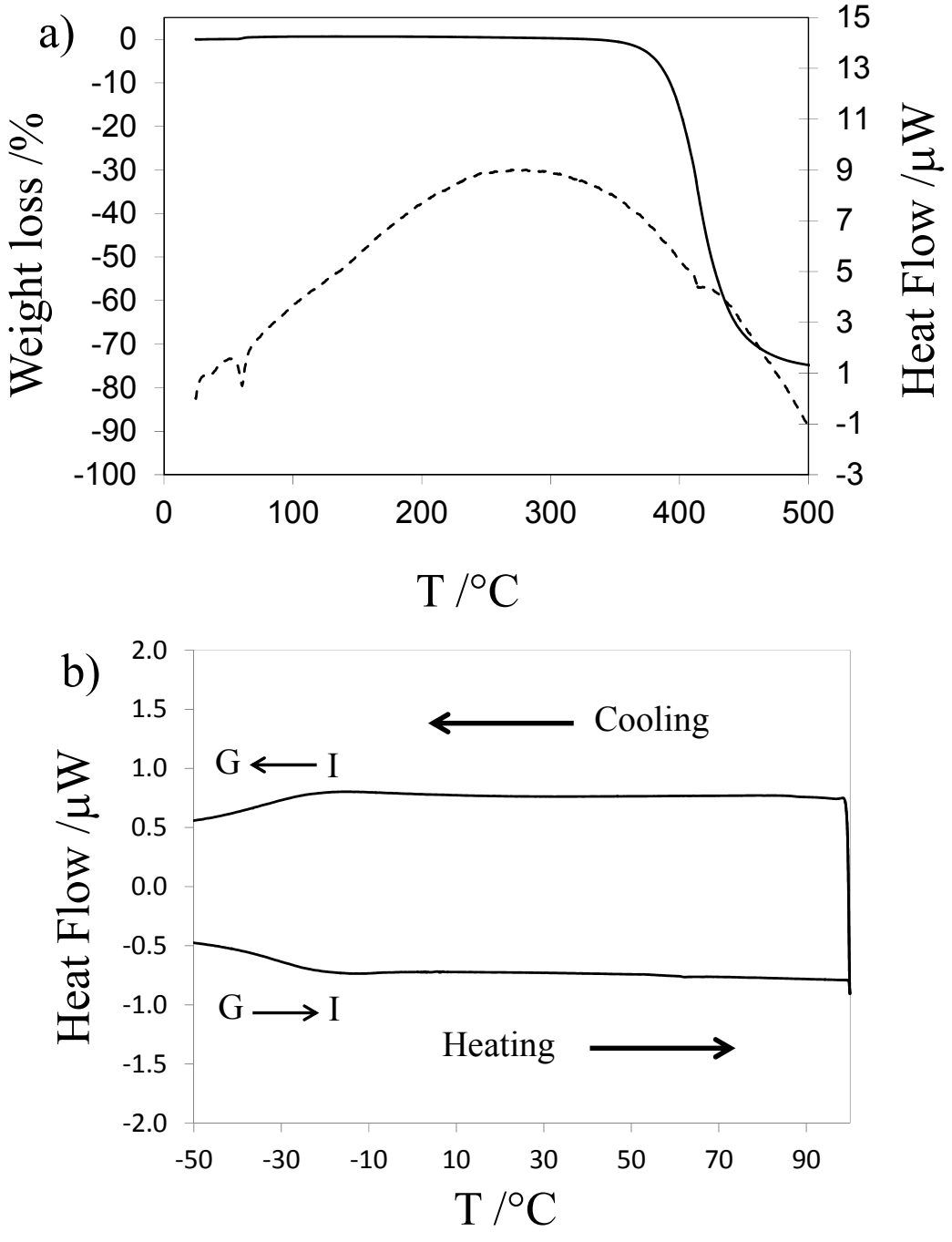

Figure S19 a) TGA of the ligand **L5** at 5°C/min and b) DSC trace of the ligand **L5** at 5°C/min.

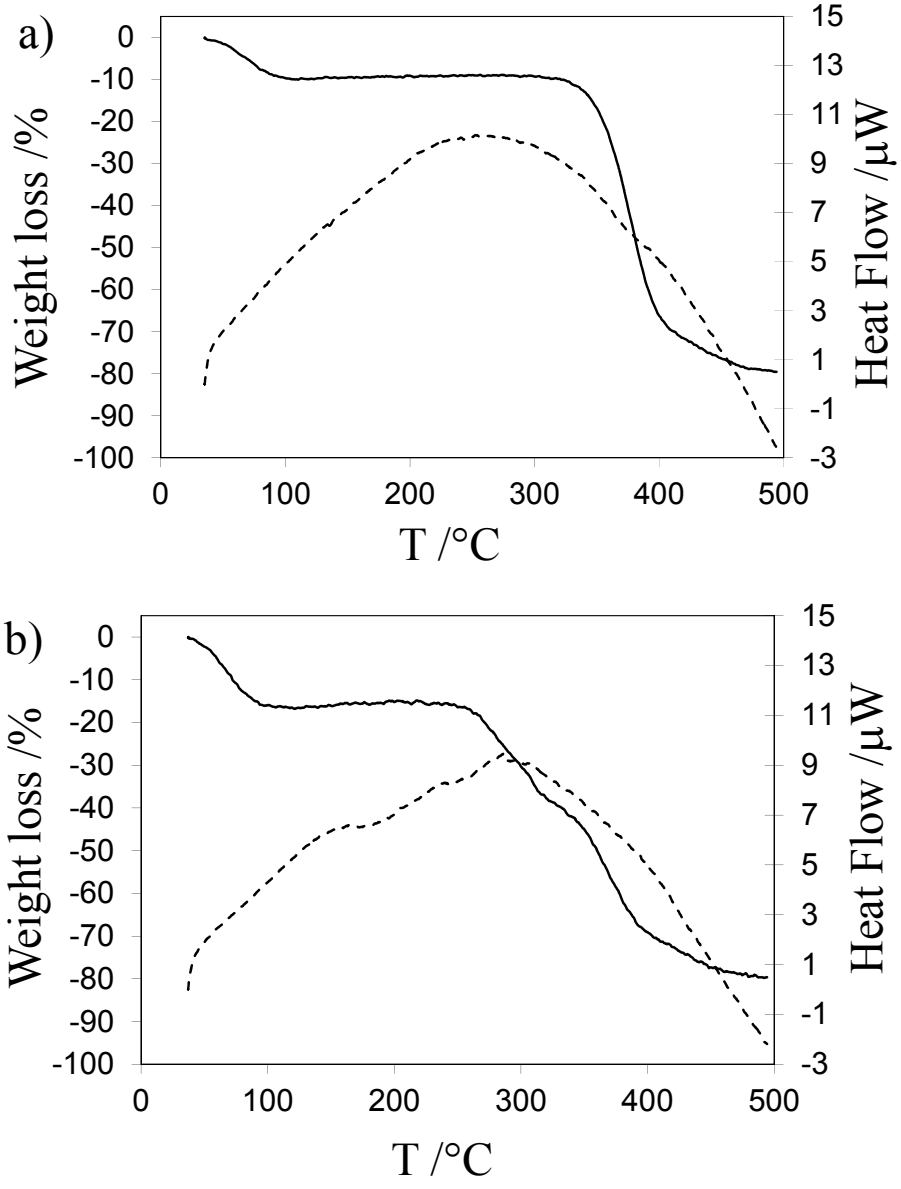

Figure S20 a) TGA of the ligand **L6** at 5°C/min b) TGA of the complex $[Y_2(\mathbf{L6})(hfac)_6]$ at 5°C/min.

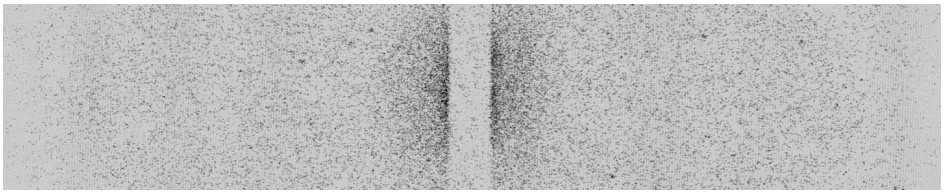

Figure S21 SA-XRD image plate of the nematic liquid crystalline phase of ligand **L6** recorded at 80°C in the -4.0° to 4.0° 2θ range.

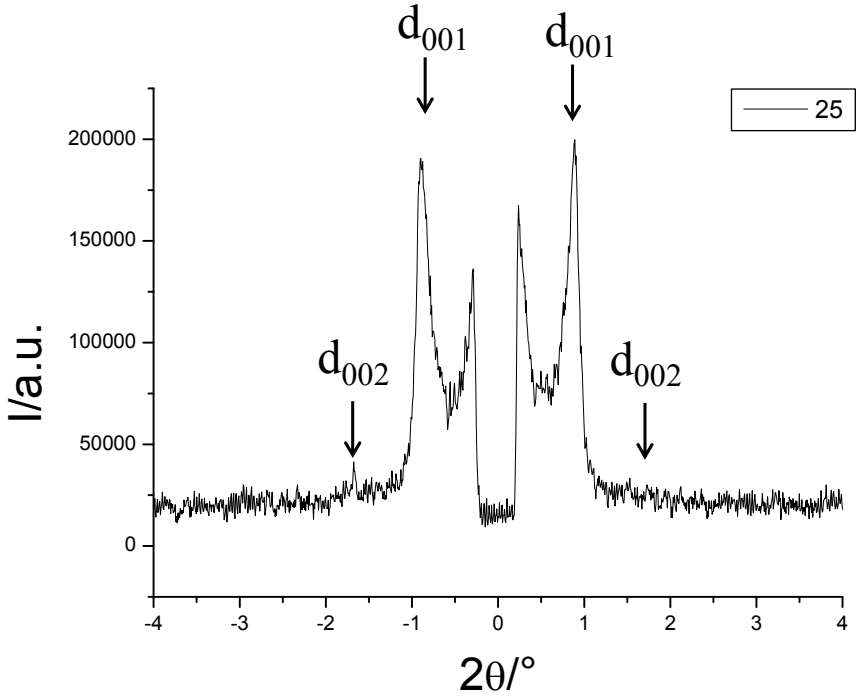

Figure S22 SA-XRD pattern of the SmA liquid crystalline phase of $[Y_2(\mathbf{L6})(hfac)_6]$ recorded at 40°C with indexation.

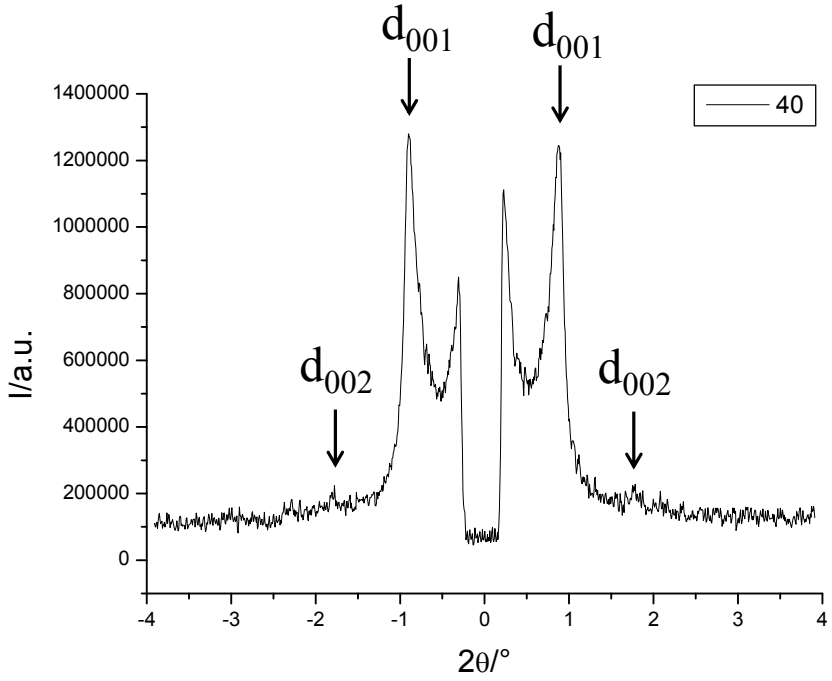

Figure S23 SA-XRD pattern of the SmA liquid crystalline phase of $[Y_2(\mathbf{L6})(hfac)_6]$ recorded at40°C with indexation.

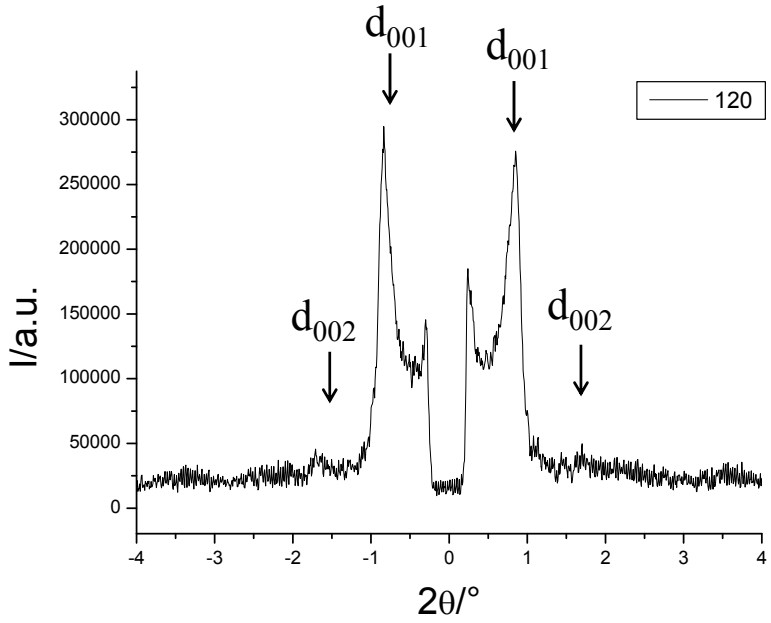

Figure S24 SA-XRD pattern of the SmA liquid crystalline phase of $[Y_2(\mathbf{L6})(hfac)_6]$ recorded at 120°C with indexation.

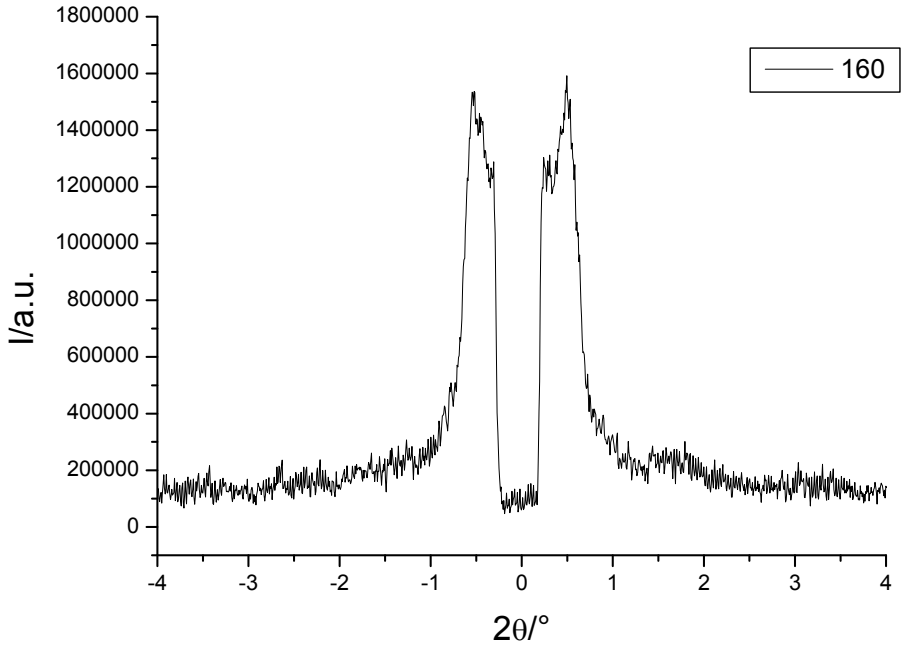

Figure S25 SA-XRD pattern of the SmA liquid crystalline phase of $[Y_2(\mathbf{L6})(hfac)_6]$ recorded at 160°C.

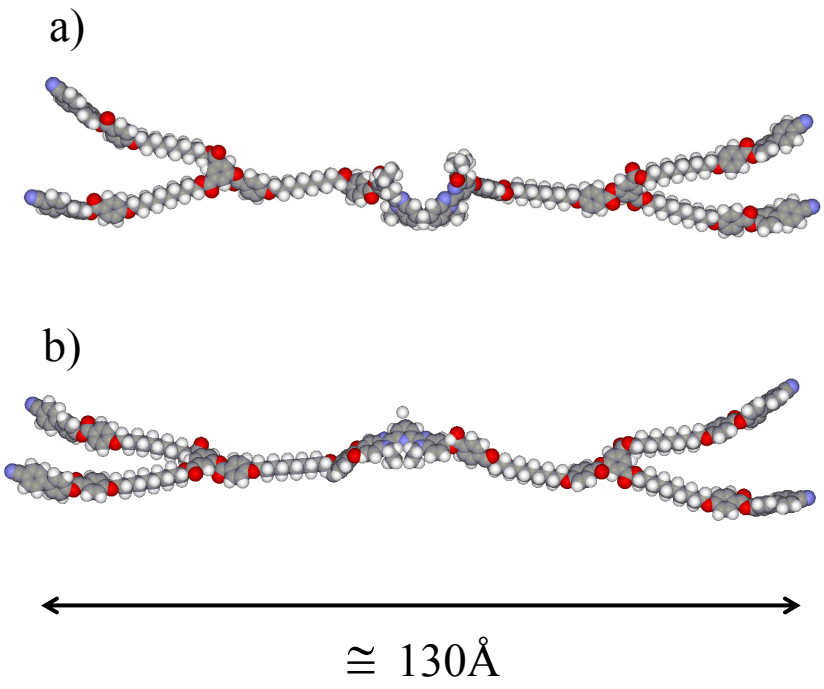

Figure S26 Rough molecular models of a) ligand **L6** and b) ligand **L9** in extended conformation.

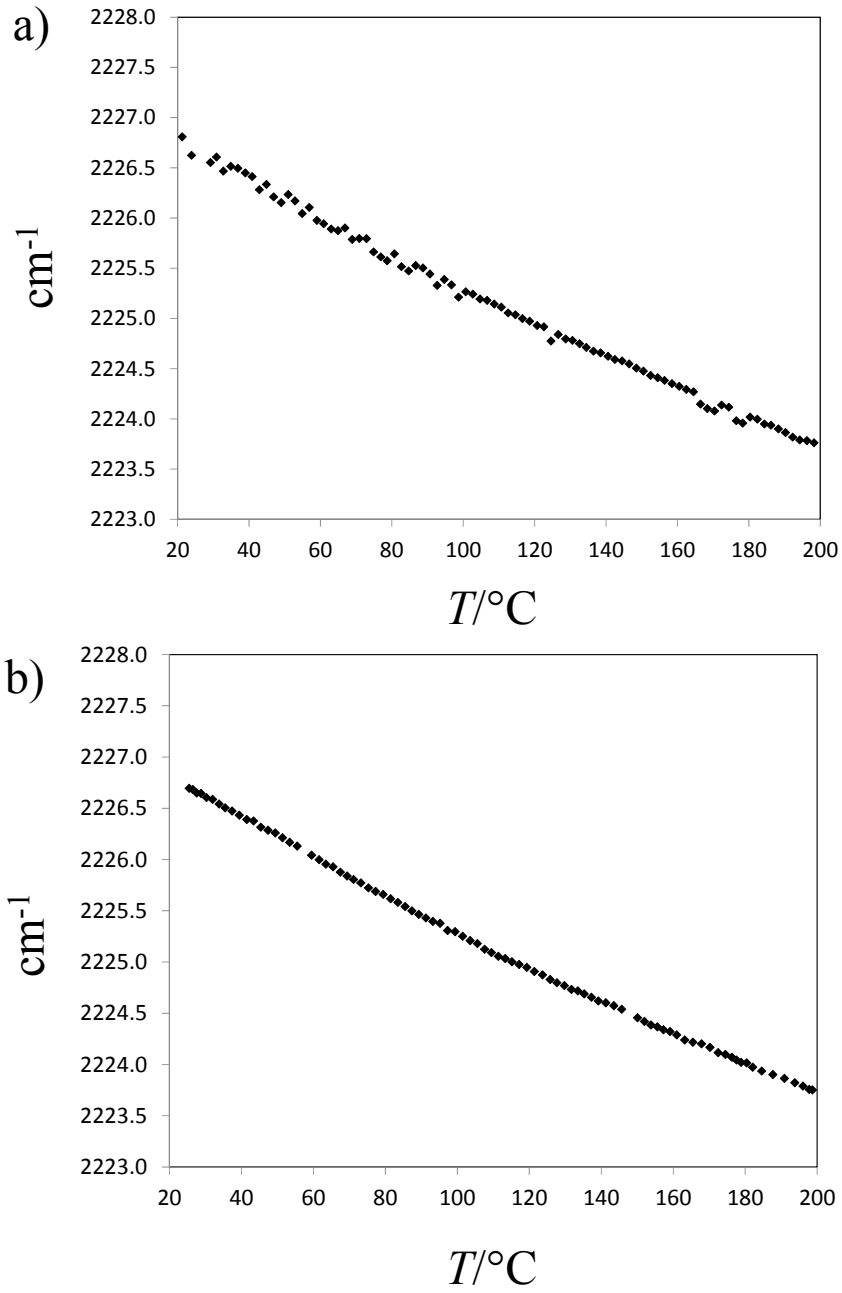

Figure S27 Temperature dependence of the energy of the CN stretching vibrational bands in complex $[Y_2(\mathbf{L6})(hfac)_6]$. a) second heating b) second cooling. (The data of the ν_{CN} band were adjusted with a Gaussian curve, see Figure S35 for a typical fit).

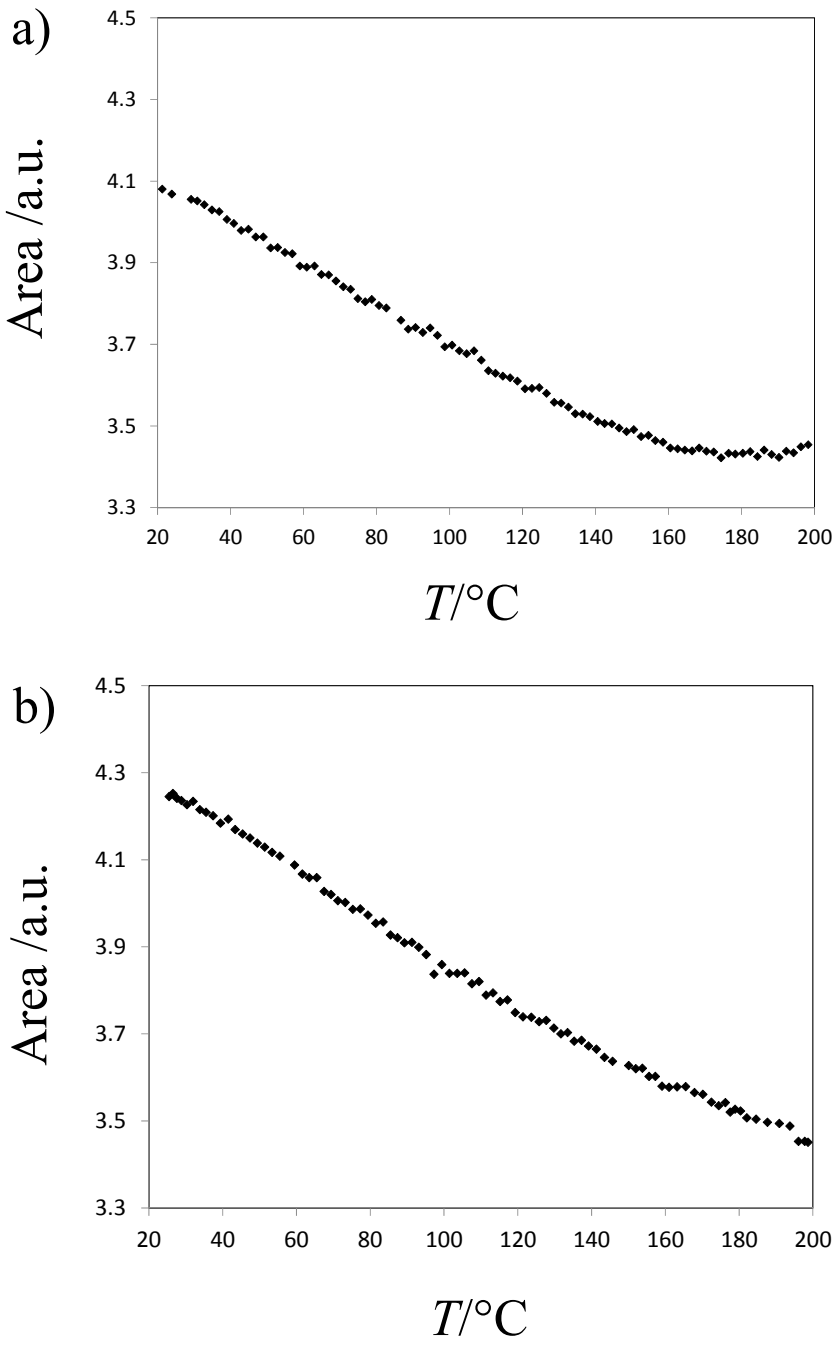

Figure S28 Temperature dependence of integrated intensities (2200 to 2250 cm^{-1}) of the CN stretching vibrational bands in complex $[Y_2(\mathbf{L6})(hfac)_6]$. a) second heating b) second cooling. (The data of the ν_{CN} band were adjusted with a Gaussian curve, see Figure S35 for a typical fit).

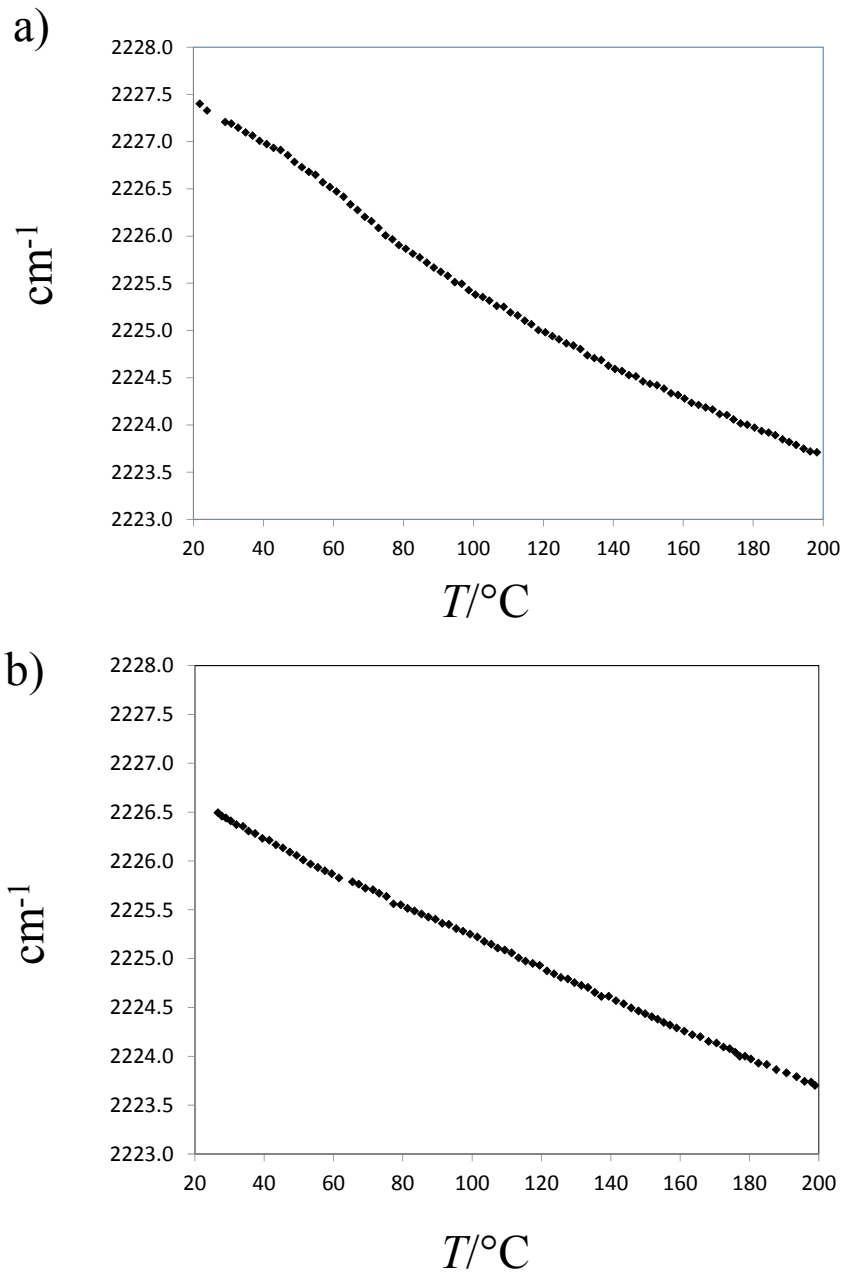

Figure S29 Temperature dependence of the energy of the –CN stretching vibrational bands in complex $[Y_2(\mathbf{L6})(hfac)_6]$. a) first heating b) first cooling. (The data of the ν_{CN} band were adjusted with a Gaussian curve, see Figure S35 for a typical fit).

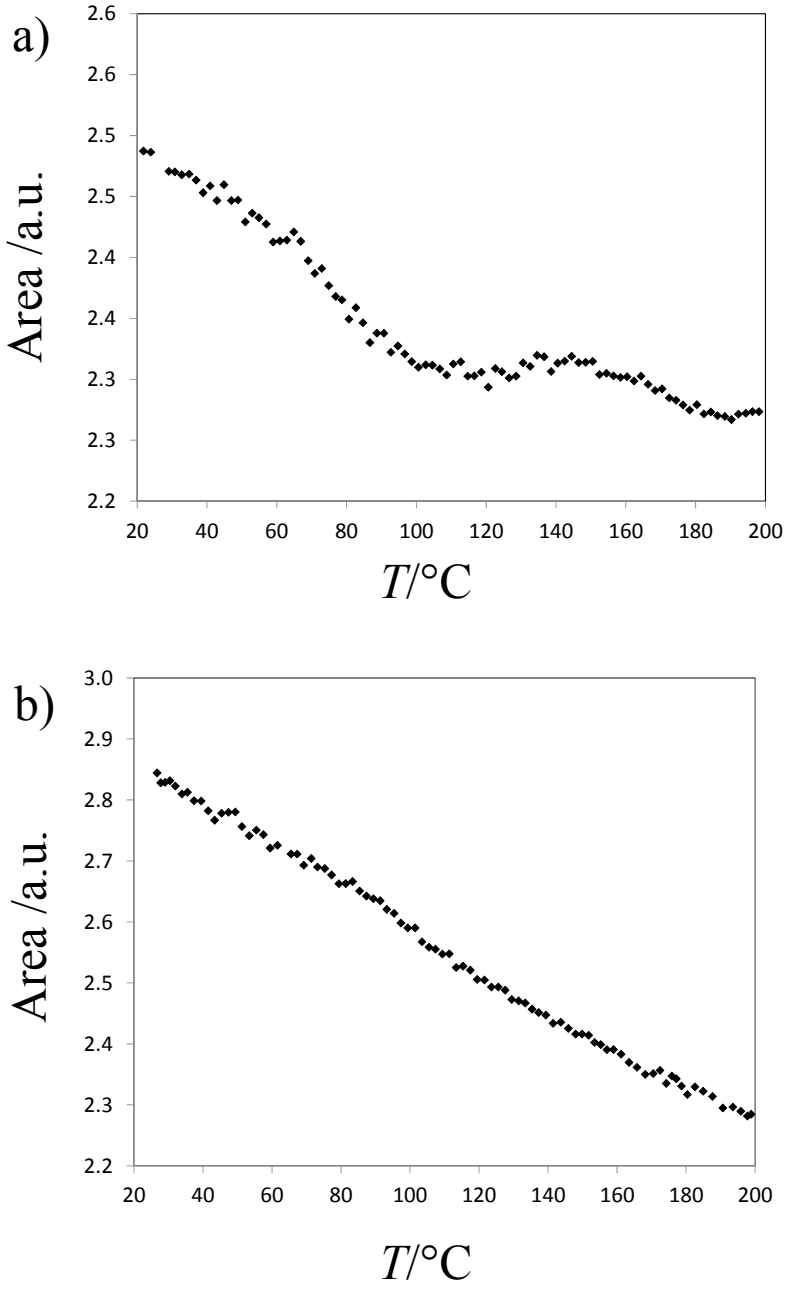

Figure S30 Temperature dependence of integrated intensities (2200 to 2250 cm^{-1}) of the –CN stretching vibrational bands in complex $[Y_2(\mathbf{L6})(hfac)_6]$. a) first heating b) first cooling. (The data of the ν_{CN} band were adjusted with a Gaussian curve, see Figure S35 for a typical fit).

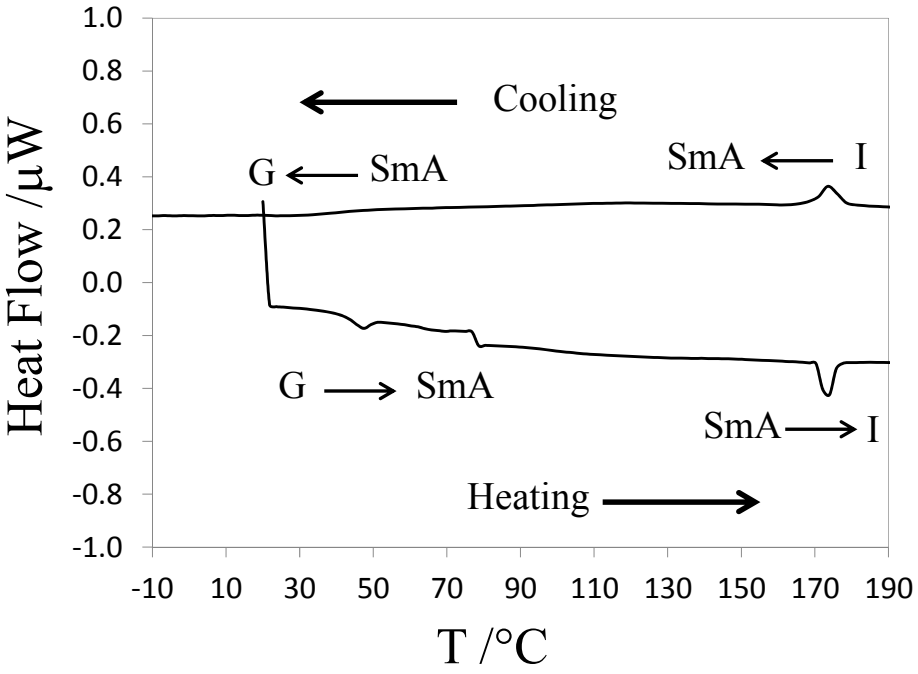

Figure S31 DSC trace of the complex $[Y_2(\mathbf{L6})(hfac)_6]$ at 5°C/min. (First heating and cooling)

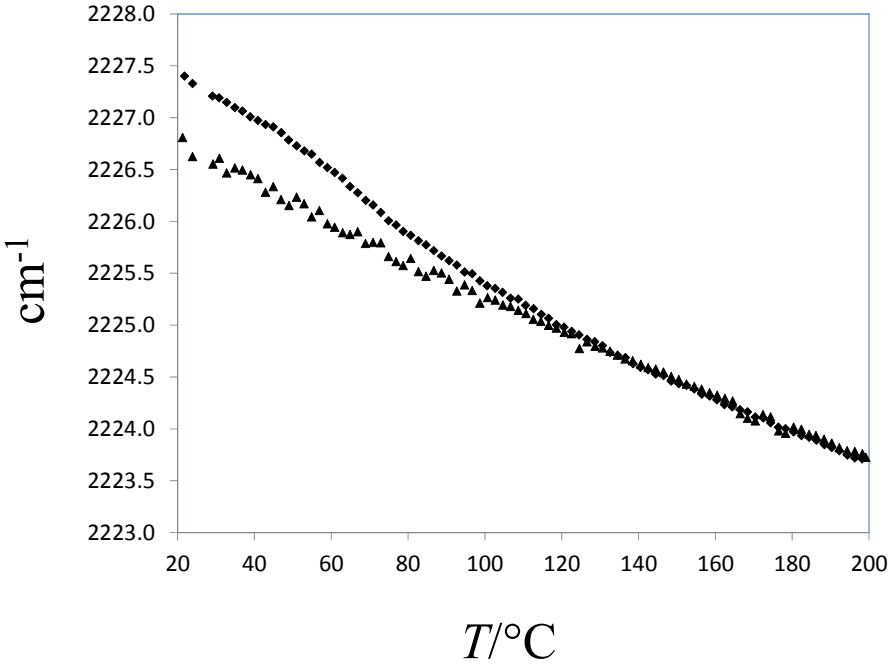

Figure S32 Temperature dependence of the energy of the CN stretching vibrational bands in complex $[Y_2(\mathbf{L6})(hfac)_6]$. ♦ first heating and ▲ second heating. (The data of the ν_{CN} band were adjusted with a Gaussian curve, see Figure S35 for a typical fit).

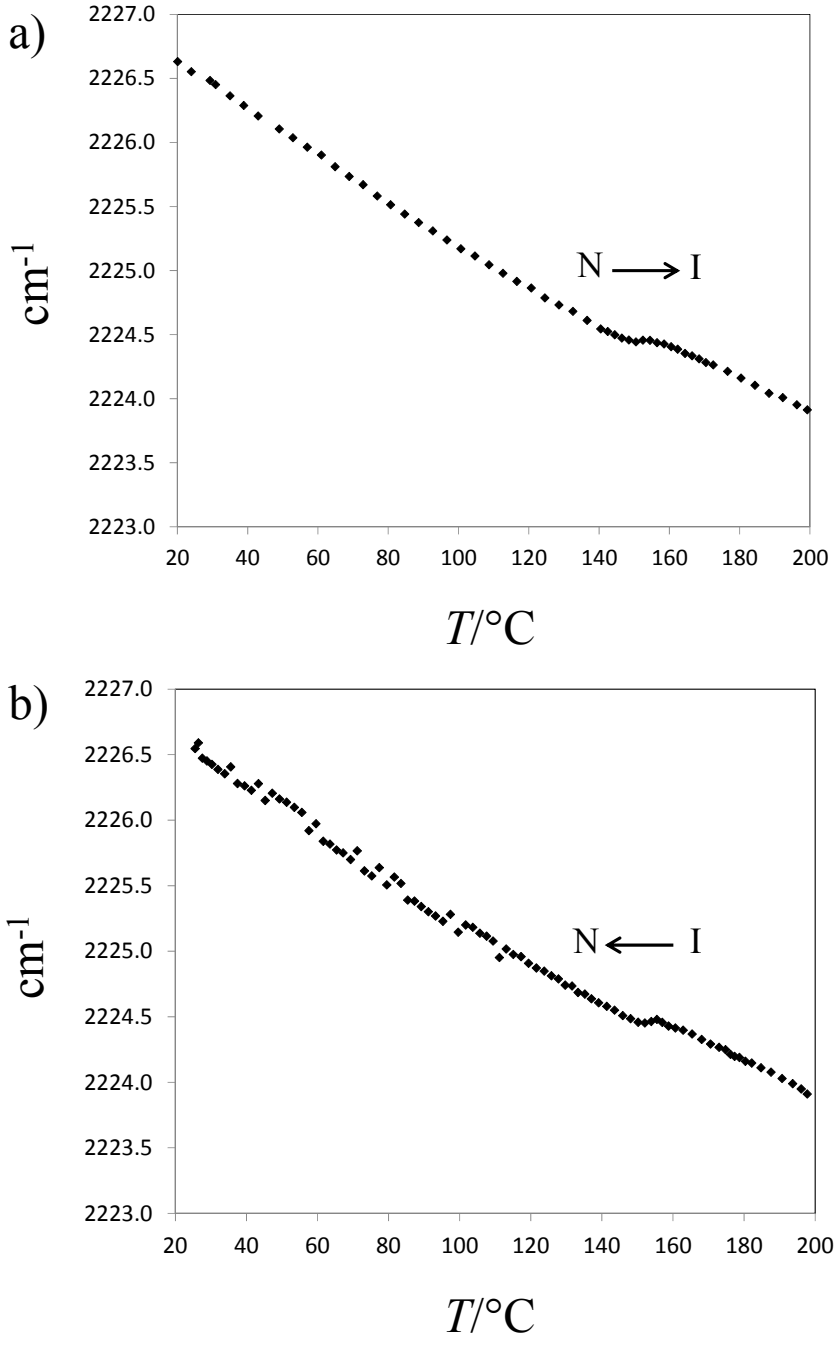

Figure S33 Temperature dependence of the energy of the CN stretching vibrational bands of ligand **L6**. a) second heating b) second cooling. (The data of the ν_{CN} band were adjusted with a Gaussian curve, see Figure S35 for a typical fit).

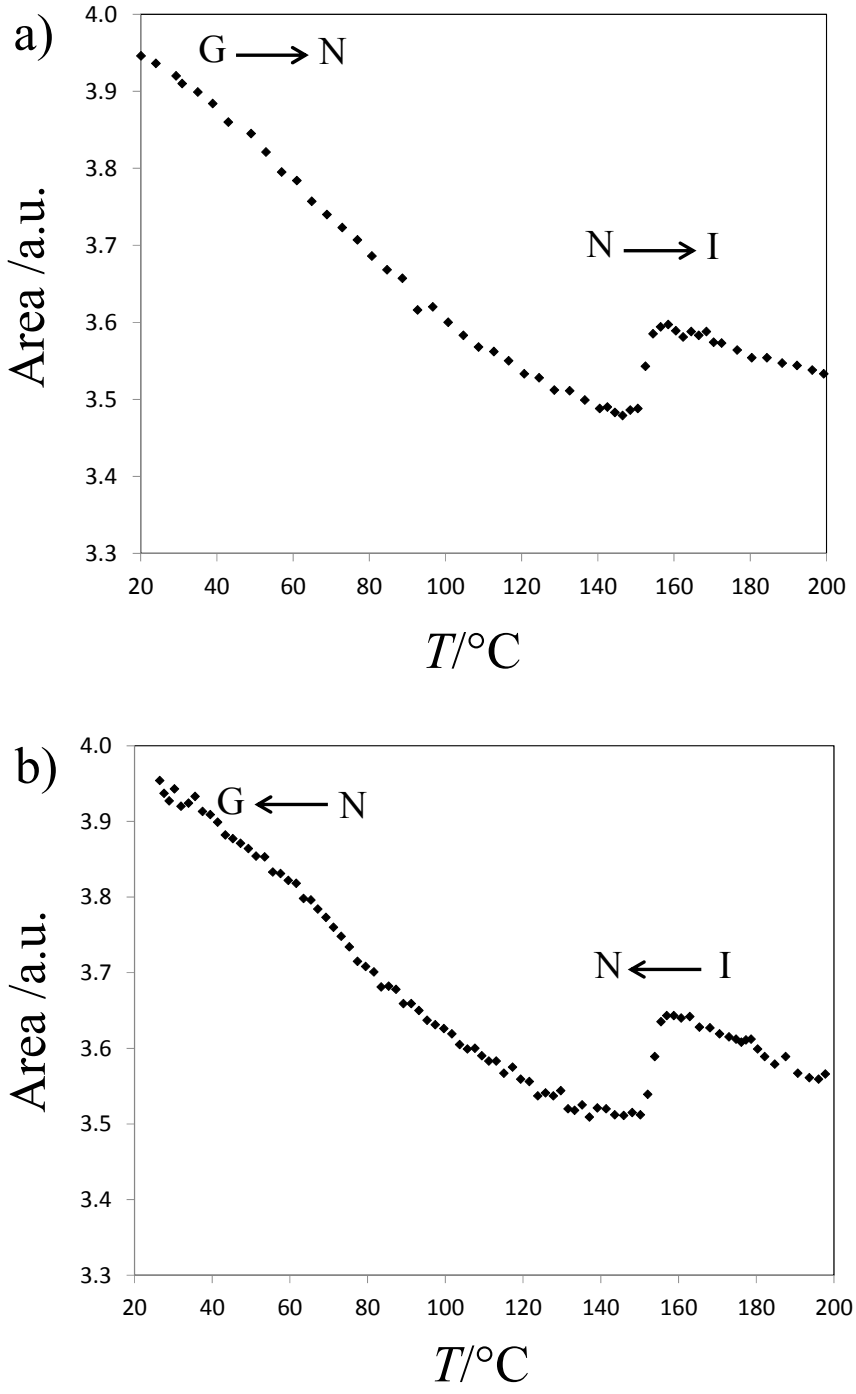

Figure S34 Temperature dependence of integrated intensities (2200 to 2250 cm^{-1}) of the CN stretching vibrational bands of ligand **L6**. a) second heating b) second cooling. (The data of the ν_{CN} band were adjusted with a Gaussian curve, see Figure S35 for a typical fit).

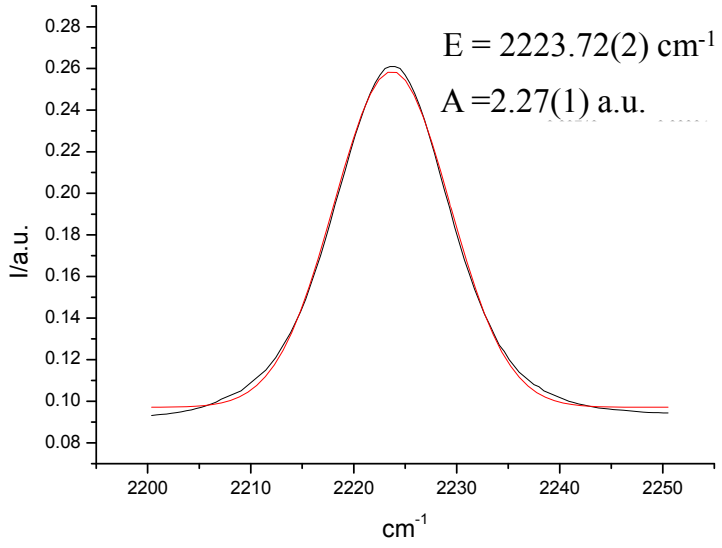

Figure S35 Typical Gaussian fit (2200 to 2250 cm^{-1}) of the CN stretching vibrational band.

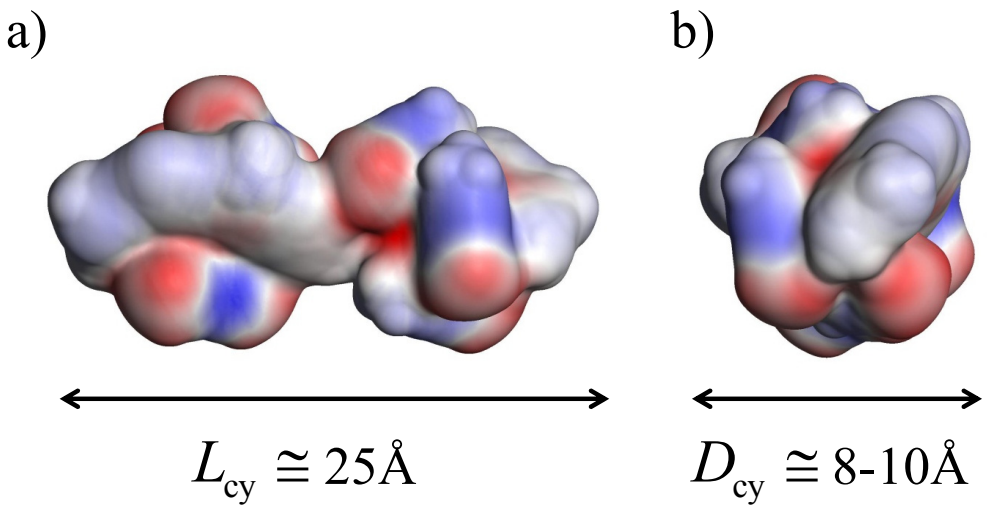

Figure S36 Connolly surface built around aromatic core of the complex using the crystal structure of $[Lu_2(\mathbf{L1})(hfac)_6]$, a) view perpendicular to the line passing through Lu1 and Lu2 b) view parallel to the line passing through Lu1 and Lu2. [8]

References

[1] G. Horvath, C. Rusa, Z. Köntös, J. Gerencser, P. Huszthy, *Synthetic Communication* **1999**, *29*, 3719-3731.

[2] P. Froidevaux, J. M. Harrowfield, A. N. Sobolev, *Inorg. Chem.* **2000**, *39*, 4678-4687.

[3] C. Piguet, G. Bernardinelli, A. Quattropani, A. F. Williams, *J. Am. Chem. Soc.* **1992**, *114*, 7440-7491.

[4] C. Piguet, B. Bocquet, G. Hopfgartner, *Helv. Chim. Acta* **1994**, *77*, 931-942.

[5] a) B. Donnio, P. Garcia-Vazquez, J.-L. Gallani, D. Guillon, E. Terazzi, *Adv. Mater.* **2007**, *19*, 3534-3539. b) Z. T. Nagy, B. Heinrich, D. Guillon, J. Tomczyk, J. Stumpe, B. Donnio *J Mater. Chem.* **2012**, *22,* 18614-18622.

[6] a) C. Piguet, J.-C. G. Bünzli, G. Bernardinelli, G. Hopfgartner, A. F. Williams, *J. Am. Chem. Soc.* **1993**, *115*, 8197-8206. b) N. Martin, J.-C. G. Bünzli, V. McKee, C. Piguet, G. Hopfgartner, *Inorg. Chem.* **1998**, *37*, 577-589. c) S. Floquet, N. Ouali, B. Bocquet, G. Bernardinelli, D. Imbert, J.-C. G. Bünzli, G. Hopfgartner, C. Piguet, *Chem. Eur. J.* **2003**, *9*, 1860-1875. d) K. Zeckert, J. Hamacek, J.-M. Senegas, N. Dalla-Favera, S. Floquet, G. Bernardinelli, C. Piguet, *Angew. Chem. Int. Ed.* **2005**, *44*, 7954-7958. (e) C. Piguet, J.-C. G. Bünzli, in *Handbook on the Physics and Chemistry of Rare Earths*, Vol. 40 (Eds.: K. A. GschneidnerJr, J.-C. G. Bünzli, V. K. Pecharsky), Elsevier Science, Amsterdam, 2009, pp. 301-553. (f) C. Lincheneau, F. Stomeo, S. Comby, T. Gunnlaugsson, *Aust. J. Chem.* **2011**, *64*, 1315-1326. (g) S. Zebret, C. Besnard, G. Bernardinelli, J. Hamacek, *Eur. J. Inorg. Chem.* **2012**, 2409-2417. (h) H.-F. Li, P.-F. Yan, P. Chen, Y. Wang, H. Xu, G.-M. Li, *Dalton Trans.* **2012**, *41*, 900-907.

[7] F. H. Allen, O. Kennard, D. G. Watson, L. Brammer, O. A. G. R. Taylor, *J. Chem. Soc. Perkin Trans. 2* **1987**, S1-S19.

[8] a) M. L. Connolly, *Science* **1983**, *221*, 709-713; b) M. L. Connolly, *J. Appl. Crystallogr.* **1983**, *16*, 548-558. b) The Connolly Surface was built with the *DS ViewerPro 5.0 software* with a probe radius of 1.4 Å.